Characterization of glycopolymers by asymmetric flow field-flow fractionation

By

Chelsea Williams

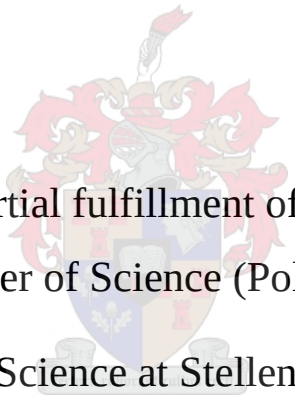

Thesis presented is in partial fulfillment of the requirements for the degree of Master of Science (Polymer Science)

at the Faculty of Science at Stellenbosch University

Supervisors: Prof H. Pasch and Prof A. Lederer

December 2020

Declaration

By submitting this thesis electronically, I declare that the entirety of the work contained therein is my own, original work, that I am the authorship owner thereof (unless to the extent explicitly otherwise stated) and that I have not previously in its entirety or in part submitted it for obtaining any qualification.

Chelsea Williams

December 2020

Dedicated to my late uncle Wern, your contribution towards my education made all this possible.

Abstract

An alternative route for studying the interactions between human serum albumin (HSA) and dendronized glycopolymers was implemented by applying a versatile asymmetric flow field-flow fractionation (AF4) technique. Dendronized polymers (DenPols) decorated with maltose moieties, have an abundance of hydrogen bonding sites that is desirable for interactions with HSA. The difficulty with the characterization of lysine maleimide DenPols and poly(ethylene glycol) (PEG) maleimide DenPols are the ultrahigh molar masses and the molecular heterogeneity. Here, we aimed to apply the gentle AF4 technique in combination with a refractive index and light scattering detectors to comprehensively characterize the lysine maleimide DenPols decorated with a maltose shell (MI-G0-MAL – MI-G3-MAL), PEG maleimide DenPol (MI-G1-PEG-MAL), human serum albumin (HSA) and complexes formed by the interaction of DenPols and HSA. An in-depth analysis of the DenPols, regarding their molar mass distribution, radius of gyration, hydrodynamic radius, dispersity, and molecular architecture was conducted. The determination of these properties was examined using batch mode dynamic light scattering (DLS), size exclusion chromatography (SEC) and AF4. Both separation techniques explicitly showed the pronounced aggregation of the DenPols. AF4 showed the DenPols being present as single macromolecules with a random coil conformation and aggregates as elongated (rod-like) or spherical conformations. Complexes formed between DenPols and HSA showed a deviation in the aggregation mechanism compared to the individual DenPols, as the conformation of the non-aggregated and aggregated structures were different. The complexation behaviour between DenPols and HSA displayed aggregated structures of hard dense spherical and swollen molecular architectures. MI-G3-MAL with more available hydrogen bonding sites showed significant changes in the conformation when interacting with HSA. The study demonstrated that the multivalent interactions of DenPols with HSA indicate the tunable aggregation and conformation of DenPols.

Abstrak

‘n Alternatiewe studieroete is gevolg vir die bestudering van die interaksie tussen menslike serumalbumien (HSA) en gedendroniseer glikopolymere. Dit was geimplementeer deur die toepassing van ‘n veelsydige onsimmetriese vloei-veldvloeifraksioneringtegniek (AF4). Gedendroniseerde polymere (DenPols) versier (gelaai) met maltose eindgroepe, het’n magdom (verskeidenheid) van waterstof bindingswerwe wat voordelig is vir interaksies van HSA. Die uitdaging met die karaktarisering van lysien maleimied DenPols en poli(etileenglikol) (PEG) maleimied DenPols, is die ultrahoë molêre eenhede en die molekulêre heterogeniteit. Hier het ons gepoog om toepassing van die sagte AF4 tegniek in kombinasie met ‘n refraktiewe indeks en ligte verspreiders aan te wend. Hierdeur kon ons die lysine maleimide wat versier is met maltose bedecking (MI-G0-MAL -MI-G3-MAL), PEG maleimide DenPol (MI-G1-PEG-MAL), HSA en komplekse wat ontstaan het deur die interaksie van DenPols en HSA omvattend karakteriseer.

‘n In diepte analise van DenPols aangaande hul “molar” massa verspreiding radius of omwenteling, hidrodinamiese verspreiding en molekulêre argitektuur was uitgevoer. Die vasberadenheid van hierdie elemente is aangedui deur die gebruik van bondelmodus dinamiese ligverspreiding (DLS), grootte-uitsluitschromatografie (SEC) en AF4 tegniek. Beide skeidingstegnieke het baie duidelik die samevoeging van DenPols gedui. AF4 lewer bewys dat DenPols teenwoordig is as ‘n enkele makromolekule met ‘n willekeurige spoelstruktuur en ‘n samevoeging as ‘n verlengde staaf of sferise struktuur. Komplekse wat gevorm is tussen DenPols en HSA het ‘n afwyking met die aggressie meganisme in vergelyking met die individuele DenPols aangesien die ooreenkomstigheid van die saamgestelde en nie saamgestelde structure verskillend was. Die komplekse gedrag tussen DenPols en HSA het samegestelde structure van harde, digte sferiese en geswolle molekulêre argitektuur. MI-G3-MAL het beskikbare waterstofverbonde werwe getoon wat beduidende veranderinge getoon het wanneer dit met HSA in interaksie is. Die studie illustreer dus die multivalente interaksie van DenPols met HSA asook die afstembare samevoeging en ooreenkomstigheid van DenPols.

Acknowledgements

I would like to thank my supervisors, Prof H. Pasch, and Prof A. Lederer, for their unwavering support, guidance, and patience during my master's thesis. I am very grateful for the opportunity you gave me to perform my experiments at Leibniz Institute of Polymer Research (Dresden, Germany).

Dr Susanne Boye (IPF Dresden), your help throughout my experiments was truly appreciated. Thank you for sharing your knowledge and expertise about AF4 with me.

I would like to thank Dr D. Appelhans from the Leibniz Institute of Polymer Research (Dresden, Germany) for providing the samples for my project.

All the members of the Pasch analytical group, thank you for your encouragement, assistance with instruments and advice.

Thank you to everyone from the polymer analytical group at IPF Dresden, thank you for making me feel welcome and for all the knowledge you shared.

Dr H. Pfukwa, thank you for your guidance and support throughout my master project.

Thank you to Prof H. Pasch, Stellenbosch University, and National Research Foundation (NRF) for the financial support during my master's thesis.

To my loving boyfriend, Bongi, thank you for all your support, constant encouragement, and motivation throughout my master project.

To my amazing family that carried me through the very difficult times of my thesis, I am eternally grateful. A special thank you to my mother Leandré, father William, grandmother Gladys, brothers David, Jaydone and aunty Delia. Your continuous support, prayers and encouragement carried me through. To my late grandfather Philip and uncle Wern, you are truly missed, it would have been great to share this moment with you.

To my supportive friends, Jaimy, Stacey, Remo, Lauren, Megan and Chandre, thank you for your support, honesty, and encouragement.

Lastly, to the Lord Almighty, thank you for giving me strength and blessing me with the opportunity to do my master project.

Table of contents

List of figures

List of tables

List of abbreviations

AF4	asymmetric flow field-flow fractionation
AFM	atomic force microscopy
ATRP	atom transfer radical polymerization
BSA	bovine serum albumin
CD	circular dichromism
CNTs	carbon nanotubes
CNCs	cellulose nanocrystals
DenPols	dendronized polymers
DLS	dynamic light scattering
D_h	hydrodynamic diameter
LiCl	lithium chloride
QCM	quartz crystal microbalance
LS	light scattering
MALLS	multiangle laser light scattering
DMAc	N, N-dimethylacetamide
dn/dc	specific refractive index increment
PBS	phosphate buffer saline
DRI	differential refractive index
FFF	field-flow fractionation
GPC, SEC	gel permeation chromatography, size exclusion chromatography
MAL	maltose
M_n	number-average molar mass
M_w	weight-average molar mass
$M_{w,0}$	molar mass of a single macromolecule
M_p	molar mass at peak maximum
MWCO	molecular weight cut off
R_g or r_{rms}	Radius of gyration or root mean square radius
R_h	hydrodynamic radius

PDI	polydispersity index
HSA	human serum albumin
PAMAM	poly (amidoamine)
PPI	poly (propylene imine)
PEIs	poly (ethylene imines)
PS	polystyrene
PEG	poly (ethylene glycol)
NaN_3	sodium azide
NMR	nuclear magnetic resonance
RI	refractive index
RAFT	reversible addition-fragmentation chain transfer polymerization
TEM	transmission electron microscopy
ThFFF	thermal field-flow fractionation
UHMM	ultrahigh molar mass
UV	ultraviolet
SLS	static light scattering

List of symbols

α	correction factor for the apparent density
A_2	second virial coefficient
c	concentration of analyte
c_0	concentration of the solute at the accumulation wall
τ	delay time
d	diameter of molecule/particle
D	diffusion coefficient
Đ	dispersity
dc/dx	change in the concentration over the mean layer thickness
F	force field applied perpendicular to the inlet flow
f	frictional drag
G	gravitational force
i	a fraction
J_x	net flux energy
k/k_B	Boltzmann constant
K	constant for a polymer and solvent system for the scaling law
K^*	optical constant
K_d	distribution coefficient
l	mean thickness layer
N_A	Avogadro's number
n_0	refractive index of the solvent
$P(\theta)$	particle scattering function
r	geometrical radius of a sphere
R	retention ratio
R_θ	Rayleigh ratio
T	temperature
υ	slope of log MM vs log R_g plot (scaling factor)
t_0	retention time of an unretained component

t_r	retention time of analyte
U	field force
V_{out}	detector flow rate
V_c	flow rate of the cross flow
ρ_{rms_i}	apparent density
V	volume of a fraction
V_e	elution volume
V_i	total volume of the solvent in the intersitial space of the pores
V_i	volume of a fraction (apparent density)
V_0	volume of the solvent outside the pores of the stationary phase (SEC)
V_0	volume of the FFF channel
V_p	volume of the particle
V_l	total volume of the mobile phase
w	the channel thickness
λ	retention parameter
λ_0	wavelength of incident
π	pi
$g(\tau)$	normalized autocorrelation function
q	scattering vector
θ	scattering angle
M	molar mass
η	viscosity
H_2O	water

Chapter 1

Introduction and objectives

Chapter 1

Introduction and objectives

1.1 Introduction

Carbohydrate-protein interactions are of critical importance for pharmaceutical therapeutics, drug delivery, and in diagnostics, specifically in the field of neurodegenerative diseases.[1–3] Since the discovery of the first ring structure (carbohydrate) in the 1930s there has been tremendous strides in the synthesis of synthetic carbohydrates to potentially mimic the interactions between natural oligosaccharides and proteins.[3] Glycopolymers are synthetic carbohydrates possessing a monosaccharide and/or an oligosaccharide as a pendent group. Recent advances have improved the synthesis of glycopolymers with complex architectures, for instance molecules with linear and hyperbranched topologies.

Dendritic glycopolymer structures have a high density of peripheral groups that enhances the potential interactions with model proteins, for instance human serum albumin (HSA), as there is an abundance of sites available for interactions. Dendronized polymers (DenPols) form part of the family of dendritic hybrids. DenPols are composed of a linear polymer backbone with multiple dendrons attached.[4-6] In this study ultrahigh molar mass lysine DenPols attached to a poly(ethylene-*alt*-maleic anhydride) backbone (MI-G0-MAL - MI-G3-MAL) and poly(ethylene glycol) (PEG) dendrons (MI-G1-PEG-MAL) decorated with a maltose shell were analyzed, see Figure 1.1. The great feature of these 3D nanosized DenPols is the abundance of H-bond active sites. Previously, the interactions between maleimide lysine DenPols and cellulose nanocrystals were investigated showing the generation dependence of the multivalent interactions.[7] These observations motivated this study on the interactions between DenPols and HSA. The interaction with a model protein, HSA, is crucial as it helps to understand the mechanism of interaction of the glycopolymers which is important for biomedical applications. [3]

The interaction mechanism between glycopolymers and HSA is quantified by fluorescence microscopy using the amino acid tryptophan shift of HSA.[8] Additionally, transmission electron microscopy (TEM), atomic force microscopy (AFM) and dynamic light scattering (DLS), quartz crystal microbalance (QCM) and ultraviolet (UV-vis) spectroscopy were used but only provide information on the conformation or size. [7,9–12]

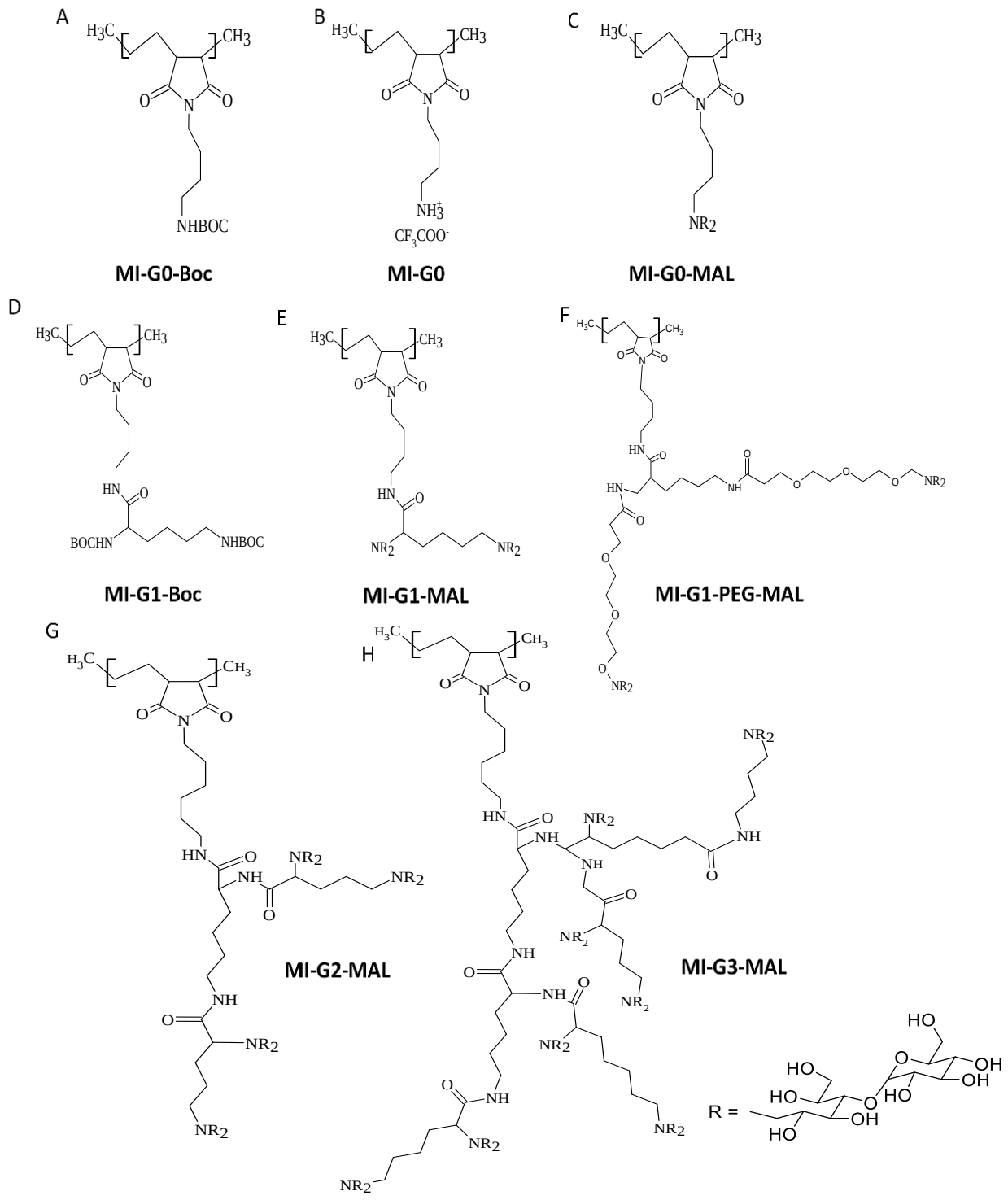

Figure 1.1. Synthesized dendronized polymers. A) MI-G0-Boc, B) deprotected MI-G0, C) MI-G0-MAL, D) MI-G1-Boc, E) MI-G1-MAL, F) MI-G1-PEG-MAL, G) MI-G2-MAL and H) MI-G3-MAL.

None of the techniques investigated the molar mass distribution, size distribution, and conformation in one measurement. By using an advanced fractionation technique such as asymmetric flow field-flow fractionation (AF4) in combination with multiangle laser light scattering (MALLS) and DLS, a comprehensive analysis of the glycopolymer-protein complexes can be achieved. Additionally, the apparent density provides information regarding the aggregated structures and the scaling law regarding the conformation.

Therefore, this study aims to develop a suitable and robust AF4 protocol for the analysis of the aggregation mechanism and conformation of the glycopolymer-HSA complexes. The present measurements will provide the necessary information about the molar mass, size, and shape of the complex between glycopolymers and HSA. To the best of our knowledge, there has been no AF4 study dedicated to the characterization of the interactions of maltose-coated maleimide DenPols with HSA.

1.2 Objectives

The general objective of this study is to comprehensively characterize the interactions between HSA and DenPols. This will be accomplished by:

1) Assessing the hydrodynamic size of deprotected MI-G0 and maltose-modified DenPols using batch mode DLS. This will provide insight into the presence of single macromolecules or aggregates in the sample.
2) Determining the molar mass distribution and dispersity of poly (ethylene-*alt*-maleic anhydride) using SEC-MALLS to calculate the theoretical molar mass of the tert-butyloxycarbonyl (Boc) protected, deprotected Boc and maltose-modified DenPols.
3) Developing an AF4-MALLS-DLS protocol that separates the DenPols as well as the HSA. In other words, the protocol must separate the DenPols with different generation numbers as well as HSA. This is to compare directly the fractograms throughout the discussion. The developed method will be used:
    I. To compare the fractograms of the DenPols by looking at the molar mass and size distributions. This will provide information regarding the elution mode of separation, whether the experimental molar masses are in good agreement with the theoretical molar masses and the presence of aggregates.

II. To determine the molar mass and size distribution of HSA and the presence of monomer, dimers, or trimers.

III. To use the developed AF4-MALLS-DLS protocol with mixtures of the DenPols with different fractions of HSA and determine the changes in the molar mass and size distribution, dispersity, apparent density and conformation with HSA, while the non-bound HSA remains separated during elution.

1.3 Layout of thesis

Chapter 1

An introductory chapter to provide a brief overview of the investigated topic for the study. The introduction will be followed by the objectives and the general layout of the thesis.

Chapter 2

In this chapter, the background information about the applications, synthesis, and conformation of the dendronized glycopolymers as well as the analytical techniques will be presented. An overview of the general interactions between carbohydrates and proteins, more specifically with human serum albumin, will be given, followed by the theory of the analytical techniques and the characterization parameters that will be used in this study.

Chapter 3

This chapter entails the materials, samples and experimental procedures that will be used in this study.

Chapter 4

In this chapter the characterization of the size of the individual DenPols with batch mode DLS is discussed. Secondly, the characterization of the molar mass distribution and dispersity of poly (ethylene-*alt*-maleic anhydride) and the Boc protected DenPols using SEC-MALLS will be discussed. An extensive analysis of the complex DenPol structure with an optimized AF4-MALLS-DLS protocol to investigate the molar and size distribution, apparent density, and the conformation will be presented. The molar mass and size of HSA, utilizing AF4-MALLS-DLS is briefly discussed. An investigation of the multivalent interactions between HSA and the DenPols

is performed with an optimized AF4-MALLS-DLS protocol with the focus on the molar mass and size distribution, dispersity, apparent density, and the conformation.

Chapter 5

The conclusions obtained from the investigations in Chapter 4 and the possible future studies for this study will be given.

1.4 References

1 D. Appelhans, B. Klajnert-Maculewicz, A. Janaszewska, J. Lazniewska and B. Voit, *Chem. Soc. Rev.*, 2015, **44**, 3968–3996.

2 G. Yilmaz and C. R. Becer, *Front. Bioeng. Biotechnol.*, 2014, **2**, 39.

3 B. Voit and D. Appelhans, *Macromol. Chem. Phys.*, 2010, **211**, 727–735.

4 A. Lederer and W. Burchard, in *Hyperbranched Polymers Macromolecules in between Deterministic Linear Chains and Dendrimer Structures*, ed. B. Z. Tang, A. S. Abd-El-Aziz, S. Craig, J. Dong, T. Masuda, C. Weber, the Royal Society of Chemistry, Cambridge, 16th ed., 2015, vol. 1, ch. 5, 88-132.

5 J. Yan, W. Li and A. Zhang, *Chem. Commun.*, 2014, **50**, 12221–12233.

6 A. D. Schlüter, A. Halperin, M. Kröger, D. Vlassopoulos, G. Wegner and B. Zhang, *ACS Macro Lett.*, 2014, **3**, 991–998.

7 J. Majoinen, J. S. Haataja, D. Appelhans, A. Lederer, A. Olszewska, J. Seitsonen, V. Aseyev, E. Kontturi, H. Rosilo, M. Österberg, N. Houbenov and O. Ikkala, *J. Am. Chem. Soc.*, 2014, **136**, 866–869.

8 D. Wrobel, M. Marcinkowska, A. Janaszewska, D. Appelhans, B. Voit, B. Klajnert-Maculewicz, M. Bryszewska, M. Štofik, R. Herma, P. Duchnowicz and J. Maly, *Colloids Surf. B*, 2017, **152**, 18–28.

9 N. Nagahori and S. I. Nishimura, *Biomacromolecules*, 2001, **2**, 22–24.

10 A. Muñoz-Bonilla, O. León, M. L. Cerrada, J. Rodríguez-Hernández, M. Sánchez-Chaves and M. Fernández-García, *J. Polym. Sci. Part A Polym. Chem.*, 2012, **50**, 2565–2577.

11 J. Ishii, M. Chikae, M. Toyoshima, Y. Ukita, Y. Miura and Y. Takamura, *Electrochem. Commun.*, 2011, **13**, 830–833.

12 N. Cakir, G. Hizal and C. R. Becer, *Polym. Chem.*, 2015, **6**, 6623–6631.

Chapter 2

Historical and theoretical background

Chapter 2

Historical and theoretical background

2.1 Dendronized polymers

Polymers have many different types of branching that can influence different structural properties, for instance mechanical strength, crystallinity, viscosity, and solubility. There are various types of branched polymers e.g. comb-like polymers, polymers with long/short chain branching, regular stars, irregular stars, dendrimers and hyperbranched polymers,[1] see Figure 2.1.

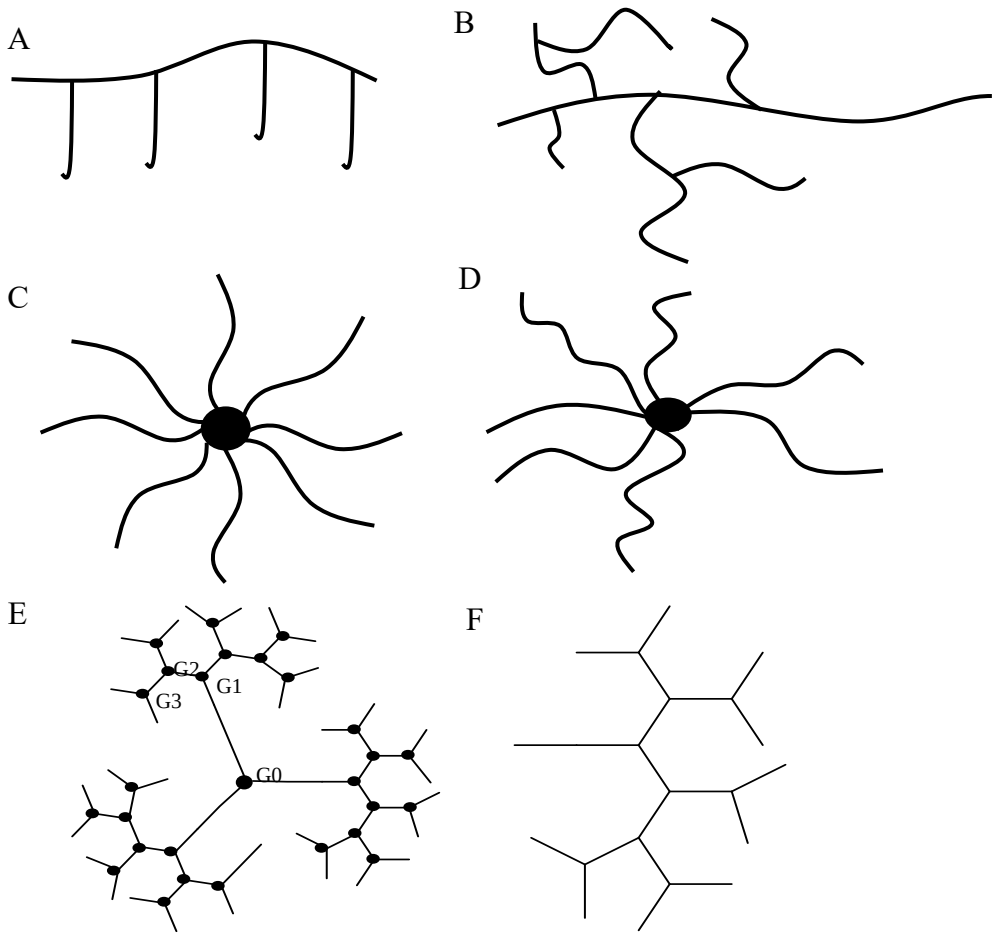

Figure 2.1. Different types of architectures for branched polymers A): comb-like, B): short and long chain branching, C): regular star, D): irregular star, E): dendrimer and F): hyperbranched.

Dendritic polymers are a group of branched polymers that are characterized by a certain sequence

of branching. These polymers contain four sub-domains namely random hyperbranched, dendrigrafts, dendrimers and dendrons.[2] Dendrimers are classified as perfectly branched polymers which are connected to a small core.[1,3] Dendrimers have a "tree-like' structure that is given due to the repetitive branching unit, the end of each branching unit is split into two, and a new unit begins, called the generation number, see Figure 2.1 E.

With the concept of dendrimers, researchers developed dendritic hybrids with attempts to reduce overcrowding. Dendritic hybrids have a high functionality and a well-defined shape with the potential to be used in many biomedical applications such as drug delivery systems (dendrimer-based bionanomaterials).[4,5] Dendritic hybrids are a blend of dendritic and linear chains; this unlocks the potential for many variations of polymer architectures with new molecular properties. With this concept in mind, dendronized polymers (DenPols) containing a linear polymer backbone with dendrons attached were invented (Figure 2.2).[1] There is a wide variety of potential applications for DenPols for instance biomedicine,[6] bioconjugates,[7,8] catalysis,[9] nanocarriers,[10] and antivirals.[11] Dendronization typically occurs by three pathways, namely, grafting to (convergent strategy), grafting from (divergent strategy) and macromonomer strategy.[3,11,12] The DenPols in this study were synthesized by grafting-from strategy, where dendrons are attached to a polymer chain and higher generations are produced from the successive binding of dendrons. The generation number can be defined as the grafted structure, in this case the dendron, on each repeat unit.[13]

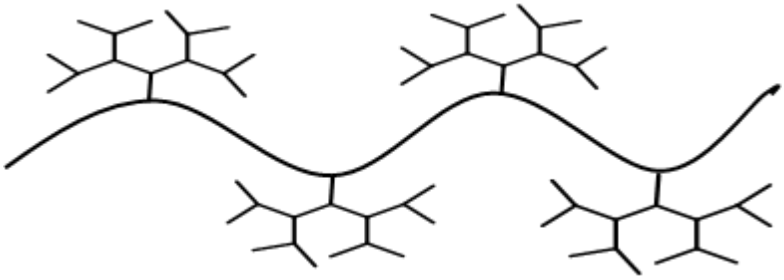

Figure 2.2 Dendronized polymer.

In this study the lysine dendrons are attached to the linear poly(ethylene-*alt*-maleic anhydride) backbone, and the first to the third generation were synthesized, see Figure 1.1.[4] In the case of MI-G0, the synthesis was performed by the protection of the amine group with tert-butoxycarbonyl (Boc), by converting the copolymer to MI-G0-Boc with the addition of *N*-Boc-protected 1,4 diaminobutane. The starting material for the synthesis of the first to the third generation is

poly{ethylene-*alt*-*N*-[-(hydroxycarbonyl-1-yl]-maleimide} (MI-A) and the reaction took place under annealing conditions with the addition of 6-aminohexanoic acid to the copolymer. A protection step was introduced for the amine group. First generation Boc-protected lysine DenPol (MI-G1-Boc) was synthesized by an amidation reaction using a Boc-protected lysine derivative and MI-A. To obtain the second-generation lysine DenPol (MI-G2-Boc), a deprotection step was introduced to remove the Boc protecting group from MI-G1-Boc using trifluoroacetic acid (TFA). The deprotected MI-G0 DenPol was converted to MI-G2-Boc with the addition of a first-generation lysine derivative under amidation conditions. The latter synthesis step was repeated for MI-G3-Boc.The DenPols presented in Figure 1.1 are the DenPols investigated for this study.

With the benefits of multifunctionality and multivalency there are also disadvantages, for instance the toxicity, lack of biocompatibility and insolubility in aqueous media.[14–16] To reduce the limitations of hyperbranched polymers, there are three main modifications to their structures, adding sugar moieties, introducing poly(ethylene glycol) (PEG) and peptide bonds.[17] For this study maltose moieties are introduced to modify the terminal groups by the process of reductive amination in a borate buffer with excess maltose[4], producing MI-G0-MAL, MI-G1-MAL, MI-G1-PEG-MAL, MI-G2-MAL, and MI-G3-MAL with the poly(ethylene-*alt*-maleimide) backbone and lysine dendrons, as well as MI-G1-PEG-MAL with PEG dendrons (Figure 1.1). Malik et al[18] discovered that the endgroups of dendrimers strongly influence the cytotoxicity, which is important for targeted drug delivery.

2.2 Glycopolymers

Glycopolymers can be defined as synthetic macromolecules containing sugar moieties in their structure.[19–21] They have gained a great deal of attention because of their potential to mimic the biological functions of carbohydrates, for example, as a lubricant for joints[19], blood coagulation[19,22] and the delivery of information for biological processes.[17,21,23] In addition, a vast range of biomedical applications like biosensors, medical adhesives and for direct therapeutic methods have been presented.[23] With all these promising applications there has been a drive towards the design and synthesis of glycopolymers with certain architectures and functionalities, hence the synthesis of dendritic glycopolymers. The synthesis route towards the specific design of glycopolymers can be achieved by conventional free radical polymerization, reversible addition-

fragmentation chain transfer polymerization (RAFT) or atom transfer radical polymerization (ATRP).[3,17,24]

Numerous techniques have previously been used to intensively characterize glycopolymer materials with heterogenous distributive properties. The techniques used provided information about the molar mass, conformation, size, and chemical structure of the material. Regarding the conformation/architecture, whether it is a globular, helical, linear random coil or rod-like structure, or aggregates are formed, atomic force microscopy (AFM)[25–27] or transmission electron microscopy (TEM)[26,28–30] were used. However, these techniques only provide information about a section of the material or a solution. Dynamic light scattering (DLS) is used for analyzing the size of the bulk material with changes in the external environment such as temperature and pH.[4,30–33] The disadvantage of DLS is that smaller molecules can easily be overlooked. Regarding the chemical structure, nuclear magnetic resonance spectroscopy (NMR) is often used to confirm the successful synthesis of glycopolymers.[15,29,34–36] To achieve separation and to characterize the molar mass and size distribution of the material, size exclusion chromatography (SEC) and asymmetric flow field-flow fractionation (AF4) in combination with light scattering detectors is used. [29,37–40] An interesting study by Rolland-Sabaté et al.[29] documented the versatility of AF4 coupled to multiangle laser light scattering (MALLS) and differential refractive index detectors (RI) by separating hyperbranched α-glucans with different sucrose concentration and quantified the molar mass distribution, size distribution and dispersity, however, the sample recovery was low.

In the present study, the chemical structure of the different generations of DenPols was characterized with ^{1}H and ^{13}C NMR. However, the broadness of the peaks influenced the sensitivity for determining the fine structure.[4] To track the successive increase in generation number, the amide, methine and N-Boc signals were used. For the maltose-modified compounds the peripheral amino groups of the DenPols were investigated. SEC-MALLS was utilized for the characterization of the molar mass and size distribution of the Boc protected compounds and AF4-MALLS-DLS was used for the glycopolymers in an acetate buffer. Aggregation of DenPols were strongly influenced by pH. The apparent density, scaling law and shape factor (R_g/R_h) were used to clarify the formation of aggregates and the conformation. The conformational analysis was complimented with cryo-TEM and AFM analysis.

The maltose shell has an abundance of H-bond active sites making it a promising material for interactions with proteins to form supramolecular assembles. This study concentrates on the characterization of multivalent interactions of dendronized maleimide copolymers decorated with a maltose shell and human serum albumin (HSA). The interactions between the glycopolymer and the protein can alter the conformation of the glycopolymer leading to a change in the shape, size, and molar mass.

2.3 Interactions between glycopolymers and proteins

Carbohydrate-protein interactions are one of the most essential components for the transfer of information between cells and cell substrates, cell-growth regulation and targeting drugs.[36,41] The binding between protein-saccharides is typically weak but when saccharides are clustered the interactions can be amplified by multivalent interactions.[24,42] The abundance of hydroxyl, amino and sulfo functional groups on pendant saccharides allows for hydrogen bonding and van der Waals interactions.[43,44] The desired interactions with proteins can be manipulated by the shape of the glycopolymers.

Typically linear glycopolymers have a random coil architecture that is useful for multivalent scaffolds and drug carriers.[45–48] Rod-like structures are common for higher generations of DenPols with a high density of dendrons, restricting the flexibility of the chain.[12,49] An interesting example are carbon nanotubes (CNTs) or graphene with a rod-like structure, covered by carbohydrate moieties exhibiting increased water solubility as found by Chen et al.[50] The rod-like structure is favourable for applications in biology for sensing devices and imaging techniques. Additionally, glycodendrimers have globular structures that are important for the complexation and encapsulation of drugs.[3,15,51] Four-arm star shaped block copolymers with a carbohydrate shell have promising applications for specific peptide delivery as they have been postulated to encapsulate peptides.[52] Controlled spindle and cubic-like shapes are important for fields in biology as they can be used as bioactive particles. [31]

Boye et al.[4] showed the strong pH dependency of the conformation, progressing from the 1st to the 3rd generation of lysine dendronized maleimide copolymers covered with maltose shells. DenPols exhibited tunable aggregation behaviour due to the amine group that can be protonated. With this

knowledge on the ability to control the aggregation behaviour and the abundance of H-bond sites, the formation of supramolecular assemblies with cellulose nanocrystals was studied. Majoinen et al.[33] investigated the formation of supramolecular assemblies between lysine dendronized poly(ethylene-*alt*-maleimide) copolymers with a maltose shell and anionic cellulose nanocrystals (CNCs) (rod-like structure) showing that multivalent interactions can be controlled by the generation number. The first and second generation glycopolymers showed distinct phase separation, attributed to the coil-like conformation whereas the third generation showed colloidal stability with a worm-like conformation (Figure 2.3). Third generation glycopolymers wrapped loosely around the CNC rod. The proposed multivalent interactions were (1) hydrogen bonds of the glucose units of the CNCs and the maltose moieties and (2) electrostatic interactions. With an increase in the sugar moieties the tertiary amines are sterically hindered. This study was motivated by the multivalent interactions between CNCs and glycopolymers. The interaction characteristics of DenPols with human serum albumin (HSA) will be investigated.

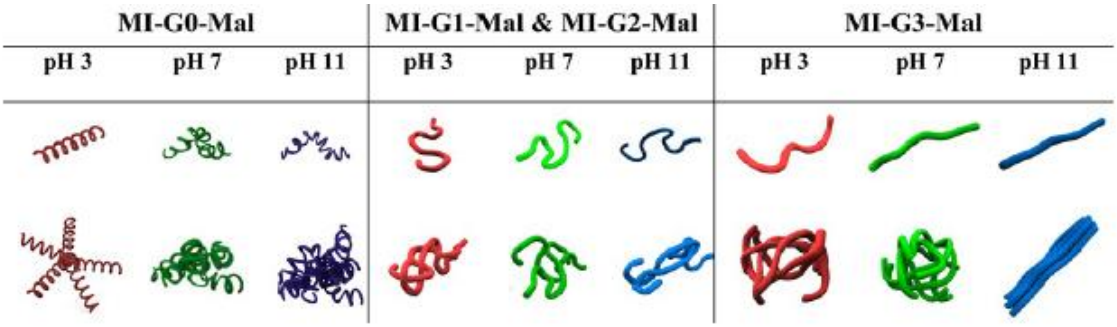

Figure 2.3. Schematic representation of the glycopolymer conformation of MI-G0-MAL - MI-G3-MAL in different pH environments.[4]

A conducive understanding of the interactions between HSA (model protein) and hyperbranched architectures is important for biomedical, pharmaceutical, drug delivery vectors and therapeutic applications.[15,53–55] Dendrimers with a poly(amidoamine) (PAMAM) core and amine endgroups binding with HSA were investigated under physiological conditions by Tian et al.[55] The authors concluded that certain sites of the HSA structure formed different interactions with the dendrimers, namely, electrostatic interactions, hydrogen bonding and hydrophobic interactions. Klajnert et al.[15] evaluated the interactions between HSA and maltose-modified poly(propylene imine) (PPI) dendrimers as a balance between the toxicity of dendrimers and the potential biomedical applications is important. The protein-dendrimer interactions were evaluated by fluorescence spectroscopy and an increase in the strength of the interactions for the fourth and fifth generation

dendrimers with HSA was observed. The enhanced interactions were attributed to a suitable spherical shape and rigid structure of the dendrimer (interaction is generation dependent) in addition to electrostatic interactions between anionic HSA and cationic dendrimer and as well as hydrogen bonding. Worbel et al[14] evaluated the interactions between maltose-modified poly(ethylene imines) (PEIs) dendrimers and HSA. The authors discovered that size and available H-bond active sites of the core are crucial for protein-nanoparticle interactions. However, all these studies focused on the conformational changes of HSA and not the conformational changes of the glycopolymers.

HSA is the most abundant protein in human plasma and is synthesized in the liver (Figure 2.4).[53] HSA plays a role in regulating the transport of hormones, fatty acids and molecules through the blood vascular system. [53–55] The molecular weight of HSA is 66.5 kg/mol.[53,56] Under physiological conditions, HSA carries a negative charge that introduces the possibility of electrostatic interactions.[57] The interaction mechanism of HSA with pharmacological drugs is important for improving the delivery and biocompatibility of the drugs.[53] The present study will provide insight on whether the DenPol-HSA interactions can be enhanced depending on the generation number by using advanced analytical techniques.

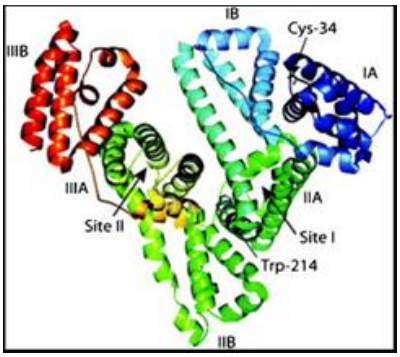

Figure 2.4. The crystal structure of HSA is composed of 585 amino acids with 17 disulfide chains and the major binding sites. [58]

This study focuses on first investigating the individual components of glycopolymers and HSA, followed by the interactions between lysine dendronized polymers and HSA. Analytical techniques have previously been used to characterize protein-carbohydrate interactions, for instance quartz crystal microbalance (QCM), differential pulse voltametry, fluorescence spectroscopy, turbidimetry, mass spectroscopy, DLS, NMR and circular dichromism (CD) and ultraviolet (UV-vis) spectroscopy.[32,41,44,59,60] The techniques only provided information about

single properties regarding size, conformation, endgroup functionalities or chemical structure of the materials.

The present study investigates the molar mass, size distribution and dispersity of the DenPols interacting with HSA by utilizing AF4-MALLS-DLS. In addition, the measured parameters can further be used to enhance our understanding of the mixtures, the apparent density (see Equation 27) to assess the presence of non-aggregated or aggregated structures in the sample, scaling law to construct a conformation plot (see equation 29) and shape factor (R_g/R_h), for the shape of the complexes formed. This is crucial for our study as it provides evidence of aggregated structures of the individual DenPols and the complexes of DenPols and HSA. A study by Boye et al[61] showed the dynamic use of AF4-MALLS-DLS-UV to track the complexation of Rose Bengal and hyperbranched poly(ethylene imine) coated with a maltose shell. Interestingly, the membrane cut-off of 5000 g/mol was larger than the molecules of Rose Bengal and thus the focusing step was used as an ultrafiltration step to remove the free dye. The amount of Rose Bengal removed was quantified and thus the amount of Rose-Bengal forming complexes was identified.

2.4 Background on analytical techniques

In depth knowledge of the different molecular heterogeneities such as chemical composition, molar mass, functionality and molecular architecture is important as it affects the properties of materials; this is achieved by using advanced separation techniques.[62,63] In order to comprehensively characterize the molar mass distribution and dispersity of poly(ethylene-*alt*-maleic anhydride), Boc-protected DenPols and glycopolymers, advanced analytical techniques will be applied.

2.4.1 Size exclusion chromatography (SEC)

SEC also referred to as Gel Permeation Chromatography (GPC) is a widely used technique for polymer analysis due to its simplicity, versatility, and vigorous measurement speed. SEC is based on the separation according to size or hydrodynamic volume of the macromolecules in a multi-porous packed column. Generally, the elution order is that larger macromolecules elute first followed by smaller macromolecules (Figure 2.5). Fractions of the analytes elute into detectors

which are coupled to the column. Possible concentration detectors are refractive index (RI) or ultraviolet (UV) and light scattering for the determination of absolute weight-average molar mass (M_w), number-average molar mass (M_n) and radius of gyration (R_g).

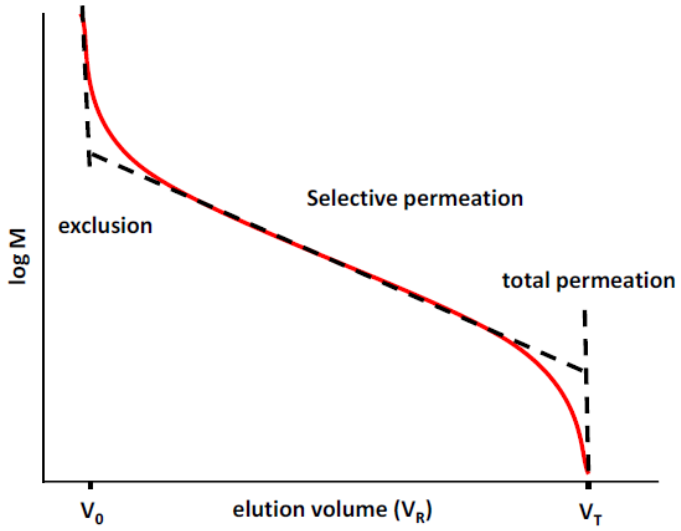

Figure 2.5. Schematic representation of the elution order of SEC. [64]

The concept of size exclusion is that the SEC column contains particles with pores of different sizes that are accessible to macromolecules of various sizes. Macromolecules should have sufficient time to diffuse into the pores and back into the mobile phase of the column. The elution volume of the polymer chains can be conveyed by:

$$V_e = V_0 + K_d V_i \quad (1)$$

where V_0 is the total volume of solvent outside of the pores, V_i is the total volume of the solvent inside the pores and K_d is the distribution coefficient. The distribution coefficient is equivalent to the ratio between the concentration of the analyte in the stationary phase and the carrier liquid. K_d is typically between 0 and 1 under ideal separation conditions, when no adsorptive interactions are taking place. The total volume, V_l, of the mobile phase, inside and outside of the pores, is expressed by:

$$V_l = V_0 + V_i \quad (2)$$

The limit of total exclusion occurs when $K_d = 0$ showing the elution of macromolecules with the void volume V_0. When macromolecules are too large to penetrate the pores of the stationary phase

the total limit of exclusion is attained. The limit of exclusion is attained when there is no retention of macromolecules in the column and the molecules elute with the void peak.

On the other hand, when small molecules can perforate all the pores in the stationary phase with equal probability the limit of total permeation is attained. The molecules will elute with the solvent peak and is referred to as the total solvent volume V_l of the column. This can be expressed by:

$V_e = V_0$ for $K_d = 0$ and (3)

$V_e = V_l$ for $K_d = 1$ (4)

To obtain a polymer peak that is well resolved, the distribution coefficient should be $0 \leq K_d \leq 1$. The elution of polymer molecules should not take place in either the exclusion or permeation limits. The column set chosen should exhibit a wide molar mass range to ensure the polymer peak is well resolved.

SEC-MALLS is a suitable analysis tool for the characterization of the molar mass distribution of the poly(ethylene-*alt*-maleic anhydride) and Boc-protected MI-G0 – MI-G1 (Figure 1.1 A and D). However, with the modification of the DenPols with maltose shells, the molar mass and branching density drastically increases. The analysis of branched ultrahigh molar mass macromolecules is challenging to analyse using SEC-MALLS, as it leads to strong interactions with the stationary phase. The strong shear forces can easily destroy a cluster of single macromolecules or complexes formed and it is not suitable for ultrahigh molar mass (beyond 10^6 g/mol) analytes. Since the goal of the study is to investigate the DenPols and the interactions between different generations of DenPols and HSA, the strong shear forces would destroy any structures formed by weak electrostatic interactions or hydrogen bonds with HSA, [65–68] making SEC unsuitable. Alternative separation methods are required to overcome the limitations of SEC. Field-Flow Fractionation (FFF) is an advanced analytical technique that will be discussed in the next section.

2.4.2 Field-Flow Fractionation

FFF is a family of analytical techniques developed for the separation and characterization of macromolecules, viruses, bacteria, and cells.[29,61,69] Initially, the dominant technique in the field of separation of polymers was SEC, but over the years there has been an increase in the application

of FFF. Invented by J. C. Giddings in 1966, separation in FFF is achieved by applying an externally generated field perpendicular to the ribbon-like channel leading to the distribution of solutes.[69,70] There are different fields that can be applied to achieve separation in FFF, namely, thermal, flow, electrical, centrifugal or sedimentation.[69,70] AF4 and thermal field-flow fractionation (ThFFF) are the most widely used FFF techniques. In AF4, separation is due to differences in the normal diffusion coefficient (*D*) whereas in ThFFF the separation is based on the thermal diffusivity (D_T) and the normal diffusion coefficient (*D*) of the sample.

2.4.2.1 Basic principles of asymmetric flow field-flow fractionation

The separation of an analyte takes places in a channel consisting of an upper impermeable plate and a bottom plate that is permeable to the eluent molecules and impermeable to the polymer molecules. The bottom plate is composed of a semi-permeable membrane with a molecular weight cut-off (MWCO) in the realm of 5-30 kg/mol, placed above a porous frit (Figure 2.6). To reduce the possibility of interactions with the membrane a suitable membrane material is chosen such as regenerated cellulose (RC), cellulose triacetate, poly(ether sulfone) (PES) or polycarbonate (PC).[71] A spacer with a specific thickness (127-508 µm) is clamped between the two plates and is composed of different materials namely Teflon, Mylar or polyimide.

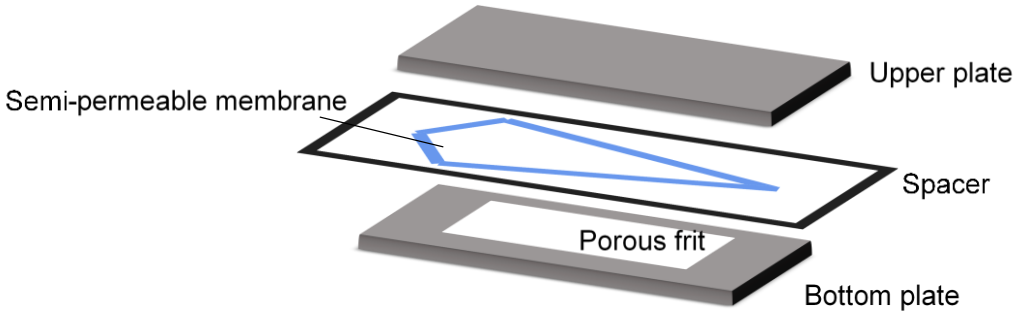

Figure 2.6. Sketch of the AF4 channel.

A field force is applied perpendicular to the channel, molecules experience a change in velocity which is *U*, a field induced flux. U_c is generated as a response of the motion of the molecules towards the accumulation wall in the negative x-direction. There is a build-up of molecules at the accumulation wall that is counteracted by diffusion forces. The counteracting motion of diffusion leads to the motion of the molecules away from the accumulation wall, in the positive x-direction,

called the net flux J_x. The diffusion coefficient D separates the components into fractions and is concentration dependent (Figure 2.7).

$$J_x = U_c - D\frac{dc}{dx} \quad (5)$$

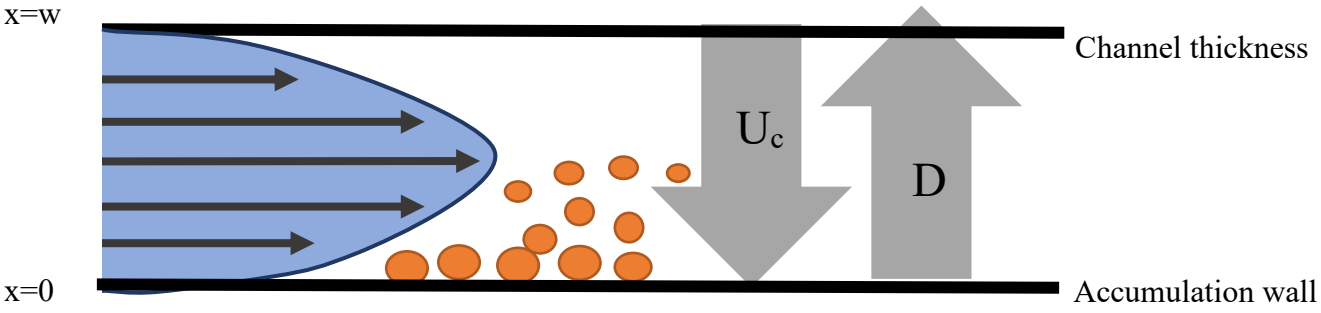

Figure 2.7. Schematic representation of the induced field U_c applied perpendicular to the channel flow and the diffusion coefficient D of the particles.

A steady state condition of the concentrated particles across the channel thickness is established when U and D are in equilibrium and the net flux $J = 0$ can be written as

$$U_c = D\frac{dc}{dx} \quad (6)$$

Upon integration and substitution of equation (6), with the assumption that U and D remain constant, the concentration profile given by:

$$c(x) = c_0 e^{(-|U|/D)x} \quad (7)$$

where c_0 is the solute concentration at the accumulation wall and x is the distance of the solute from the accumulation wall. There is the development of a concentration profile, which decreases exponentially as molecules move further from the accumulation wall. The mean layer thickness is the average distance from the accumulation wall to the centre of the sample component and can be written as

$$l = \frac{D}{|U|} \quad (8)$$

The retention parameter λ when the solute interacts with the field is expressed by

$$\lambda = \frac{l}{w} = \frac{D}{|U|w} \quad (9)$$

where the width of the channel is represented by *w*. Equation (9) shows the dependence of retention parameter on the diffusion coefficient of the sample. Each individual component in the channel has a specific retention parameter value λ.

The concentration profile generated in the channel can be written as

$$c(x) = c_0 e^{\left(\frac{-x}{l}\right)} = c_0 e^{\left(\frac{-x}{\lambda w}\right)} \tag{10}$$

The frictional drag *f* can be related to the diffusion coefficient *D* and the field induced by the force *U* which is given by

$$D = \frac{kT}{f} \qquad \text{and} \tag{11}$$

$$U = \frac{F}{f} \tag{12}$$

The following parameters k, T and F are the Boltzmann constant, temperature, and applied force. To represent an expression for the retention parameter for a general FFF system the parameters need to substituted leads to

$$\lambda = \frac{l}{w} = D = \frac{kT}{Fw} \tag{13}$$

The retention ratio, describes the retention of molecules with a specific diffusion coefficient, in comparison to molecules that are unretained by the applied force under the given experimental conditions expressed by

$$R = \frac{v}{\langle v \rangle} \tag{14}$$

where *v* is the migration velocity of the prescribed molecules and $\langle v \rangle$ is the average fluid velocity, respectively. In Equation (14), the migration velocity represents the mean particle velocities which can also be written as $v = \frac{\langle cv \rangle}{\langle c \rangle}$.[72] The retention ratio can be expressed solely by a dimensionless parameter

$$R = 6\lambda\left(coth\frac{1}{2\lambda} - 2\lambda\right) \tag{15}$$

Additionally, the retention ratio can be expressed by void time of the unretained component, t_0, and t_R, the mean residence time of the retained component, is expressed by

$$R = \frac{t_0}{t_R} \tag{16}$$

When λ approaches zero then R can be approximated to $R \sim 6\lambda$, with this approximation there is an inherent error of 20 % when R=0.25.[73] Thus t_R can be represented as a function of t_0 and λ.

$$t_R = \frac{t_0}{6\lambda} = \frac{|F|wt_0}{6kT} \; for \; \lambda <<< 1 \tag{17}$$

The theory represented explains the fractionation of an FFF technique when an external field is applied to a sample and the response of the sample to the applied force. Each sub-technique has a unique retention parameter and field force F. The field force for normal AF4 is given by

$$F = f|U| = \frac{kT|U|}{D} = 3\pi\eta|U|d \tag{18}$$

The components of the equation are η the viscosity of the mobile phase, d the diameter of the particle, D which is the diffusion coefficient and U which is the field induced velocity.

Regarding AF4 specifically, the flow velocity U is related to the cross flow as it is the ratio of the cross flow V_c and the area of the accumulation wall A_{aw}. Furthermore, the ratio between the volume of the channel V_0 and the channel thickness w is equal to A_{aw}. Substituting the parameters into the equation $\lambda = D/Uw$ results in the expression for the retention parameter for AF4 which is given by

$$\lambda = \frac{DV_0}{V_c w^2} \tag{19}$$

The parameters in the equation are V_0 which is the void volume, V_c is the cross flow and w is the channel thickness. Equation (19) shows that the normal mode of separation is dependent on the size. The t_r is related to $t_0/6\lambda$ which result in the equation of t_r which can be equated to

$$t_r = \frac{w^2 V_c}{6DV_{out}} \tag{20}$$

where the flow rate of the channel V_{out} is equal to V_c/t_0. This explains symmetrical FFF but with AF4 the cross flow at the non-permeable wall is negligible. Thus, the retention time (t_r) can be explained with a logarithmic function of V_{out} and V_c which is shown by

$$t_r = \frac{w^2}{6D} \ln\left(1 + \frac{V_c}{V_{out}}\right) \tag{21}$$

In this study AF4 fractionation will be used as the fractionation technique in combination with light scattering and concentration detectors (Figure 2.8).

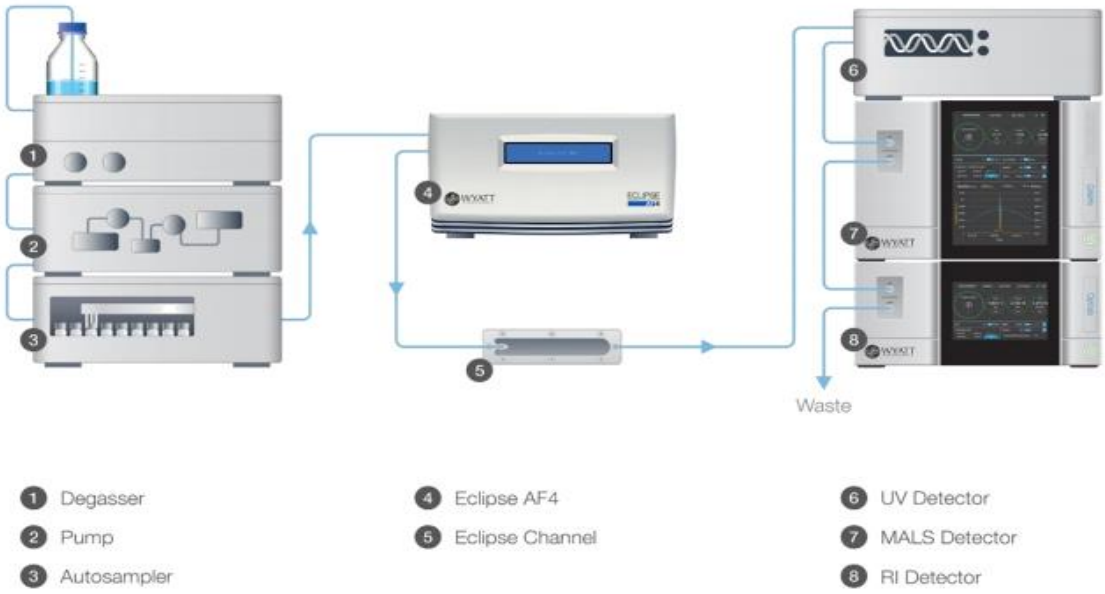

Figure 2.8. Schematic representation of the AF4 set up in Dresden, Germany. The DLS is embedded in the MALLS detector. (obtained from Wyatt manufacturer).

The high aspect ratio of the channel generates a parabolic flow profile with the channel flow. The cross flow is applied perpendicular to the channel moving the analyte towards the accumulation wall. The first step is the injection step, where a known volume of sample enters through the inlet of the channel. Depending on the diffusion coefficient of the macromolecules they will align in different flow streams of the parabolic flow profile. When the sample is injected into the channel the macromolecules all disperse. To ensure that the macromolecules are concentrated and constrained in a narrow zone, a focusing step is applied with the active cross flow (Figure 2.9 B).

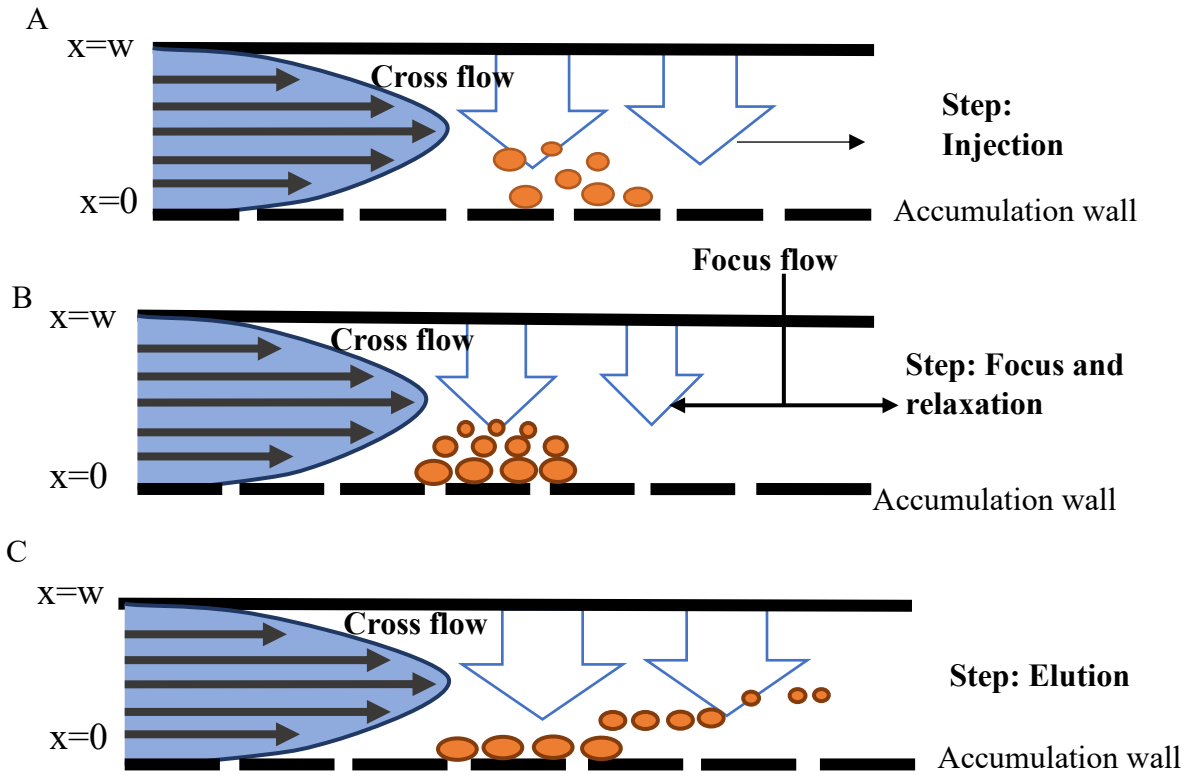

Figure 2.9. Schematic representation of the different steps of the AF4 technique. (A) The eluent is injected into the channel, (B) the focus/relaxation step and (C) the elution step with normal mode.

The focus flow is a flow applied in the opposing direction of the longitudinal flow to ensure that the macromolecules form a narrow band to minimize band broadening. Once the focusing time elapses, the focus flow stops, and the macromolecules will elute in their respective flow streams towards the detectors. If separation is solely based on the normal diffusion coefficient (Brownian motion) it is called normal elution mode. Small particles move faster, elute first, and therefore are in flow streams further from the accumulation wall whereas larger particles are closer to the accumulation wall.[69,74] The cross flow profile can be adjusted systematically to retain molecules of a particular size (Figure 2.9 C).

The different operating modes of AF4 are normal, steric and hyper-layer mode, and are based on separation characteristics such as selectivity and resolution.[69] Steric mode encompasses macromolecules with a diameter greater than 1µm. Due to the large size of the particles, Brownian motion is too weak to counter the cross flow. The diffusion becomes negligible and larger particles form a thin layer close to the accumulation wall. Smaller particles remain close to the accumulation

wall in the slower flow streams and larger particles protrude out of the thin layer to faster flow streams. The elution mode is dependent on the physical barrier of the accumulation wall called the 'steric'. Therefore, larger particles elute first, followed by smaller particles.[69,74] Hyper-layer mode has the same elution sequence as steric mode, therefore, it is difficult to differentiate between the two modes. Large macromolecules have insufficient contact time with the accumulation wall and instead are influenced by an opposed force that moves particles away from the accumulation wall towards faster flow streams. When these particles have moved a length larger than their diameter from the accumulation wall it is called hyperlayer.[75]

The gentle separation mechanism and the advantage of separating ultrahigh molar mass analytes makes AF4-MALLS-DLS ideal for the comprehensive characterization of MI-G0, MI-G0-MAL, MI-G1-MAL, MI-G1-PEG-MAL, MI-G2-MAL and MI-G3-MAL, as well as HSA. The interaction between the DenPols and HSA can also be characterized as there are minimized shear forces for the destruction of aggregates that are not stable. The separation method needs to be applied to fractionate the polymer into smaller homogenous fractions, to be used to calculate the apparent density, shape factor and scaling law.

2.5 Detectors

Detectors are required to convert the physical or chemical properties to a measurable response. The detectors used in this study are the refractive index (RI), multiangle laser light scattering (MALLS) and dynamic light scattering (DLS) detectors. The type of detector is dependent on the nature of the sample and the desired information.

2.5.1 Refractive index detector

The differential refractive index (RI) detector is a universal concentration sensitive detector. The detector measures the difference between the refractive index of the solvent and refractive index response of the analyte. An important parameter is the specific refractive index increment (dn/dc) as it is needed in combination with light scattering detectors to calculate the absolute molar mass of the polymer.[76,77]

2.5.2 Dynamic light scattering (DLS)

DLS also known as photon correlation spectroscopy (PCS) or quasi-elastic scattering (QELS) is a well-established technique. DLS measures the hydrodynamic size and size distribution of particles which are dissolved or dispersed in a solvent.[78,79] The advantage of DLS is that it is non-invasive and only small amounts of sample are required.[78,79] While dispersed or dissolved in a solvent, particles undergo Brownian motion and the diffusion coefficients (D_τ) of the particles or macromolecules are measured. Small particles diffuse at higher speeds resulting in faster fluctuations and thus a faster rate of the correlation function, whereas larger particles and aggregates diffuse slower and have slower fluctuations.[78,80] The technique determines the fluctuations by a mathematical process called the autocorrelation function which analyses the correlation of the fluctuation of light intensity over time. The normalized autocorrelation function for a monodispersed polymer is given by

$$g(\tau) = e^{-Dq^2r} \tag{22}$$

where *D* is the mutual diffusion coefficient, τ is the delay time and q is the scattering vector which is represented by

$$q = \frac{4\pi n_0}{\lambda} \sin\left(\frac{\theta}{2}\right) \tag{23}$$

The components in the equation are λ which is the incident light wavelength in a vacuum, n_0 which is the refractive index of the solvent and θ which is the scattering angle. Equation (23) holds true for solutions with small monodisperse particles. Larger particles move slowly and have a small diffusion coefficient. The relationship between the speed of a particle and the particle size can be expressed by the Stokes-Einstein equation as follows

$$D = \frac{k_B T}{6\pi\eta R_H} \tag{24}$$

where k_B is Boltzmann constant, T is the temperature, η is the viscosity of the solvent and R_H is the hydrodynamic radius.[78] There are two distribution methods, namely cumulant analysis method and non-negative least squares (NNLS). Cumulant analysis method is used for monomodal

distributions where no prior information is required, and the average values of the diffusion coefficient is provided. The NNLS method is used for non-monomodal distributions.[78]

2.5.3 Multiangle laser light scattering (MALLS)

MALLS measures the absolute molar mass and distribution of polymers after the elution from SEC or FFF systems as well as with direct injection into the detector. The data obtained from light scattering detectors can be fitted to different models, the most utilized models are the Zimm, Debye and Berry models.[81] The models mentioned allow for the determination of the root mean square radius (r_{rms}), also called the radius of gyration (R_g). The r_{rms} is determined from the slope of a curve, which is based on the angular dependence of the intensity of scattered light.

A MALLS detector measures the light from polymers or particles in a sample from an array of scattering angles in comparison to the initial entering light. MALLS detectors have a different number of observing angles per detector and each angle is different to the other. Figure 2.10 shows a schematic representation of a 18-angle MALLS detector.

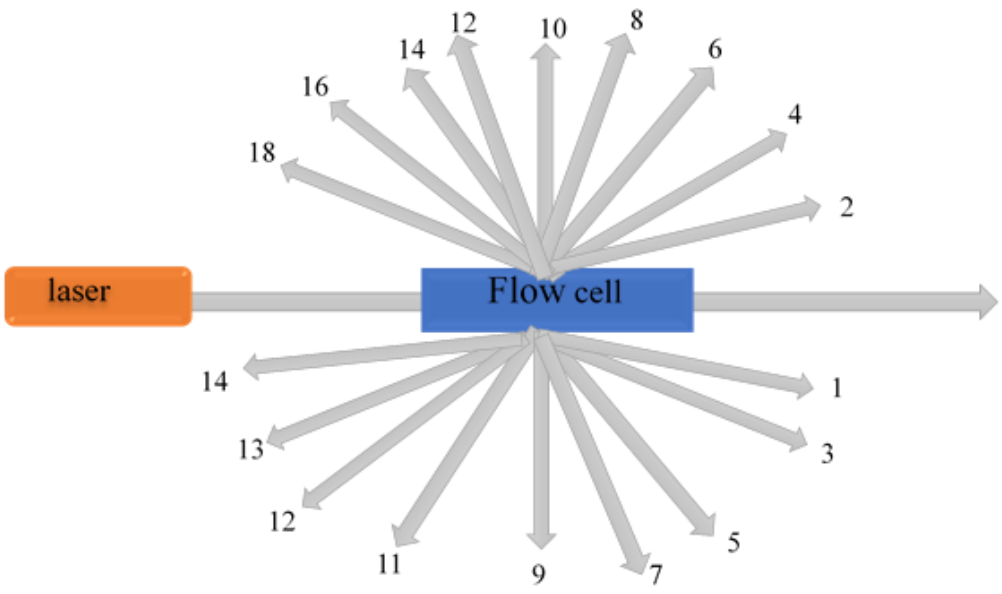

Figure 2.10. Schematic representation of an 18-angle MALLS detector.

The most common is the Debye equation and it is given by

$$\frac{R_\theta}{K^*} = MP(\theta) - 2A_2cM^2P^2(\theta) \quad (25)$$

where R_θ, K^*, c, M, $P(\theta)$ and A_2 are the Rayleigh ratio, an optical constant, concentration of the sample in solution, molar mass and the particle scattering factor and the second virial coefficient. The optical constant is described by

$$K^* = \frac{4\pi^2 n_0^2}{\lambda_0^4 N_A} \times \left(\frac{dn}{dc}\right)^2 \quad (26)$$

where n_0 is the refractive index of the solvent, , λ_0 is the wavelength of the incident light, N_A is Avogadro's number and the dn/dc is the specific refractive index increment.[75,82] Plotting $\frac{R_\theta}{K^*}$ vs. $sin^2(\frac{\theta}{2})$ provides insightful information about the molar mass and R_g. The molar mass can be determined from the intercept of the extrapolated plot to the zero angle ($\theta = 0$) whereas the slope of the plot is associated to the R_g.

2.6 Conformation parameters

The coupling of AF4 with MALLS, DLS and RI detectors allows for the measurements of several macromolecular conformation parameters. The apparent density parameter provides structural information regarding the physical parameters determined from AF4-MALLS. Apparent density is a parameter used to distinguish the aggregated structures from the non-aggregated structures in a material.[83] The formation of aggregated structures from non-aggregated structures is visualised by a reduction in the apparent density with an increase in molar mass.[84] The expression for the apparent density calculation using the molar mass and R_g is expressed by:

$$\rho_{rms,i} = \frac{M_w}{V\,(R)_i N_A}.\alpha \quad (27)$$

where V is the volume of a hard sphere with a radius, r, N_A is Avogadro's number and α can be expressed as

$$\alpha = \frac{V_{sphere}\,(R)}{V_{sphere}\,(r)} = \frac{R^3}{r^3} = \frac{(\frac{\sqrt{3}}{5}x\,r)^3}{r^3} = (\frac{3}{5})^{\frac{3}{2}} \quad (28)$$

The apparent density expression describes the mass in a certain volume of a hard sphere. Therefore, α is introduced as a correction parameter for R_g that is used for the calculations.

To provide clarity of the shape of the non-aggregated and aggregated species, the scaling law can be implemented. The scaling law provides vital information about the shape of macromolecular objects and can be expressed by:

$$R_g = kM^{\upsilon} \tag{29}$$

where k is the constant obtained from the y-intercept for a specific polymer in the solvent and temperature, M is the molar mass and ν is the scaling factor. The slope of the plot log (R_g) vs log (M) is the scaling factor parameter. The scaling factor is representative of different structures, 0.33 is typical for a sphere, 0.5-0.6 for a random coil macromolecule and values approaching 1 for rods.

When AF4 or SEC are coupled to concentration and light scattering detectors, information about the molar mass, radius and their distributions can be acquired. These powerful analytical tools will be used to investigate the DenPols, HSA and the DenPol-HSA mixtures.

2.7 References

1 A. Lederer and W. Burchard, in *Hyperbranched Polymers Macromolecules in between Deterministic Linear Chains and Dendrimer Structures*, ed. B. Z. Tang, A. S. Abd-El-Aziz, S. Craig, J. Dong, T. Masuda, C. Weber, the Royal Society of Chemistry, Cambridge, 16th ed., 2015, vol. 1, ch. 5, 88-132.

2 D. A. Tomalia and J. M. J. Fréchet, *J. Polym. Sci. Part A Polym. Chem.*, 2002, **40**, 2719–2728.

3 A. Zhang, L. Shu, Z. Bo and A. D. Schlüter, *Macromol. Chem. Phys.*, 2003, **204**, 328–339.

4 S. Boye, D. Appelhans, V. Boyko, S. Zschoche, H. Komber, P. Friedel, P. Formanek, A. Janke, B. I. Voit and A. Lederer, *Biomacromolecules*, 2012, **13**, 4222–4235.

5 D. Appelhans, B. Klajnert-Maculewicz, A. Janaszewska, J. Lazniewska and B. Voit, *Chem. Soc. Rev.*, 2015, **44**, 3968–3996.

6 X. Liu, W. Lin, D. Astruc and H. Gu, *Prog. Polym. Sci.*, 2019, **96**, 43–105.

7 G. G. Kochendoerfer, S. Y. Chen, F. Mao, S. Cressman, S. Traviglia, H. Shao, C. L. Hunter, D. W. Low, E. N. Cagle, M. Carnevali, V. Gueriguian, P. J. Keogh, H. Porter, S. M. Stratton, M. Con Wiedeke, J. Wilken, J. Tang, J. J. Levy, L. P. Miranda, M. M. Crnogorac, S. Kalbag, P. Botti, J. Schindler-Horvat, L. Savatski, J. W. Adamson, A. Kung, S. B. H. Kent and J. A. Bradburne, *Science (80)*, 2003, **299**, 884–887.

8 G. Fuhrmann, A. Grotzky, R. Lukić, S. Matoori, P. Luciani, H. Yu, B. Zhang, P. Walde, A. D. Schlüter, M. A. Gauthier and J. C. Leroux, *Nat. Chem.*, 2013, **5**, 582–589.

9 Y. Y. Huang, X. Yang, Y. Feng, F. Verpoort and Q. H. Fan, *J. Mol. Catal. A Chem.*, 2014, **393**, 150–155.

10 M. Kumari, S. Gupta, K. Achazi, C. Böttcher, J. Khandare, S. K. Sharma and R. Haag, *Macromol. Rapid Commun.*, 2015, **36**, 254–261.

11 J. Yan, W. Li and A. Zhang, *Chem. Commun.*, 2014, **50**, 12221–12233.

12 J. I. Paez, M. Martinelli, V. Brunetti and M. C. Strumia, *Polymers (Basel).*, 2012, **4**, 355–395.

13 S. Costanzo, L. F. Scherz, T. Schweizer, M. Kröger, G. Floudas, A. Dieter Schlüter and D. Vlassopoulos, *Macromolecules*, 2016, **49**, 7054–7068.

14 D. Wrobel, M. Marcinkowska, A. Janaszewska, D. Appelhans, B. Voit, B. Klajnert-Maculewicz, M. Bryszewska, M. Štofik, R. Herma, P. Duchnowicz and J. Maly, *Colloids Surf. B*, 2017, **152**, 18–28.

15 B. Klajnert, D. Appelhans, H. Komber, N. Morgner, S. Schwarz, S. Richter, B. Brutschy, M. Ionov, A. K. Tonkikh, M. Bryszewska and B. Voit, *Chem. - A Eur. J.*, 2008, **14**, 7030–7041.

16 G. Yilmaz, E. Guler, C. Geyik, B. Demir, M. Ozkan, D. O. Demirkol, S. Ozcelik, S. Timur and C. Remzi Becer, *Mol. Syst. Des. Eng*, 2018, **3**, 150.

17 S. G. Spain, M. I. Gibson and N. R. Cameron, *J. Polym. Sci. Part A Polym. Chem.*, 2007, **45**, 2059–2072.

18 N. Malik, R. Wiwattanapatapee, R. Klopsch, K. Lorenz, H. Frey, J. W. Weener, E. W. Meijer, W. Paulus and R. Duncan, *J. Control. Release*, 2000, **65**, 133–148.

19 V. Ladmiral, E. Melia and D. M. Haddleton, *Eur. Polym. J.*, 2004, **40**, 431–449.

20 K. Babiuch and M. H. Stenzel, in *Encyclopedia of Polymer Science and Technology*, John Wiley & Sons Inc., USA, 1st edn, 2002, vol. 1, ch. 1, pp. 1–58.

21 B. Voit and D. Appelhans, *Macromol. Chem. Phys.*, 2010, **211**, 727–735.

22 J. J. Barchi, *J. Nat. Prod.*, 2004, **67**, 1956–1957.

23 I. Pramudya and H. Chung, *Biomater. Sci.*, 2019, **7**, 4848–4872.

24 Y. Miura, *Polym. J.*, 2012, **44**, 679–689.

25 A. N. Round, M. Berry, T. J. McMaster, A. P. Corfield and M. J. Miles, *J. Struct. Biol.*, 2004, **145**, 246–253.

26 M. Toyoshima, T. Oura, T. Fukuda, E. Matsumoto and Y. Miura, *Polym. J.*, 2010, **42**, 172–178.

27 P. Laurino, R. Kikkeri, N. Azzouz and P. H. Seeberger, *Nano Lett.*, 2011, **11**, 73–78.

28 H. Schlaad, L. You, R. Sigel, B. Smarsly, M. Heydenreich, A. Mantion and A. Maić, *Chem. Commun.*, 2009, 1478–1480.

29 A. Rolland-Sabaté, S. Guilois, F. Grimaud, C. Lancelon-Pin, X. Roussel, S. Laguerre, A. Viksø-Nielsen, J.-L. Putaux, C. D'Hulst, G. Potocki-Véronèse and A. Buléon, *Anal. Bioanal. Chem.*, 2014, **406**, 1607–1618.

30 S. Muthukrishnan, M. Zhang, M. Burkhardt, M. Drechsler, H. Mori and A. H. E. Müller, *Macromolecules*, 2005, **38**, 7926–7934.

31 X. Li, M. Bao, Y. Weng, K. Yang, W. Zhang and G. Chen, *J. Mater. Chem. B*, 2014, **2**, 5569–5575.

32 A. Muñoz-Bonilla, O. León, M. L. Cerrada, J. Rodríguez-Hernández, M. Sánchez-Chaves and M. Fernández-García, *J. Polym. Sci. Part A Polym. Chem.*, 2012, **50**, 2565–2577.

33 J. Majoinen, J. S. Haataja, D. Appelhans, A. Lederer, A. Olszewska, J. Seitsonen, V. Aseyev, E. Kontturi, H. Rosilo, O. Monika, N. Houbenov and O. Ikkala, *J. Am. Chem. Soc.*, 2014, **136**, 8–11.

34 J. Madeira Do O, F. Mastrotto, N. Francini, S. Allen, C. F. Van Der Walle, S. Stolnik and G. Mantovani, *J. Mater. Chem. B*, 2018, **6**, 1044–1054.

35 Y. M. Chabre, C. Contino-Pépin, V. Placide, C. S. Tze and R. Roy, *J. Org. Chem.*, 2008, **73**, 5602–5605.

36 D. Appelhans, B. Klajnert-Maculewicz, A. Janaszewska, J. Lazniewska and B. Voit, *Chem.*

Soc. Rev., 2015, **44**, 3968–3996.

37 N. R. Cameron, S. G. Spain, J. A. Kingham, S. Weck, L. Albertin, C. A. Barker, G. Battaglia, T. Smart and A. Blanazs, *Faraday Discuss.*, 2008, **139**, 359–368.

38 P. Besenius, S. Slavin, F. Vilela and D. C. Sherrington, *React. Funct. Polym.*, 2008, **68**, 1524–1533.

39 A. Hkansson, M. Ulmius and L. Nilsson, *Carbohydr. Polym.*, 2012, **87**, 518–523.

40 E. Chiaramonte, L. Rhazi, T. Aussenac and D. R. White, *J. Cereal Sci.*, 2012, **56**, 457–463.

41 N. Nagahori and S. I. Nishimura, *Biomacromolecules*, 2001, **2**, 22–24.

42 Y. M. Chabr and R. Roy, *Chem. Soc. Rev.*, 2013, **42**, 4657–4708.

43 Y. Miura, *J. Polym. Sci. Part A Polym. Chem.*, 2007, **45**, 5031–5036.

44 J. Majoinen, J. S. Haataja, D. Appelhans, A. Lederer, A. Olszewska, J. Seitsonen, V. Aseyev, E. Kontturi, H. Rosilo, M. Österberg, N. Houbenov and O. Ikkala, *J. Am. Chem. Soc.*, 2014, **136**, 866–869.

45 B. D. Polizzotti and K. L. Kiick, *Biomacromolecules*, 2006, **7**, 483–490.

46 Z. Ma and X. X. Zhu, *J. Mater. Chem. B*, 2019, **7**, 1361–1378.

47 N. E. Davis, L. S. Karfeld-Sulzer, S. Ding and A. E. Barron, *Biomacromolecules*, 2009, **10**, 1125–1134.

48 A. D. Schlüter and J. P. Rabe, *Angew. Chemie (International Ed. English)*, 2000, **39**, 864–883.

49 A. D. Schlüter, A. Halperin, M. Kröger, D. Vlassopoulos, G. Wegner and B. Zhang, *ACS Macro Lett.*, 2014, **3**, 991–998.

50 Y. Chen, A. Star and S. Vidal, *Chem. Soc. Rev.*, 2013, **42**, 4532–4542.

51 D. Wrobel, D. Appelhans, M. Signorelli, B. Wiesner, D. Fessas, U. Scheler, B. Voit and J. Maly, *Biochim. Biophys. Acta - Biomembr.*, 2015, **1848**, 1490–1501.

52 S. R. S. Ting, G. Chen and M. H. Stenzel, *Polym. Chem.*, 2010, **1**, 1392–1412.

53 P. Lee and X. Wu, *Curr. Pharm. Des.*, 2015, **21**, 1862–5.

54 S. C. Rozinek, R. J. Thomas and L. Brancaleon, *Biochem. Biophys. Reports*, 2016, **7**, 295–302.

55 W. De Tian and Y. Q. Ma, *Chem. Soc. Rev.*, 2013, **42**, 705–727.

56 J. Anguizola, R. Matsuda, O. S. Barnaby, K. S. Hoy, C. Wa, E. DeBolt, M. Koke and D. S. Hage, *Clin. Chim. Acta*, 2013, **425**, 64–76.

57 B. S. Farmer, K. Terao and J. W. Mays, *Int. J. Polym. Anal. Charact.*, 2006, **11**, 3–19.

58 S. Barbosa, P. Taboada and V. Mosquera, in *Bio-nanoimaging: Protein Misfolding and Aggregation*, ed. V. N. Uversky, Y. Lyubchenko, Elsevier Inc., Amsterdam, 1st edn. 2014,

vol. 1, ch. 32, pp. 345–362.

59 J. Ishii, M. Chikae, M. Toyoshima, Y. Ukita, Y. Miura and Y. Takamura, *Electrochem. Commun.*, 2011, **13**, 830–833.

60 N. Cakir, G. Hizal and C. R. Becer, *Polym. Chem.*, 2015, **6**, 6623–6631.

61 S. Boye, N. Polikarpov, D. Appelhans and A. Lederer, *J. Chromatogr. A*, 2010, **1217**, 4841–4849.

62 H. Pasch, *Adv. Polym. Sci.*, 2000, **150**, 2–66.

63 T. H. Mourey, *Int. J. Polym. Anal. Charact.*, 2004, **9**, 97–135.

64 M. Gaborieau and P. Castignolles, *Anal. Bioanal. Chem.*, 2011, **399**, 1413–1423.

65 F. J. Stadler, J. Kaschta, H. Münstedt, F. Becker and M. Buback, *Rheol. Acta*, 2009, **48**, 479–490.

66 M. Gerle, K. Fischer, S. Roos, A. H. E. Müller, M. Schmidt, S. S. Sheiko, S. Prokhorova and M. Möller, *Macromolecules*, 1999, **32**, 2629–2637.

67 S. Podzimek, T. Vlcek and C. Johann, *J. Appl. Polym. Sci.*, 2001, **81**, 1588–1594.

68 W. Fraunhofer and G. Winter, *Eur. J. Pharm. Biopharm.*, 2004, **58**, 369–383.

69 M. E. Schimpf, K. D. Caldwell and J. C. Giddings, in *Field-flow fractionation handbook*, ed. M. E. Schimpf, K. D. Caldwell and J.C. Giddings, John Wiley & Sons, Inc., New York, 1st edn, 2000, vol. 1, ch. 1, pp. 3-31.

70 F. A. Messaud, R. D. Sanderson, J. R. Runyon, T. Otte, H. Pasch and S. K. R. Williams, *Prog. Polym. Sci.*, 2009, **34**, 351–368.

71 M. Wagner, S. Holzschuh, A. Traeger, A. Fahr and U. S. Schubert, *Anal. Chem.*, 2014, **86**, 5201–5210.

72 J. C. Giddings, *J. Chem. Phys.*, 1968, **49**, 81–85.

73 S. K. Ratanathanawongs Williams, M.-A. Benincasa and A. A. Ashames, in *Encyclopedia of Analytical Chemistry*, ed. R. A. Meyers, John Wiley & Sons, Inc., New York, 1st edn, 2016, vol. 1, ch. 2008a, pp. 1-24.

74 F. A. Messaud, R. D. Sanderson, J. R. Runyon, T. Otte, H. Pasch and S. K. R. Williams, *Prog. Polym. Sci.*, 2009, **34**, 351–368.

75 Stepan Podzimek, *Light Scattering, Size Exclusion Chromatography and Asymmetric Flow Field Flow Fractionation*, John Wiley & Sons, Inc., Hoboken, New Jersey, 1st edn, 2011, vol. 1, ch. 5, pp. 259-303.

76 C. Kim, A. Deratani, F. Bonfils and F. dé ric Bonfils, *J. Liq. Chromatogr. Relat. Technol.*, 2009, **33**, 37–45.

77 H. Zhao, P. H. Brown and P. Schuck, *Biophysj*, 2011, **100**, 2309–2317.

78 J. Stetefeld, S. A. McKenna and T. R. Patel, *Biophys. Rev.*, 2016, **8**, 409–427.

79 F. Ross Hallett, *Food Res. Int.*, 1994, **27**, 195–198.

80 S. Bhattacharjee, *J. Control. Release*, 2016, **235**, 337–351.

81 A. Oliva, M. Llabres and J. Farina, *Curr. Drug Discov. Technol.*, 2005, **1**, 229–242.

82 M. Andersson, B. Wittgren and K. G. Wahlund, *Anal. Chem.*, 2003, **75**, 4279–4291.

83 M. Glantz, A. Håkansson, H. Lindmark Månsson, M. Paulsson and L. Nilsson, *Langmuir*, 2010, **26**, 12585–12591.

84 L. Nilsson, *Food Hydrocoll.*, 2013, **30**, 1–11.

Chapter 3

Experimental

Chapter 3

Experimental

3.1 Experimental material, solvents, and chemicals

3.1.1 Chemicals used for dynamic light scattering (DLS)

- Phosphate buffered saline (PBS) tablets purchased from Sigma-Aldrich (Sigma-Aldrich, South Africa)
- Sodium azide (NaN_3) purchased from Sigma-Aldrich (Sigma -Aldrich, South Africa)
- Water (H_2O) (Millipore from the H_2O filtration system in the laboratory)

3.1.2 Chemicals used for size exclusion chromatography (SEC)

- *N*,*N*-dimethylacetamide (DMAc) purchased from Sigma-Aldrich (Sigma-Aldrich, Germany)
- Lithium chloride (LiCl) purchased from Sigma-Aldrich (Sigma-Aldrich, Germany)
- Deionized H_2O, treated with ultraviolet (UV) light (Purelab Plus UV/UF equipment, USF Elga, DE)

3.1.3 Chemicals used for asymmetric flow field-flow fractionation (AF4)

- PBS tablets obtained from Sigma-Aldrich (Sigma-Aldrich, Germany)
- NaN_3 obtained from Sigma-Aldrich (Sigma -Aldrich, Germany)
- UV treated, deionized H_2O (Purelab Plus UV/UF equipment, USF Elga, DE)
- Bovine serum albumin (BSA) purchased from Sigma-Aldrich (Sigma-Aldrich, Germany)

3.2 Polymer standards

Polystyrene (PS) calibration standards obtained from Polymer Laboratories (PL) (Polymer Laboratories, Church Stretton, Shropshire, UK). The polymer calibration standards were used for the calibration of SEC-MALLS system.: Their nominal molar masses M_p were, 1.3, 5.46, 20.65, 96.0 and 377.4 kg/mol.

3.3 Samples and sample preparation

3.3.1 Samples

The DenPol samples were supplied and synthesized in the Department of Bioactive and Responsive Polymers at the Leibniz-Institut für Polymerforschung Dresden (Dresden, Germany). The synthesis of the DenPols is explained in detail by S.Boye and collegues (Figure 1.1).[1]

Human serum albumin (HSA) was purchased from Sigma-Aldrich (Sigma-Aldrich, South Africa).

3.3.2 Sample preparation for dendronized polymers

The phosphate buffer with a concentration of 10 mM and pH 7.4 was prepared with PBS tablets, 0.02 % sodium azide (w/v) (prevents microbial growth) and deionized water that was UV treated and ultrafiltrated. The concentration of the DenPols for all AF4 measurements was 1 mg/mL, obtained by weighing 1 mg of MI-G0, MI-G0-MAL, MI-G1-MAL, MI-G1-PEG-MAL, and adding 1 mL of the 10 mM PBS eluent and kept for 24 hours at room temperature. The preparation of 1 mg/mL of MI-G2-MAL and MI-G3-MAL was obtained by weighing 1 mg of the DenPol and adding 1 mL of 10 mM PBS followed by stirring at elevated temperatures of 70 °C for several hours until solutions were visually clear. The samples were filtered with a 0.45 µm nylon filter.

3.3.3 Sample preparation for human serum albumin (HSA)

The eluent was prepared in the same manner as described in Section 3.3.2. The concentration of the HSA samples was 0.1, 0.25 and 0.5 mg/mL dissolved in 10 mM PBS and left for 4 hours until a visually clear solution was observed. For the preparation of the HSA solutions, 1 mg of HSA was diluted with 2 mL, 4 mL, and 10 mL of 10 mM PBS, respectively, to obtain the desired concentrations.

3.3.4 Sample preparation of the dendronized polymer and HSA mixtures

The preparation of the mixtures was achieved by first preparing 1 mg/mL of the DenPols in 10 mM PBS with a concentration of 1 mg/mL following the protocols mentioned in section 3.3.2. Regarding MI-G2-MAL and MI-G3-MAL the solution was first left to cool to room temperature before preparing the mixtures. To prepare the mixtures, different masses of HSA, 0.1, 0.25 and 0.5 mg, were added to 1 mL of MI-G0, MI-G0-MAL, MI-G1-MAL, MI-G1-PEG-MAL, MI-G2-MAL, and MI-G3-MAL. Different ratios of mixtures were prepared (1:0.1), (1:0.25) and (1:0.5) with the

concentration of the DenPols remaining constant. The mixtures were stirred for 24 hours at room temperature.

3.4 Calculated theoretical molar masses of the single macromolecule repeating units of poly (ethylene-*alt*-maleic anhydride) copolymer (MA) and the DenPols

Poly(ethylene-*alt*-maleic anhydride) (**MA**): 126.11 g/mol; **MI-G0-Boc**: 296.36 g/mol; deprotected **MI-G0**: 310.27 g/mol; **MI-G0-Mal**: 832.85 g/mol; **MI-G1-Boc**: 524.65 g/mol; deprotected **MI-G1**: 552.47 g/mol ; **MI-G1-Mal**: 1689.71 g/mol ; **MI-G1-PEG-Boc**: 1018.71 g/mol; deprotected **MI-G1-PEG** : 930.88 g/mol ; **MI-G1-PEG-Mal**: 2068.13 g/mol ; **MI-G2-Boc**: 1009.29 g/mol ; deprotected **MI-G2**: 1064.91 g/mol ; **MI-G2-Mal**: 3331.12 g/mol ; **MI-G3-Boc** : 1921.46 g/mol ; deprotected **MI-G3**: 2032.71 g/mol ; **MI-G3-Mal**: 6341.26 g/mol.

3.5 Instrumentation

3.5.1 Dynamic light scattering (DLS)

For each measurement three runs were performed using a glass cuvette with an open round aperture. The cuvette was filled with a sample volume of 1 mL and concentrations of 0.5 mg/mL to 3 mg/mL at a temperature of 25 °C. The equilibration time for each sample was programmed for 5 min prior to all measurements. For temperature dependent measurements the cuvette was filled with sample volumes of 1 mL with a concentration of 1 mg/mL with temperature increments of: 37 °C, 40 °C, 60 °C and 80 °C. The equilibration time for all temperature measurements was programmed for 10 min. Off-line measurements of the hydrodynamic diameter (D_h) and dispersity (PDI) were performed using a DLS detector (Malvern Zetasizer Nano ZS, Malvern Instruments, Worcestershire, U.K.) by measurement with a backscatter detection angle at 173°.

Samples of 0.1, 0.25, 0.5 and 1 mg/mL were analyzed in cyclic olefin copolymer cuvettes with an open square aperture. Three measurements were performed for each experiment at 25 °C and the cuvette required a minimal volume of 4 µL. Before the commencement of measurements, the equilibration time was 5 min. Off-line measurements were performed using a DLS instrument (DynaPro® Nanostar®, Wyatt Technologies, U.S.A) with a backscatter detection angle of 90°. The DLS data was treated with DYNAMICS 7.9.0.5 software.

3.5.2 Size exclusion chromatography (SEC) system

The experiments were performed using a PolarGel-M column (Polymer Labaratories, U.K.), differential refractive index (dRI) detector (K2301, Knauer, DE), and a miniDAWN MALS detector (TREOS II, Wyatt Technologies, U.S.A.). The flow rate of 1 mL/min for the experiments were monitored by Agilent isocratic pump series 1200 (Agilent Tech, U.S.A). The eluent used for the measurements was *N*,*N*-dimethylacetamide (DMAc) with 3 g/L of lithium chloride (LiCl).

3.5.3 Asymmetric flow field-fractionation (AF4) system

The AF4 experiments were performed at ambient temperatures using an AF4 instrument (Eclipse DualTec, Wyatt Technology, Europe, DE) which was coupled to MALLS- (DAWN HELEOS ll, Wyatt Technology Europe, DE) with an integrated DLS detector that measures from one of the angles and an RI detector (Optilab rEX, Wyatt Technology, Santa Barbara, USA). The Eclipse DualTec system was connected to an isocratic pump (Agilent Technologies 1200, Agilent, USA) which included a degasser. The aqueous AF4 channel was connected to an Eclipse DualTec valve which regulates the channel flow, injection flow, cross flow and focus flow. A regenerated cellulose membrane with a molecular weight cut-off (MWCO) of 10 kDa (Wyatt Technology Europe, DE) was placed inside the channel on top of the porous frit. The long channel had a tetrafluoroethylene (PTFE) spacer with a defined thickness of 350 µm. The backpressure was maintained by using suitable tubing.

3.6 Calibration of RI and MALLS detector with PS standards in DMAc with LiCl (SEC-MALLS)

The RI detector was calibrated using a PS 62 kg/mol calibration standard as isotropic scatterer in DMAc with LiCl. The concentration of the PS standard was 2 mg/mL and a dn/dc value of 0.146 mL/g. The flow rate was maintained as 1 mL/min for the calibration of the RI detector. The calibration of the RI detector was performed to obtain accurate concentration values for the polymers.

The MALLS detector was calibrated by following a protocol containing two steps. The initial step was the calibration of the 90° angle. The MALLS detector was calibrated with the same PS 62 kg/mol calibration standard, with a concentration of 2 mg/mL and a dn/dc value of 0.146 mL/g. The normalization procedure was the second step of the calibration protocol. The constants for all

the remaining angles, excluding the 90° angle were determined using the ASTRA 7.3.2 software. To validate the calibration, PS 1.3, 5.46, 20.65, 96.0 and 377.4 kg/mol were used.

3.7 Calibration of the MALLS detector with BSA standard in PBS (AF4)

The calibration and normalization of the MALLS detector was performed with a BSA standard as it is an isotropic scatterer (R_g smaller than 10 nm) in 10 mM PBS buffer. The molar mass of the BSA monomer is 66.7 kg/mol. The sample was prepared by measuring 1 mg of BSA dissolved in 1 mL of filtered PBS buffer, resulting in a concentration of 1 mg/mL. The dn/dc of BSA in PBS is 0.185 mL/g. The injection volume was 50 µL. The AF4 method for calibration was a channel flow rate and detector flow rate of 1 mL/min. The sample was injected at 0.45 mL/min and focused for 3 min at 3 mL/min. A constant cross flow of 4 mL/min was employed over a period of 15 min.

3.8 Specific refractive index increments (dn/dc) of dendronized polymers and HSA

The dn/dc values were determined externally using the Optilab rEX (Wyatt Technology, Europe GmbH, Germany). The samples were dissolved in 10 mM PBS and left for 24 hours. The solution was prepared by weighing 10 mg of the sample in a 5 mL volumetric flask and dissolving in 10 mM PBS to make a 2 mg/mL solution, followed by 4 dilutions which were each injected directly into the RI detector with a glass syringe. The data processing was completed using ASTRA software (version 7.3.2) (Table 3.1).

Table 3.1. The specific refractive index increment (dn/dc) values for the samples with varying generation number.

DenPol name	dn/dc (mL/g)
MI-G0	0.130
MI-G0-MAL	0.153
MI-G1-MAL	0.153
MI-G1-PEG-MAL	0.153
MI-G2-MAL	0.153
MI-G3-MAL	0.153

The dn/dc for human serum albumin in literature was 0.189 mL/g.[2]

The dn/dc values for SEC measurements in DMAc with 3 g/L were obtained from literature as 0.117 mL/g for the poly(ethylene-*alt*-maleic anhydride) and the average dn/dc for the Boc protected dendronized polymers was 0.09 mL/g.[1]

3.9 References

1. S. Boye, D. Appelhans, V. Boyko, S. Zschoche, H. Komber, P. Friedel, P. Formanek, A. Janke, B. I. Voit and A. Lederer, *Biomacromolecules*, 2012, **13**, 4222–4235.

2. H. Zhao, P. H. Brown and P. Schuck, *Biophys. J.*, 2011, **100**, 2309–17.

Chapter 4

Results and discussion

Chapter 4

Results and discussion

4.1 Introduction

Over the years the tremendous power of AF4 coupled to various light scattering and concentration detectors has been proven with the analysis of complex polymers.[1–5] The combination of an advanced fractionation technique and light scattering detectors provides important information about molecular properties such as molar mass, size, conformation, apparent density and shape as a function of molar mass.[6–8] With this insight, the potential of specific materials for biomedical applications can be explored. The benefits of fractionation occurring in an empty channel such as in AF4 is important for high molar mass polymers to minimize shear degradation and the destruction of macromolecules or their assemblies.[1]

The purpose of this study is the characterization of lysine-dendronized polymers (DenPols) and poly(ethylene glycol) (PEG) DenPols modified with maltose shells by applying batch mode DLS as well as SEC and AF4 separation techniques. Thus, a comprehensive characterization of the molar mass, size, and their distributions as well as apparent densities and conformations of these structures shall be performed. Previously, SEC-MALLS-RI and AF4-MALLS-RI were applied to determine the molar mass and size of DenPols.[9] In this study, the first step was to study the influence of concentration and temperature on the aggregation behaviour of the DenPols using batch mode DLS. This was followed by SEC-MALLS to study the molar mass of poly(ethylene-*alt*-maleic anhydride), MI-G0-Boc, and MI-G1-Boc (see Figure 1.1 A and D in Section 1.1). An optimized AF4 method was utilized to obtain information regarding the molar mass and size of MI-G0, MI-G0-MAL, MI-G1-MAL,MI-G1-PEG-MAL, MI-G2-MAL and MI-G3-MAL (see Figure 1.1 B, C, E, F, G and H in Section 1.1). These values enabled calculations of the conformational parameters to improve the understanding of the DenPols' architecture. The second section of this work is devoted to the application of the developed technique to mixtures of different fractions of HSA and the glycopolymers. The optimization of the AF4 method in combination with RI, MALLS, and DLS detectors (all as part of one detector set-up) provided a real-time determination of the hydrodynamic sizes, radii of gyration and molar mass distributions.

SEC is not suitable for the characterization of DenPols with many branches and ultrahigh molar masses. In contrast, AF4 proves to be a powerful tool for the fractionation of large aggregates. AF4 was successfully applied for the complete characterization of highly branched polymers and DenPol-HSA complexes. From this analysis vital information regarding the change in apparent density and conformation of DenPols was obtained.

4.2 Analysis of DenPols with dynamic light scattering

Dynamic light scattering (DLS) is a versatile tool used to investigate the influence of concentration, generation number and temperature on the particle size of complex materials. The batch mode analysis of samples is non-invasive and information about the size and size distribution of glycopolymers can easily be determined.[10,11] The broad molar mass distribution, chemical heterogeneity and branching distribution of DenPols present challenges for characterization.[12] Investigating the change in concentration and applying temperature as an external stimulus will provide insights into the stability of DenPols in solution.

Phosphate buffer saline (PBS) solution was chosen as the solvent as it resembles the physiological environment of the human body having similar osmolarity and ion concentration. The water-based buffer is non-toxic towards cells and maintains a constant pH of 7.4.[13]

4.2.1 Analysis of the different concentrations of DenPols

A comparison between DenPols in water and PBS is displayed in Figure 4.1. Figure 4.1 A shows the measured hydrodynamic diameter (D_h) of MI-G0, MI-G0-MAL, MI-G1-MAL, MI-G1-PEG-MAL, MI-G2-MAL, and MI-G3-MAL in water as obtained by DLS. There is a sharp increase in D_h to 200 nm for MI-G0 with the concentration of 3 mg/mL. The large increase in D_h is not visible for the DenPols decorated with maltose shells. This suggests that there is a possibility of self-aggregation as the end groups of MI-G0 can form electrostatic interactions. The cationic charge of the amine group and the negative charge of the triflate group can be influenced by the changing pH. This suggests that the modification of MI-G0 with maltose reduces the possibility of electrostatic interactions thereby reducing the aggregation. Maltose-decorated glycopolymers show slight changes in D_h which indicates that the spatial arrangement of the maltose moieties in the glycopolymer plays a role in reducing aggregation.[14]

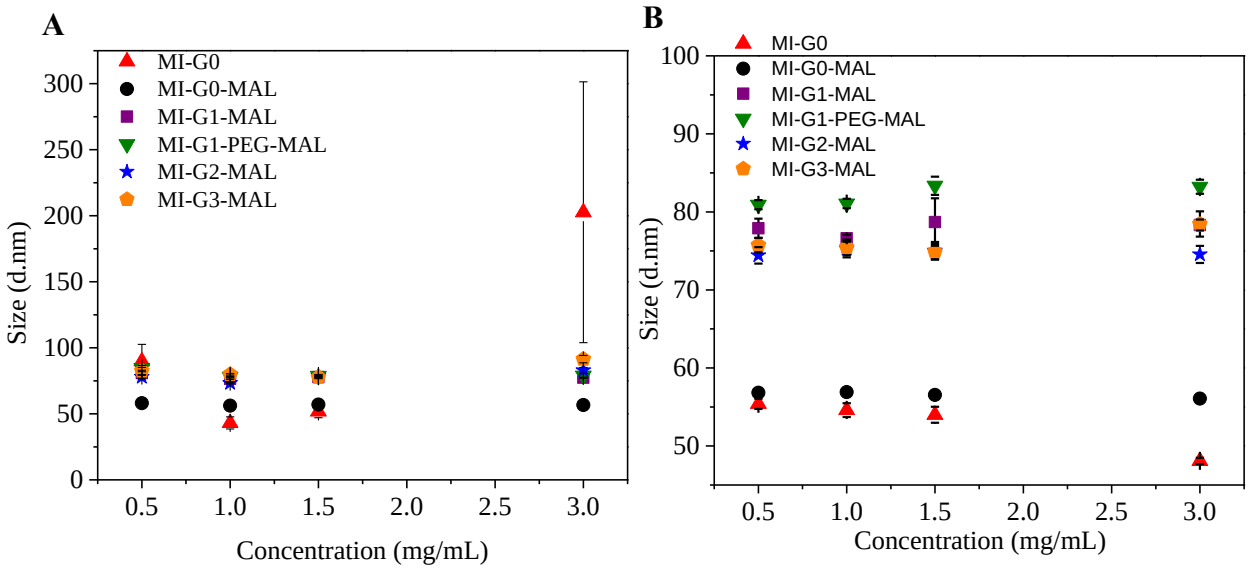

Figure 4.1. Comparison between z-average sizes of different concentrations of MI-G0, MI-G0-MAL, MI-G1-MAL, MI-G1-PEG-MAL, MI-G2-MAL and MI-G3-MAL in A) water with 0.02 % (w/v) sodium azide and B) 0.01 M PBS with 0.02 % (w/v) sodium azide.

As seen in Figure 4.1 B there are slight changes in D_h with an increase in concentration. The D_h of MI-G0-MAL is larger than MI-G0 which was not displayed in water. There is an increase in D_h from MI-G0-MAL to the 1st generation DenPols. However, progressing from 1st generation to the 2nd and 3rd generation, there is minimal alterations in D_h. It should be noted that with increasing generation number the DenPols have an increased branching density along the polymer backbone, but the length of the polymer backbone does not change. This can be explained by the increase in the persistence length while the contour length of the DenPols remains the same, leading to small changes in the hydrodynamic size. The persistence length is a geometric property that quantifies the stiffness of an object and the contour length is defined as the maximum physical length of possible extension.[15] An alternative explanation is that MI-G1-MAL is not present as a single macromolecule but as a cluster of single macromolecules. In addition, MI-G2-MAL and MI-G3-MAL were heated at 70 °C for several hours to achieve a visibly clear solution and these elevated temperatures can lead to the disruption of hydrogen bonding. Studies by Choperena et al.[16] and Mizan et al.[17] showed that elevated temperatures decrease the strength of hydrogen bonds.

The dependence of the size of MI-G0-MAL – MI-G3-MAL on the increase in concentration is small. A slight increase of the D_h in the range of 3-6 nm is observed with a concentration of 3 mg/mL for MI-G1-PEG-MAL and MI-G3-MAL. The slight change in size does not indicate that aggregation is concentration dependent. A comparison between the size of the DenPols in water

and PBS shows the importance of a controlled pH environment for the stability of the DenPols. Therefore, the focus will be on the behaviour of DenPols in PBS.

Table 4. 1.The z-average hydrodynamic diameter and dispersity measurements of MI-G0, MI-G0-MAL, MI-G1-MAL, MI-G1-PEG-MAL, MI-G2-MAL, and MI-G3-MAL in 10 mM PBS.

Sample	**Concentration (mg/mL)**	**Z-average hydrodynamic diameter (D_h) (nm)**	**PDI**
MI-G0	0.5	55.4 ± 0.66	0.33
	1.0	54.6 ± 0.88	0.34
	1.5	54.0 ± 1.02	0.40
	3.0	48.1 ± 0.41	0.44
MI-G0-MAL	0.5	56.8 ± 0.36	0.27
	1.0	56.9 ± 0.18	0.28
	1.5	56.5 ± 0.31	0.27
	3.0	56.1 ± 0.21	0.28
MI-G1-MAL	0.5	77.9 ± 1.24	0.34
	1.0	76.6 ± 0.44	0.39
	1.5	78.7 ± 3.04	0.39
	3.0	78.3 ± 0.70	0.42
MI-G1-PEG-MAL	0.5	80.9 ± 0.59	0.29
	1.0	81.0 ± 0.60	0.29
	1.5	83.4 ± 1.17	0.32
	3.0	83.2 ± 0.90	0.30
MI-G2-MAL	0.5	74.4 ± 1.06	0.34
	1.0	75.3 ± 1.07	0.32
	1.5	75.0 ± 1.11	0.34
	3.0	74.6 ± 1.09	0.38
MI-G3-MAL	0.5	75.7 ± 0.93	0.38
	1.0	74.9 ± 1.00	0.33
	1.5	74.5 ± 1.00	0.33
	3.0	78.5 ± 1.62	0.40

As seen in Table 4.1 the concentration of glycopolymers has a minimal influence on the size of the DenPols. The polydispersity index (PDI) is a dimensionless parameter that is defined as the approximate width of the size distribution determined from the cumulants analysis. The PDI value

corresponds to the square of the width of the peak divided by the average. The PDI of all the DenPols is in the realm of 0.27 to 0.40. For a monodisperse sample, the PDI is below 0.1; as the DenPols PDI exceeds 0.1, they can be viewed as heterogenous objects. This illustrates that DenPols are polydisperse species with different sizes and are not necessarily dissolved on a macromolecular level.

4.2.2 Analysis of DenPols exposed to elevated temperatures

To study the influence of temperature on the size of DenPols, the DenPols were exposed to temperatures of 25, 37, 40, 60 and 80 °C. A comprehensive understanding about the conformation of DenPols with an increase in temperature is important for various fields, such as biomedical applications.

As can be seen by DLS measurements of MI-G0 and MI-G0-MAL - MI-G3-MAL in Figure 4.2, there are slight changes in the size in response to elevated temperatures. Changes in D_h between 1 to 4 nm were observed. These differences are minimal and do not indicate that temperature triggers aggregate formation. This corroborates with a previous study, that temperature does not influence the aggregation behaviour of lysine dendronized glycopolymers.[9]

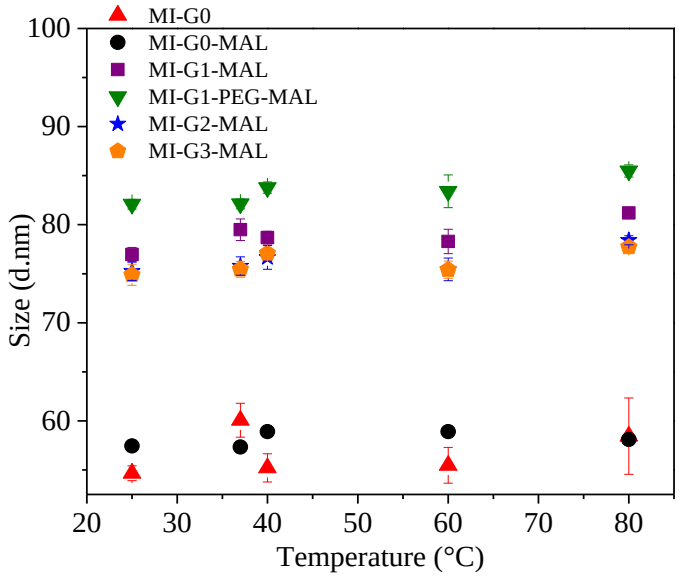

Figure 4.2. Comparison of the hydrodynamic diameter of MI-G0 (filled red triangle), MI-G0-MAL (filled black circle), MI-G1-MAL (filled purple square), MI-G1-PEG-MAL (filled olive inverted triangle), MI-G2-MAL (filled blue star) and MI-G3-MAL (filled orange pentagon) with temperature increments of, 25 °C, 37 °C, 40 °C, 60 °C and 80 °C in 10 mM PBS.

From the results obtained by DLS it can be concluded that a defined buffer is essential for DenPols to have a controlled pH for the stability of D_h. The concentration of the DenPols and temperature of the environment has a minimal influence on the aggregation behaviour. The broad size dispersity of the DenPols makes analysis challenging with batch mode DLS. Thus, a suitable separation technique is required to separate the sample into homogenous fractions to thoroughly analyze the size and molar mass. To address the problem, a separation technique in combination with a light scattering detector is implemented.

4.3 Analysis of poly(ethylene-*alt*-maleic anhydride) (MA), MI-G0-Boc and MI-G1-Boc with SEC-MALLS

Size exclusion chromatography (SEC) coupled to light scattering and concentration detectors provides critical information regarding the molar mass of species. The molar mass of the polymer backbone is necessary for the calculation of the theoretical molar masses of the single macromolecules of the respective DenPols. The molar mass readings of poly(ethylene-*alt*-maleic anhydride) (MA) obtained from SEC was used to calculate the number of alternating units present in the polymer backbone.

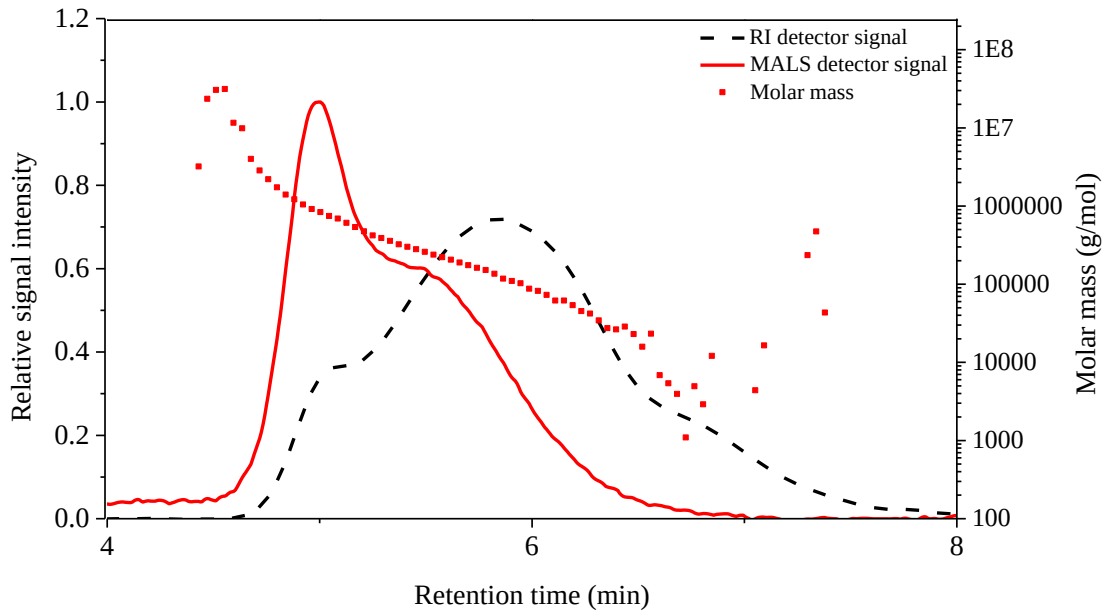

Figure 4.3. SEC elugram and molar mass readings of poly(ethylene-alt-maleic anhydride) in DMAc with 3 g/L LiCl.

The SEC elugram for the MA shows a broad molar mass distribution that ranges from 10^4 *to* 10^6g/mol, showing the molar mass heterogeneity of MA, see Figure 4.3.

The light scattering and RI detector signals show bimodalities with the presence of a low molar mass peak and an early eluting high molar mass shoulder, indicating aggregate formation. It is evident that the high molar mass shoulder has a lower concentration compared to the low molar mass species. To resolve the aggregate formation, an alternative eluent could be used.[18] However, the dissolution of BOC-protected polymers MI-G0-Boc and MI-G1-Boc are a challenge in aqueous and organic solvents.[9] The experimental M_n of poly(ethylene-*alt*-maleic anhydride) was determined as 78 800 g/mol (see Table 4.2) and was used to calculate the number of repeat units present in the polymer backbone. This was achieved by dividing the M_n by the molar mass of the MA monomer, 126.11 g/mol. The number of alternating units was calculated as 625.

Table 4.2. Molar mass of repeating unit, average molar mass and dispersity of MA, MI-G0-Boc and MI-G1-Boc, in DMAc with 3 g/L LiCl, measured with SEC-MALLS-RI.

Sample	M_w **(repeating unit) (g/mol)**	M_n **(g/mol)**	M_w **(g/mol)**	Đ (M_w/M_n)
MA	126.11	78 800	259 000	3.3
MI-G0-Boc	296.36	154 000	730 000	4.9
MI-G1-Boc	524.66	343 000	2 370 000	6.1

The BOC-protected polymers MI-G0-Boc and MI-G1-Boc were analyzed in DMAc with LiCl and water to determine the average molar mass and Đ (Figure 4.4). A comparison of the RI detector signals shows a decrease in signal intensity of MI-G1-Boc compared to MI-G0-Boc. This can be attributed to possible interactions with the stationary phase. The high molar mass shoulder at early elution times in the MALLS signal for both BOC-protected species indicates pronounced aggregation. The molar mass readings show abnormal SEC elution behaviour for MI-G1-Boc: decrease in the molar mass followed by a slight abnormal upswing in the molar mass data after 7 min. This phenomenon is typical for highly branched polymers,[19] but the elution behaviour of such materials is not completely understood. There are several explanations, namely, adsorption[20], large macromolecules diffusing in and out of the pores for a prolonged time[21], presence of micogels[22] or the Argentinean bolas effect (i.e. the entanglement of a section of a polymer in the column packing).[19,23] However, in this case, the most probable explanation for the effect is the low

concentration of high molar mass fractions, which cannot strongly influence the molar mass calculations.

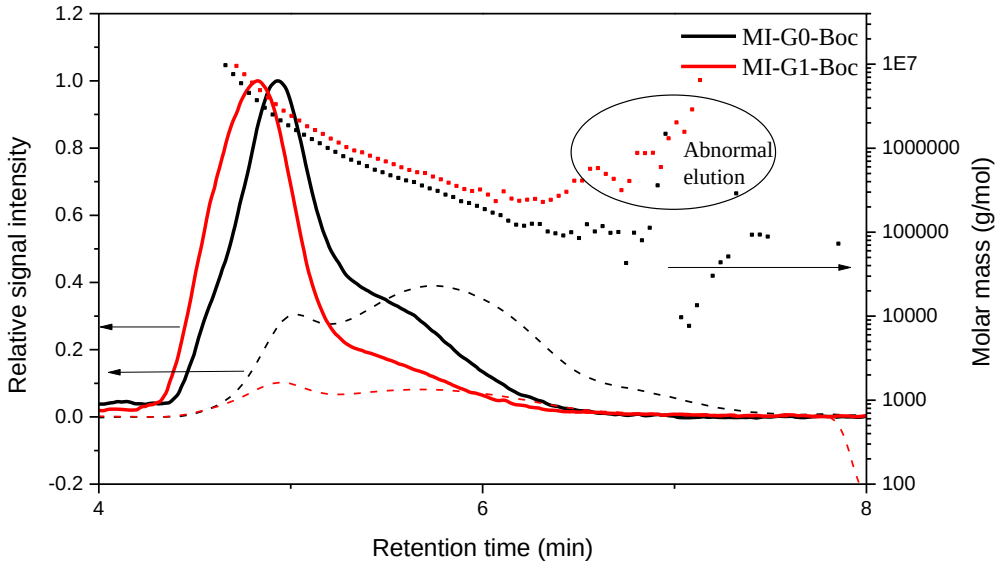

Figure 4. 4. SEC elugrams of MALLS detector signal (solid line), RI detector signal (dashed line) and molar mass (filled squares) readings of MI-G0-Boc and MI-G1-Boc in DMAc with 3 g/L LiCl and water.

Table 4.2 shows an increase in M_n and M_w values with generation number of the Boc-protected DenPols and is accompanied by a more disperse MI-G1-Boc sample. The theoretical molar mass of MI-G0-Boc is 185 kg/mol and MI-G1-Boc is 330 kg/mol with a number average degree of polymerization calculated as 625 (with the assumption of 100 % modification). The experimental $M_n$of MI-G0-Boc is only slightly lower than the theoretical molar mass. The starting material for the dendronization of lysine-DenPols modified with maltose shell for MI-G1-MAL – MI-G3-MAL is different to MI-G0-MAL (explained in Section 2.1).[9] This can explain the reason for the larger experimental molar mass of MI-G1-Boc than the theoretical molar mass. However, the high molar mass shoulder can lead to an overestimation of the molar mass. Boye et al.[9] explained that with an increase in the generation number, the tendency of the Boc-protected polymers to form aggregates

increases, leading to the overestimation of the molar mass. Nevertheless, the deviation of the experimental M_n from the theoretical is minimal.

4.3.1 Theoretical molar mass calculations of MI-G0, MI-G0-MAL, MI-G1-MAL, MI-G1-PEG-MAL, MI-G2-MAL, and MI-G3-MAL from SEC-MALLS-RI measurements

The theoretical molar mass values were obtained from the degree of polymerization of 625 calculated from the molar mass of the polymer backbone and is presented in Table 4.3.

Table 4.3. Theoretical molar mass calculations of MI-G0, MI-G0-MAL, MI-G1-MAL, MI-G1-PEG-MAL, MI-G2-MAL, and MI-G3-MAL, with the degree of polymerization of 625.

	Polymerisation degree (DP)	**M_w of repeating units (g/mol)**	**Total M_n (g/mol)**
MI-G0	625	310.27	~160 000
MI-G0-MAL	625	848.84	~530 000
MI-G1-MAL	625	1629.61	~1 020 000
MI-G1-PEG-MAL	625	2096.50	~1 300 000
MI-G2-MAL	625	3267.57	~2 040 000
MI-G3-MAL	625	6341.26	~3 960 000

The values calculated in Table 4.3 cannot be directly measured using SEC for the maltose-modified glycopolymers. Maltose modification of the DenPols requires the deprotection of the Boc-protecting group. Followed by the DenPols submerged in a borate buffer with excess maltose. Once the DenPols are modified with the maltose shell, the glycopolymers are no longer soluble in organic solvents, only in aqueous solutions. The change in solubility of the DenPols emphasizes the change in their overall structure. This is because the maltose shell introduces a high concentration of endgroups along the polymer backbone that have the capability of forming hydrogen bonds. The number of endgroups increase exponentially with generation number and can lead to very strong interactions with the column. Additionally, shear forces can result in uncontrolled degradation of aggregates during elution in the column. Furthermore, the excessive branching of DenPols presents the possibility of co-elution. To perform reliable molar mass determinations in the absence of a stationary phase, AF4 will be used.

4.4. Analysis of dendronized polymers and human serum albumin using asymmetric flow field-flow fractionation coupled to MALLS, DLS and RI detectors

The primary objective of this work was to develop a robust and suitable AF4 protocol for the characterization of the individual components of DenPols and HSA as well as DenPol-HSA complexes. The samples were examined in detail to determine the molar masses, size, apparent density, and architectures of the DenPols depending on the generation number.

4.4.1. AF4 optimization

The AF4 measurements were performed to (1) determine the properties of individual DenPols and HSA and (2) determine the properties of DenPol and HSA mixtures. Applying the same AF4 protocol for the characterization allows the direct comparison of fractograms. The most important parameters for the optimization of an AF4 technique are:

- Channel flow rate/detector flow rate
- Cross flow rate program (constant/linear decay/exponential decay)
- Focus/relaxation rate and time
- Elution time
- Channel thickness
- Membrane material and its molar mass cut-off
- Liquid carrier composition

There are three cross flow programs, namely, constant, linear, and exponential decay. Constant flow is when the cross flow remains the same throughout the designated elution time. A constant cross flow has limitations as the resolution is dependent on the time that the species is retained in the channel. To overcome or to reduce some of the limitations of a constant cross flow, an exponential decay can be implemented. Exponential decay is expressed by the following equation:

$$Q_c(t) = Q(0)e^{\left(-\frac{ln\,2}{t_{\frac{1}{2}}}t\right)} \qquad (30)$$

where $Q_c(t)$ is the cross flow rate as a function of time t once the elution mode of the protocol commences, $Q(0)$ is the cross flow at the beginning of the experiment and $t_{\frac{1}{2}}$ is the half-life of the exponential decay. A linear flow decay is the constant incremental decrease of the cross flow for a designated time.

The rationale for the method development was to start with a high constant cross flow to retain the small protein in the channel for a sufficient time, for the separation of the monomer and dimer of HSA. HSA has a similar structure to bovine serum albumin (BSA), which is typically used for the calibration of the aqueous AF4 system. The method applied for the calibration of the AF4 system is described in Section 3.7. The method utilized for the calibration was implemented for the characterization of HSA. Implementation of a high cross flow allows the elution of HSA but not the large DenPols. This is to ensure that when the mixtures are analyzed, the non-bound HSA will elute in the beginning of the fractionation process. The second elution step for the DenPols is to apply an exponential flow decay to achieve separation. An exponential flow decay has been investigated for polydisperse macromolecules and exhibited good resolution and consistent selectivity over the broad size distribution.[24] An exponential cross flow (F_x) gradient was applied as it overcomes disadvantages of a linear flow decay, especially when polymers with a broad molar mass and size distribution need to be separated. The disadvantages of a linear decay are a decrease in the RI detector signal over a long elution period, resulting in a low signal-to-noise ratio. The cause of the low signal-to-noise ratio is the continuous elution of sample through the duration of the measurement. This is valid when the same amount of sample is injected leading to a lower discrete concentration. In addition, the linear decay approaches the sensitivity limit of the 45° light scattering angle faster; this is caused by larger particles (with a small diffusion coefficient) dwelling in the channel. When considering the desired protocol, the sensitivity of the light scattering angles are important. With these rationales, method A was developed.

The first AF4 experimental protocol, method A, was performed with a channel flow rate (F_c) and detector flow rate of 1 mL/min. Before the commencement of the experiment, the focus flow was 3 mL/ min to equilibrate the system for 1 min. The respective sample was introduced into the channel with an injection volume of 50 µL and a sample load of 12.5 to 55 µg at 0.45 mL/min followed by a focus flow of 3 mL/min for 3 min. After the focus time elapsed, the focus flow stopped, and the elution mode started. A constant F_x was maintained at 4 mL/min for 10 min (for the elution of HSA). This also provides sufficient time for the elution of the void peak. A void peak corresponds to the elution of sample that has no retention in the channel, either ultrahigh molar mass ($< 1\ \mu m$) polymers or small molecules. After 10 min, an exponential F_x gradient of 4 mL/min to 0.15 mL/min in 30 min was used followed by a decrease in the cross flow to 0 mL/min

and was maintained for 10 min. No cross flow for 10 min was used to flush out any large particles that were retained in the channel.

Figure 4.5 shows a comparison between the light scattering signals of MI-G1-MAL and MI-G3-MAL applying method A. The void peak elutes with the commencement of the elution mode. The ultrahigh molar mass and the broad molar mass distribution of the DenPols made baseline separation unachievable. Both MI-G1-MAL and MI-G3-MAL samples elute when the exponential decay begins, and the cross flow began to reduce from 4 mL/min. Once the cross flow is stopped (0 mL/min) the light scattering detector indicates the elution of an individual peak. The late eluting peak can be because of larger polymers that were retained in the channel and were not given efficient time to elute due to their size. An alternative explanation is that there was non-specific adsorption of the polymers to the semi-permeable membrane leading to the later elution.[25] Increasing the measurement time for the exponential decay can improve the resolution of the later eluting peak.

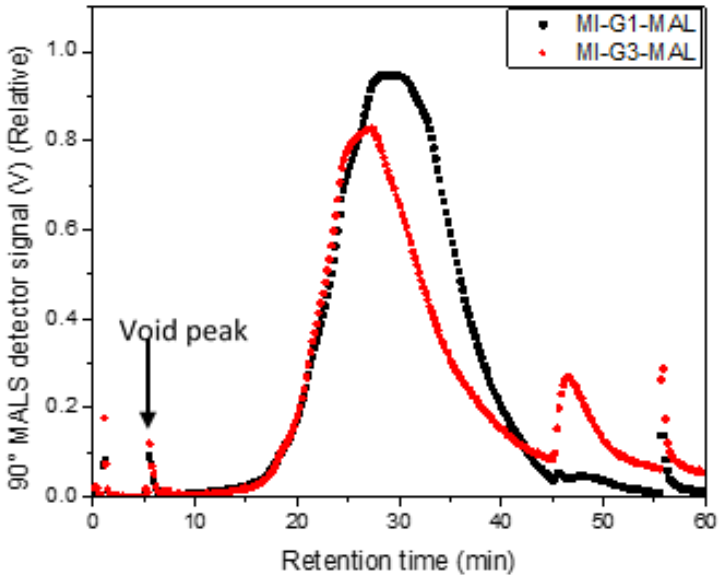

Figure 4.5. Fractograms of 1.0 mg/mL of MI-G1-MAL (solid black square) and MI-G3-MAL (solid red square) in 10 mM PBS applying Method A. 90° MALLS detector signal.

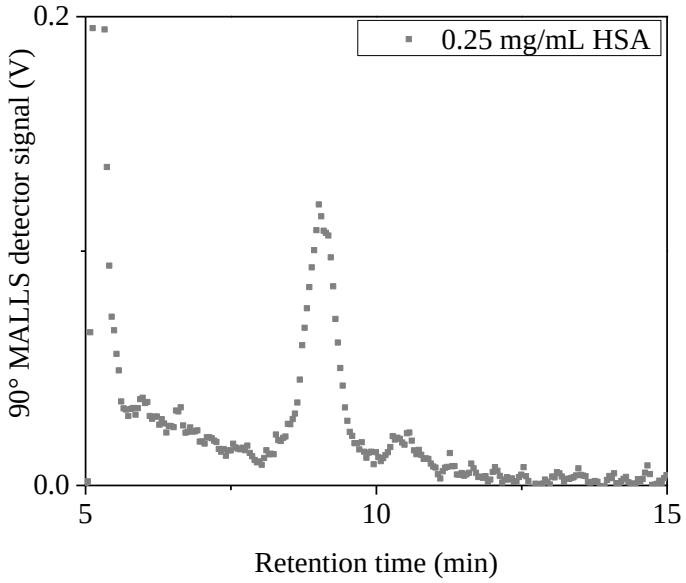

Figure 4.6. Fractograms of 0.25 mg/mL of HSA (solid grey square) in 10 mM PBS applying Method A. 90° MALLS detector signal.

To investigate the elution of HSA during the constant flow of 4 mL/min for 10 min, 0.25 mg/mL of HSA was analyzed, with method A. The MALLS fractogram shows the elution of two peaks, suspected as the monomer and dimer peaks of HSA in the initial 10 min of the elution step, see Figure 4.6.

To evaluate the experimental protocol for the mixtures, a comparison between mixtures of MI-G1-MAL and MI-G3-MAL interacting with 0.1 mg HSA is displayed in Figure 4.7 A. The fractogram displays the non-bound HSA and the DenPol-HSA complexes. The MALLS signal shows a similar peak shape for both DenPols and the individual peak elutes after the cross flow stops. In this instance, the light scattering signal of peak eluting after the cross flow is reduced to 0 mL/min has a higher intensity than the main peak for MI-G3-MAL: HSA (1:0.1). This suggests the presence of suspected aggregates formed by interactions of MI-G3-MAL with HSA. For larger species, light scattering detectors need sufficient time for the measurements especially for online DLS measurements, as larger polymers move slower and thus have slower Brownian motion.[10,26] Figure 4.7 B shows the elution of the HSA monomer peak during the constant cross flow of 10 min.

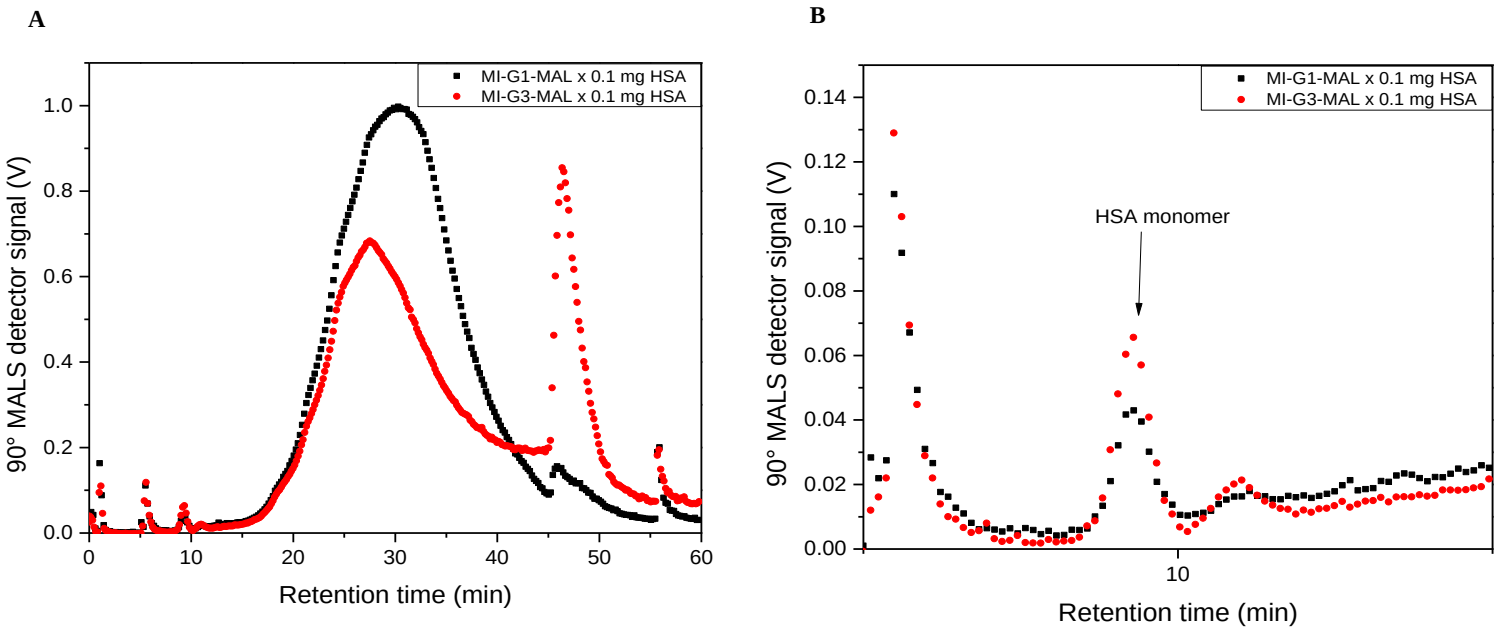

Figure 4.7. Fractograms of 1.1 mg/mL of A) MI-G1-MAL: HSA (1:0.1) and MI-G3-MAL:HSA (1:0.1) and B) 0-15 min of the fractogram of HSA in 10 mM PBS applying Method A. 90° MALLS detector signal.

To optimize the operational parameters for the characterization of DenPols, the F_c and the F_x rates were adjusted. The channel flow rate was decreased for the detectors to have sufficient time to detect larger particles and the elution time was increased. To provide the detectors with sufficient time for analysis, without making alterations to the resolution, two parameters were adjusted. An increase in the cross flow enhances the resolution and reducing the channel flow increases the resolution. Therefore the channel flow was reduced to provide sufficient analysis time for the detectors and the cross flow was reduced to maintain the resolution.[25–27]

F_c was decreased to 0.6 mL/min and F_x to 3 mL/min. The optimized AF4 method B used for all the experiments was as follows: The channel flow rate and the detector flow rate were maintained at 0.6 mL/min for all AF4 measurements (unless stated otherwise). At the beginning of the experiment, the cross flow is maintained at 3 mL/min for 1 min to equilibrate the system. An autosampler was used to inject the samples into the channel at a flow rate of 0.45 mL/min, followed by the focus step for 3 min at 3 mL/min. A constant cross flow of 3 mL/min was kept for 10 min. After 10 min, an exponential cross flow beginning at 3 mL/min and reduced to 0.15 mL/min for 40 min was used. For the final elution step, the cross flow decreased from 0.15 mL/min to 0 mL/min. The final 10 min there was no cross flow, to ensure that all analytes eluted (Figure 4.8).

The concentration of the DenPols was maintained at 1 mg/mL. The of HSA concentration was 0.1, 0.25 and 0.5 mg/mL in 10 mM PBS. Regarding the DenPols and HSA mixtures the concentration was approximately 1.1, 1.25 and 1.5 mg/mL. The injection volume was adjusted to 100 µL to increase the sample volume in the channel as the programmed gradient of the injected sample decreases the RI detector signal. Furthermore, for online DLS measurements the sample load was increased to 300 µL to obtain an accurate R_h value. Overloading effects, for instance, band broadening and shift in retention times,[28] for DLS measurements can be ignored.

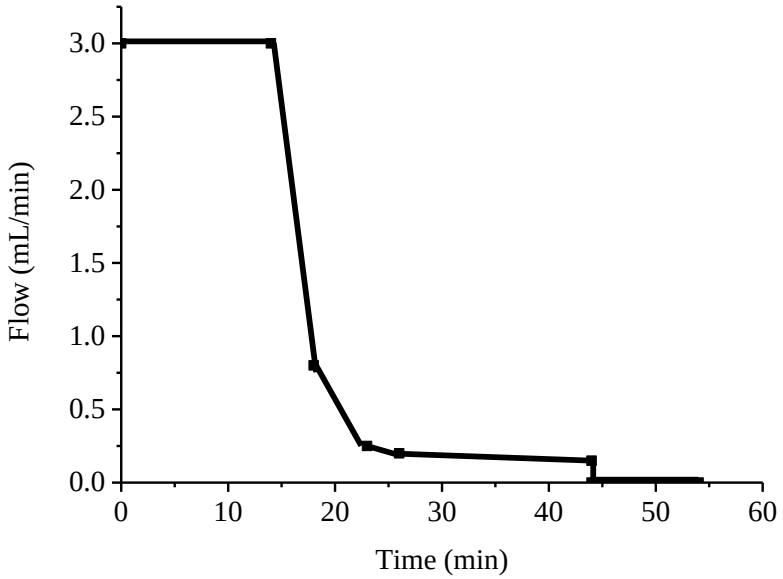

Figure 4.8. Cross flow profile for method B.

4.4.2 Analysis of DenPols with AF4-MALLS-DLS

A comparison between the MALLS detector signals, molar masses, and radii readings of MI-G0 and MI-G0-MAL are shown in Figure 4.9. As seen in Figure 4.9 the MALLS detector signal shows an increase in the signal intensity after the modification of MI-G0 with a maltose shell. This is because of the addition of maltose moieties that increases the molar mass of the polymer leading to an increased scattering intensity. With an increase in the molar mass, a shift in the retention time is typically expected but the DenPols have a broad molar mass and size distribution. Due to the branching along the polymer backbone, a high dispersity of the DenPols is expected. At a retention time of approximately 35 min, the MI-G0 peak presents a slight shoulder, that indicates the

possibility of a different structure with a larger molar mass. Molar mass readings increase gradually towards ultrahigh molar mass regions (above with 1×10^7 g/mol). To provide clarity about the presence of aggregates the radii readings show an increase as a function of retention time. Therefore, the species are expanding as the molar mass rises.

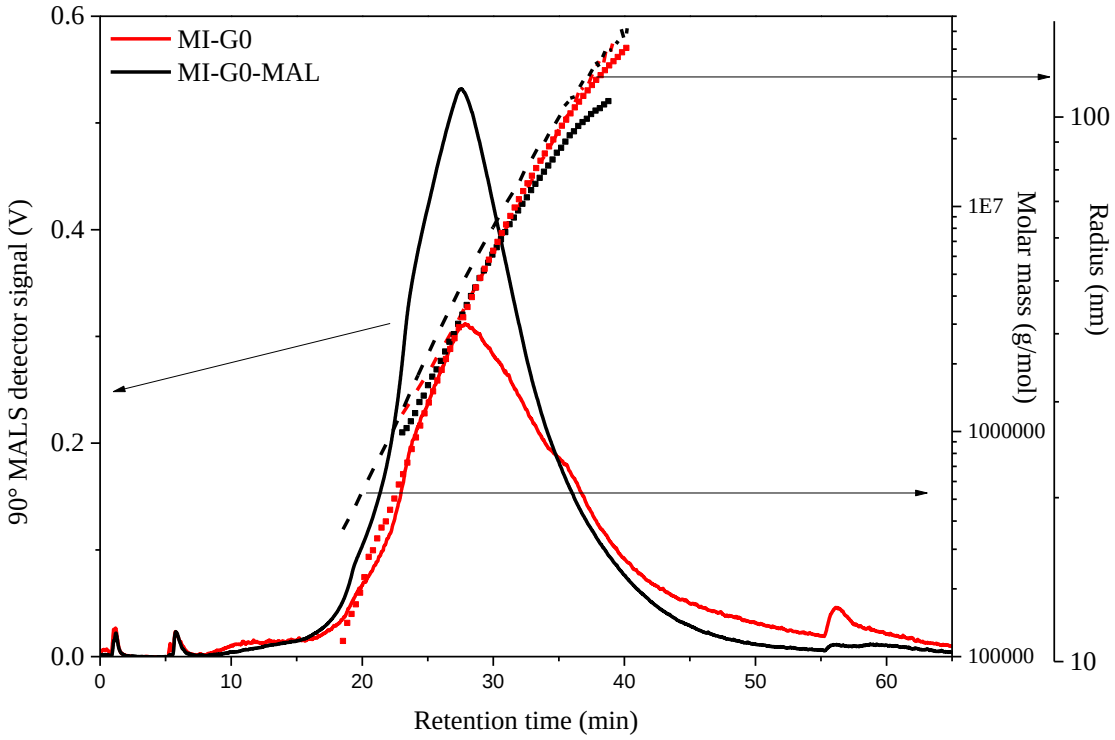

Figure 4.9. AF4 fractograms of MI-G0 and MI-G0-MAL; solid line (90° MALLS detector signals), dash line (radius) and symbols (molar masses) of MI-G0 (filled black square) and MI-G0-MAL (filled red triangle).

A comparison between the 90° MALLS detector signal of MI-G1-MAL and MI-G1-PEG-MAL is shown in Figure 4.10. The key difference between the 1st generation DenPols is the chemical composition of the dendrons, MI-G1-MAL has lysine dendrons and MI-G1-PEG-MAL has poly(ethylene glycol) (PEG) dendrons. The addition of PEG is generally to improve the biocompatibility of polymers, as it is non-toxic and non-ionic.[29,30] The difference in the dendron chemical composition provides insight into the role that the dendrons play in the aggregation behaviour. Theoretical molar mass calculations indicate that MI-G1-PEG-MAL has a larger molar mass than MI-G1-MAL. Therefore, the observed increase in the light scattering signal intensity of MI-G1-PEG-MAL is expected as a larger structure scatters more light. Upon lowering the cross flow to zero the remaining sample in the channel elutes without additional separation. An individual peak elutes with a low MALLS signal intensity, possibly because of interactions with

the membrane or non-specific adsorption. In the case of the radii readings, there is an expansion of the structure with elution time (see Figure 4.10).

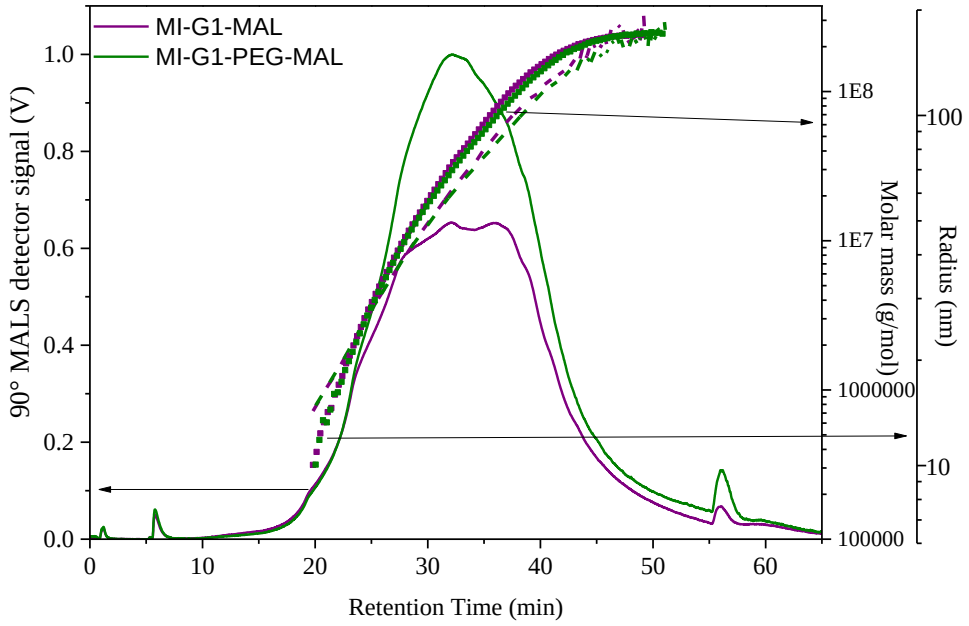

Figure 4.10. AF4 fractograms of samples MI-G1-MAL and MI-G1-PEG-MAL, solid line (90° MALS detector signals), dash line (radius) and symbols (molar mass) of MI-G1-MAL (filled purple square) and MI-G1-PEG-MAL (filled green triangle).

The fractograms and molar mass readings for MI-G0-MAL - MI-G3-MAL are shown in Figure 4.11. The fractograms clearly illustrate the broad molar mass distribution of the DenPols in 10 mM PBS. The glycopolymers from the 1st generation to the 3rd generation elute for the complete 40 min of the exponential flow decay. With an increase in the generation number there is expected to be an increase in the MALLS detector signal intensity due to the additional maltose moieties. However, MI-G2-MAL does not adhere to the same trend, which can be attributed to the difficulty with the dissolution as elevated temperatures were applied to obtain a visibly clear solution. The observation of the individual peak after the cross flow has been reduced to zero, is present for all generations. This agrees with SEC-MALLS measurements with the high molar mass shoulder. The molar mass of the later eluting species is greater than 1×10^9 g/mol and cannot be quantified as this high molar mass approaches the limit of the light scattering detector.

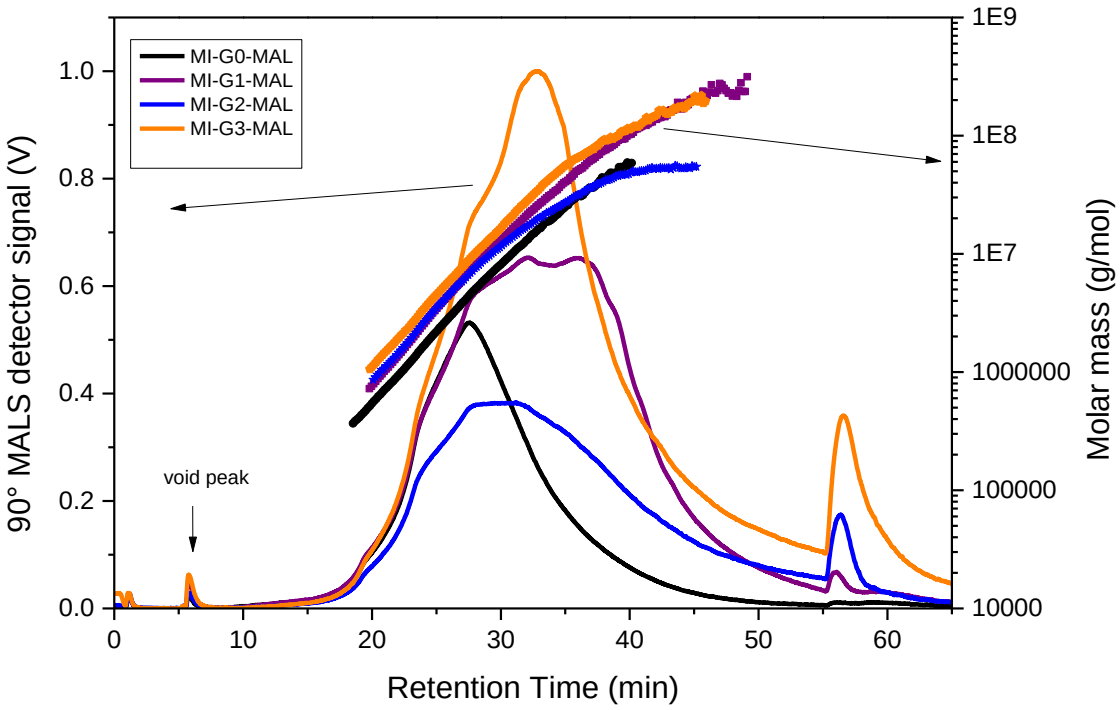

Figure 4.11. AF4 fractograms of MI-G0-MAL – MI-G3-MAL, solid line (90° MALS detector signals) and symbols (molar mass) of MI-G0-MAL (filled black circle), MI-G1-MAL (filled purple square), MI-G2-MAL (filled blue star) and MI-G3-MAL (filled orange pentagon).

The RI fractograms for the maltose-modified samples are shown in Figure 4.12. MALLS detector signals show high molar mass species eluting at approximately 55 min, however, there are no peaks present in RI detector response, suggesting that the concentration is too low to be detected.[31] The light scattering detector is more sensitive than the RI detector. There is a small peak after 55 min for MI-G3-MAL, suggesting that the amount of aggregates increases with higher generation number. It can be concluded that the aggregates (high molar mass species) are a marginal amount of the entire sample.

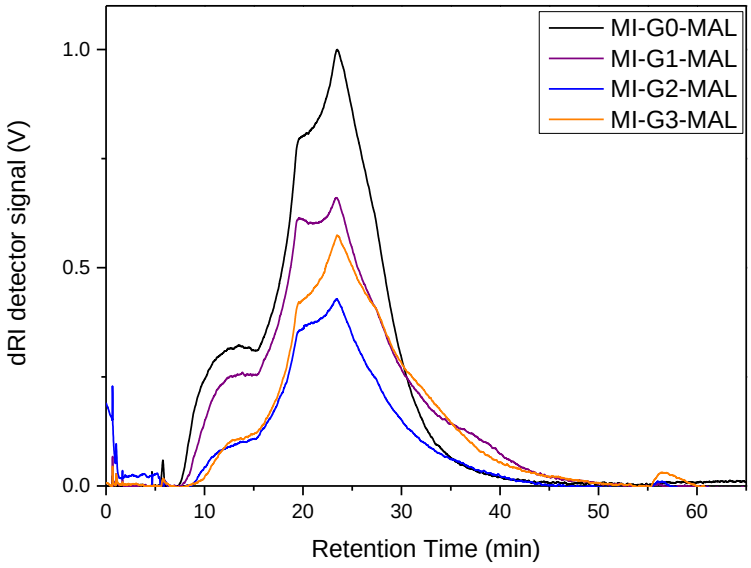

Figure 4.12. AF4 fractograms of MI-G0-MAL – MI-G3-MAL: solid line (RI detector signals) of MI-G0-MAL (black), MI-G1-MAL (purple), MI-G2-MAL (blue) and MI-G3-MAL (orange).

There is an increase in the radii with retention time seen in Figure 4.13. Larger structures with higher molar masses indicate that there are not only single macromolecules present in the species but clusters of single macromolecules. These observations suggest the formation of aggregates in the sample and the importance of fractionation for obtaining detailed information about the

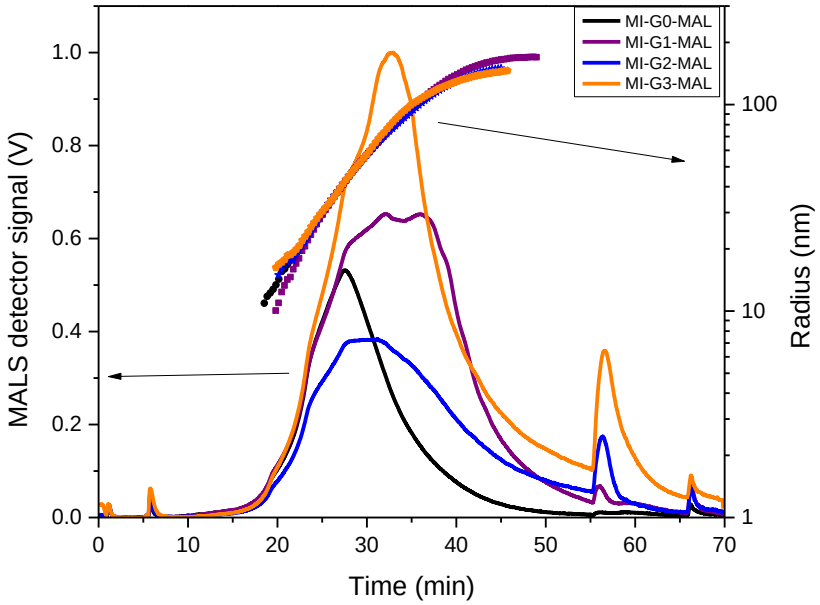

Figure 4.13. AF4 fractograms of MI-G0-MAL – MI-G3-MAL: solid line (RI detector signals) and symbols (Radius) of MI-G0-MAL (black), MI-G1-MAL (purple), MI-G2-MAL (blue) and MI-G3-MAL (orange).

samples.

4.4.3. Mathematical models for molar mass determination of DenPols

The combination of AF4 with MALLS in conjunction with a concentration detector enables the determination of absolute molar masses without using molar mass standards for calibration. To calculate molar masses, the Debye plot uses mathematical models to convert the light scattering response to molar mass and radius of gyration (R_g).

Table 4.4. The intercept and slope expressions for the Zimm and Berry models compiled from the Debye plot.

Model	Intercept	Slope $\left[sin^2\left(\frac{\theta}{2}\right) = 0\right]$
Zimm	M^{-1}	$\frac{16\pi^2(R_g)^2}{3\lambda^2 M}$
Berry	$M^{-\frac{1}{2}}$	$\frac{8\pi^2(R_g)^2}{3\lambda^2 M^{1/2}}$

The Zimm and Berry mathematical models in Table 4.4 indicate the intercept and slope expressions used to obtain the molar mass and radius of gyration readings from the MALLS and concentration detector signals. There are typically different errors with light scattering measurements that influence the precision of the molar mass and radius values.[32] The Berry extrapolation method is useful for large molecules whereas the Zimm method is for molecules in the range of 20-50 nm.[33] The mathematical extrapolations become challenging for large macromolecules compared to small molecules where a linear relationship can be assumed. To prove the importance of selecting the correct model, a comparison between the calculated molar masses obtained from Zimm and Berry models is examined for MI-G3-MAL and compared with the approximate theoretical molar masses calculated from SEC-MALLS-RI, see Table 4.5.

Table 4.5. Comparison between Berry and Zimm mathematical models for the calculation of molar mass and rdius of gyration for MI-G3-MAL.

Method	$M_{w,theoretical\ molar\ mass}$ (kg/mol)	M_w(kg/mol)	M_n(kg/mol)	R_g(nm)
Zimm	3 960	35 000	2 700	421
Berry	3 960	20 900	4 200	126

Generally, with all models there is an increase in error with larger polymers. The same data obtained from the light scattering detector are used but the quantification is dependent on the model used. The first observation is the large difference between the molar mass determined from the two plots, where M_w is 35 000 kg/mol (Zimm) compared to 20 900 kg/mol (Berry). Both values indicating pronounced aggregation in comparison to the theoretical molar masses. The Berry plot provides good accuracy for objects of different sizes and for large molecules with linear fits.[1] Generally, the Berry plot is used for polymers with molar masses greater than 500 kg/mol as a polynomial fit improves the accuracy for larger molecules, allowing accurate molar mass determinations.[34] The values obtained from the Berry plot provides a better accuracy for MI-G3-MAL with a molar masses above 500 kg/mol and thus was the chosen extrapolation method. In addition, the R_g reading of 421 nm is above the typical limitation of 50 nm polymer size for the Zimm plot.

4.4.4. Discussion of molar masses, radii, and conformations of DenPols.

DenPols are challenging to characterize as there chains are flexible but very large, these two features increase the difficulty of defining their dimensions.[35] The mathematical models provide the average values of the $R_{g,z}$, M_n and M_w which enables the interpretation of the overall conformation of the polymers. These average values can be directly compared with the theoretical molar mass values of the DenPols.

Table 4.6. Molar mass, dispersity, and radii values of DenPols determined from AF4-MALLS-DLS in 10 mM PBS.

	$M_{W,0,theoretical}$ (kg/mol)	$M_{w,AF4}$ (kg/mol)	M_n (kg/mol)	Đ (M_w /M_n)	$R_{g,z}$ (nm)	$R_{h,z}$ (nm)
MI-G0	~160	5 500	2 600	2.13	80.6 ± 15.0	54.2± 15.6
MI-G0-Mal	~530	3 800	1 200	3.12	71.8 ± 1.6	48.5± 1.6
MI-G1-Mal	~1 020	15 200	2 600	9.33	122.1 ± 2.1	62.1± 4.9
MI-G1-PEG-Mal	~1 260	17 100	2 200	7.61	117.7 ± 0.6	65.6± 1.1

MI-G2-Mal	~2 040	13 200	3 100	9.94	101.1 ± 5.5	69.6± 8.3
MI-G3-Mal	~3 960	20 900	4 200	4.8	126.0 ± 7.5	56.3± 5.5

For clarity, the $R_{g,z}$ value is the z-average of the entire peak. Average molar masses and radii values in Table 4.6 were calculated with the Berry mathematical model from AF4-MALLS-DLS measurements. Average molar mass is crucial to provide a comprehensive understanding of the properties of DenPols. There is an increase in M_n with the generation number of the maltose-decorated glycopolymers. This increase is expected as the number of maltose units rises exponentially with generation number. All the DenPols experimental molar mass readings are larger than the theoretical molar mass values, indicating the presence of aggregates in the species. Surprisingly, the experimental M_w of MI-G0 is very large compared to the theoretical molar mass of 160 kg/mol. The primary distinction between MI-G0 and MI-G0-MAL are the maltose units along the polymer chain. The end groups of the MI-G0 structure is a triflate (negative charge) and an amine (positive charge) group. Triflate stabilization is owed to the resonance stabilization and the negative charge is spread over the three oxygen atoms.[36] The amine group has a cationic charge that is no longer shielded by the maltose shell. The amine group could possibly form strong intermolecular interactions, this could result in the suspected aggregation.

It is evident that the experimental molar mass of all the DenPols is greater than the theoretical molar mass, suggesting suspected aggregation in the species. It would be expected that the highest generation DenPol, in this case MI-G3-MAL, with most available H-bond sites would form stronger intermolecular interactions and therefore be more likely to form aggregates. The dispersity's (M_w/M_n**)** are all greater than 1 indicating a heterogenous molar mass distribution, which corroborates with the broad elution peaks.

There is no distinct trend in the $R_{g,z}$ and $R_{h,z}$ values, with an increase in generation number. The $R_{g,z}$ values of MI-G0-MAL, MI-G2-MAL, and MI-G3-MAL increase with generation number. The $R_{g,z}$ value of MI-G1-MAL is similar to MI-G3-MAL, indicating larger clusters of MI-G1-MAL. However, $R_{h,z}$ of MI-G1-MAL, MI-G1-PEG-MAL and MI-G2-MAL is slightly larger than MI-G3-MAL.

The large differences between the experimental and theoretical molar mass values, motivated the evaluation of the aggregation number.

4.4.5. Analysis of the DenPols aggregation number ($M_w/M_{w,0}$)

The aggregation number illustrates the number of single macromolecules present in an aggregate. The aggregation number of the macromolecules can be calculated by dividing the experimental M_w (listed in Table 4.6) by the theoretical molar mass of a single macromolecule (listed in Table 4.6). The aggregation numbers of the DenPols are presented in Table 4.7, with none of the DenPols present as single macromolecules.

Table 4.7. The aggregation number ($M_w/M_{w,0}$) determined from the experimental weight-average molar mass readings and the theoretical molar mass values of the DenPols: MI-G0, MI-G0-MAL, MI-G1-MAL, MI-G1-PEG-MAL, MI-G2-MAL and MI-G3-MAL in 10 mM PBS.

Sample	**Aggregation number ($M_w/M_{w,0}$)**
MI-G0	34
MI-G0-MAL	7
MI-G1-MAL	15
MI-G1-PEG-MAL	15
MI-G2-MAL	6
MI-G3-MAL	5

Noticeably, MI-G0 has a large aggregation number of 34 that suggests there is pronounced aggregation, as stable aggregates are formed that are not destroyed due to slight shear in the channel. The trend in Table 4.7 indicates a decrease in the aggregation number with an increase in the generation number except for the 1st generation DenPols, with an aggregation number of 15. MI-G3-MAL has an aggregation number of 5 suggesting marginal aggregation compared to the lower generation DenPols. The decrease in the aggregation suggests that the aggregates of MI-G2-MAL and MI-G3-MAL are not stable and are possibly destroyed by minimized shear during elution or by the elevated temperatures required for dissolution. Alternatively, the respective conformations of MI-G2-MAL and MI-G3-MAL are not suitable for aggregate formation. In contrast, 1st generation DenPols form stable aggregates even when exposed to high cross flow. It was expected that with an increase in the number of functional groups there is more hydrogen

bonding leading to stable associates. To provide clarity on the aggregation mechanism the apparent density will be evaluated.

4.4.6 Analysis of the DenPols apparent density

The high aggregation number of the DenPols requires more knowledge to clearly understand the aggregation mechanism. To understand the aggregation mechanism the apparent density parameter was evaluated. The apparent density calculation is explained in equations 27 and 28. This parameter provides information regarding the non-aggregated and aggregated structures present in the species. The apparent density calculations were performed with R_g and molar mass data obtained from AF4-MALLS measurements (see Table 4.6).

Figure 4.14 reveals a change in the apparent density as a function of molar mass for MI-G0. The apparent density moves from a maximum of approximately 12 kg/m^3 to a minimum of approximately 6 kg/m^3 with a slight increase at ultrahigh molar masses. The change in the apparent density suggests a change in the compactness of MI-G0 with an increase in the molar mass; this suggests that there are clusters of single macromolecules at high molar masses. These observations provide an explanation for the high average molar mass values.

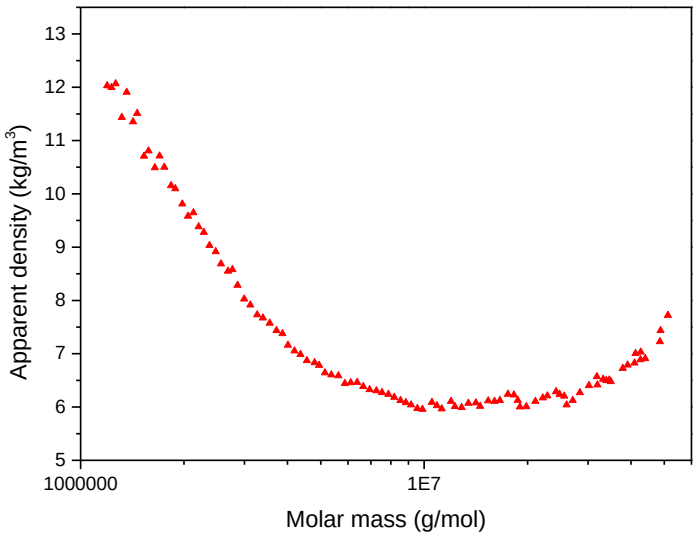

Figure 4.14. Apparent density vs the molar mass of MI-G0, calculated based on data from AF4-MALLS.

It is observed that the apparent density of MI-G1-MAL and MI-G1-PEG-MAL is larger compared to MI-G0, see Figure 4.15. The maximum apparent density of MI-G1-MAL is approximately 130

kg/m^3 and for MI-G1-PEG-MAL it is approximately 60 kg/m^3. An explanation for this observation is that a higher apparent density is also related to a polymer with higher branching density compared to a polymer that is less branched.[8] An example is with amylopectin (an α(1→ 4) glucan) which has a lower degree of branching and exhibits a considerably lower apparent density compared to glycogen (α(1→ 6) glucan) with a higher degree of branching.[8,15]

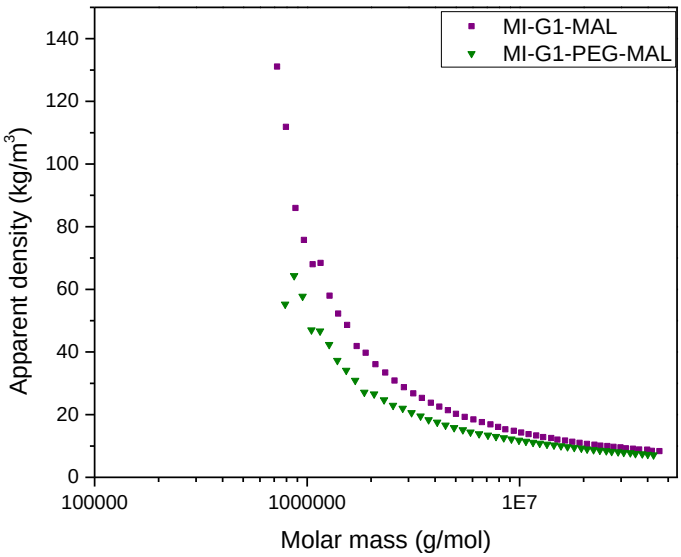

Figure 4.15. Apparent density of MI-G1-PEG-MAL and MI-G1-MAL over the molar mass distribution, calculated based on data from AF4-MALLS.

For both MI-G1-MAL and MI-G1-PEG-MAL there is a similar dependence on molar mass as there is a decrease in the apparent density with an increase in the molar mass in Figure 4.15. However, MI-G1-PEG-MAL has a lower apparent density than MI-G1-MAL. This observation can be attributed to the high hydrophilicity of poly(ethylene oxide) (PEO) present in the dendrons, the PEO can stretch the dendrons away from the backbone, leading to a lower apparent density of the single macromolecules or less dense, hydrogel-like aggregates.

The apparent density values of MI-G0-MAL, MI-G1-MAL, MI-G2-MAL, and MI-G3-MAL can be seen in Figure 4.16. All the DenPols display a similar aggregation mechanism, starting with a high apparent density and decreasing towards ultrahigh molar masses. Interestingly, MI-G1-MAL has a maximum apparent density of 130 kg/m^3 compared to MI-G3-MAL of 40 kg/m^3, with the greatest branching density. Towards higher molar masses, the apparent density of MI-G3-MAL is larger than MI-G1-MAL.

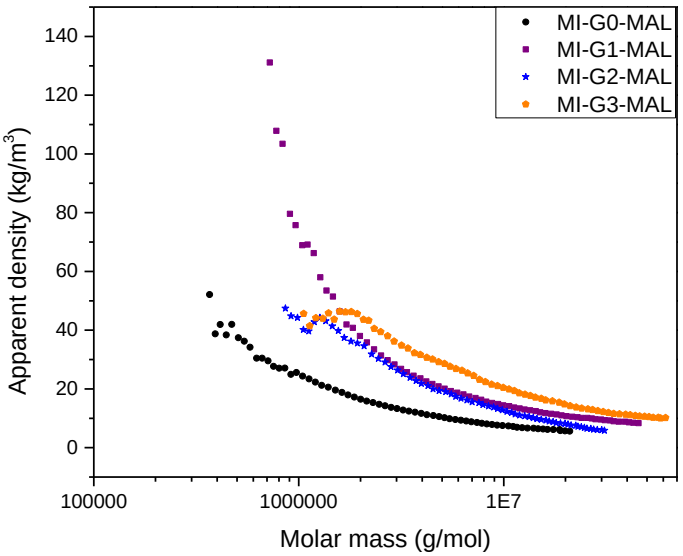

Figure 4.16. Apparent density over the molar mass distribution of MI-G0-MAL (solid black circle), MI-G1-MAL (solid purple square), MI-G2-MAL (solid blue star) and MI-G3-MAL (solid orange pentagon).

Nonetheless, the apparent density confirms that at lower molar masses there are non-aggregated structures, suspected to be the single macromolecules. Towards higher molar masses there are aggregated structures formed from clusters of single macromolecules. The apparent density provides information regarding the aggregation of the structures but not the conformation of the DenPols. To describe the shape of the aggregates, the physical parameters determined from AF4-MALLS-DLS measurements will be evaluated.

4.4.7 Analysis of the conformation of DenPols by applying the shape factor (R_g/R_h)

The ratio between R_g and R_h is the ρ parameter, or the shape factor, providing insight about the conformation and shape of respective species. Burchard et al.[37,38] showed that certain ratios correspond to particular shape factor values. For a homogenous sphere it is 0.775, for elongated (rod-like) structures the value is 2 and for macromolecules it is between 1 and 2. The shape factor for a hyperbranched polymer is 1.23. When the shape factor is smaller than 0.7, the species are considered swollen macromolecules, for example microgels. DenPols are categorized as branched macromolecules and thus the shape factor is expected to be between 1 and 2.

The average R_g and R_h were used to calculate the average shape factor value of the DenPols, see Table 4.8. As anticipated the average shape factors are in the range of 1 and 2, with values closer to 1 as spherical structure and values towards 2 as elongated structures. The broad size distribution and complexity of the structure results in shape factors for each DenPol varying from a linear random coil polymer to a randomly branched polymer. Interestingly, MI-G1-MAL shows an architecture corresponding to an elongated structure, which suggests an anisotropic shape. More rigid, rod-like architectures are typical for third generation DenPols with larger branching density.[39,40] The increased branching density restricts the flexibility of the polymer backbone resulting in a more rigid structure. MI-G0 and MI-G0-MAL ratio values are representative of linear chain random coils.[37]

Table 4.8. The average shape factor (R_g/R_h) calculated for MI-G0, MI-G0-MAL, MI-G1-MAL, MI-G1-PEG-MAL, MI-G2-MAL and MI-G3-MAL with radius values obtained from AF4-MALS-DLS measurements.

DenPols	**Shape factor (R_g/R_h)**
MI-G0	1.50
MI-G0-MAL	1.48
MI-G1-MAL	1.97
MI-G1-PEG-MAL	1.79
MI-G2-MAL	1.45
MI-G3-MAL	1.72

These average values provide the shape of the DenPols. To have a clear description of the entire sample, the shape factor as a function of molar mass was determined. The shape factors over the molar mass distribution of MI-G0, MI-G0-MAL, MI-G1-MAL, MI-G1-PEG-MAL, MI-G2-MAL, and MI-G3-MAL are represented in Figure 4.17. All the DenPols were in the region between 1 and 2 expected for macromolecules. The region corresponds to a broadly distributed linear coil or to a randomly distributed macromolecule. An exception is MI-G3-MAL where ratio values begin at approximately 0.7 suggesting a hard sphere conformation at lower molar masses. The broad molar mass region is due to the polydispersity and complexity of hyperbranched polymers. What is striking is that as the molar masses of the DenPols increase, there is a tendency towards

anisotropy, which corresponds to values greater than 2. Anisotropy is typical for a rod-like object with an axial ratio of 25 that has a R_g/R_h ratio of 2.1.[8] This shape was seen for xanthan gum or mesaquite gum in solution.[37] However, the R_g/R_h of the DenPols does not surpass 2, thus, the structures are elongated but pure anisotropic conformations are not achieved. The transition of conformations can be attributed to the formation of clusters of DenPols, thereby forming aggregates, which agrees with the apparent density. Nilsson et al.[6] reported a similar change in the conformation of casein micelles where the micelles existed as hard spheres and formed clusters of aggregates with an elongated rod-like conformation. Literature has shown that depending on the generation number the conformation can change from a Gaussian coil to rod-like.[41] Thus, it is also possible that DenPols can exist with populations that have different conformations. The apparent density calculations correspond to the idea that elongated aggregates are formed from linear branched random coils except for MI-G3-MAL.

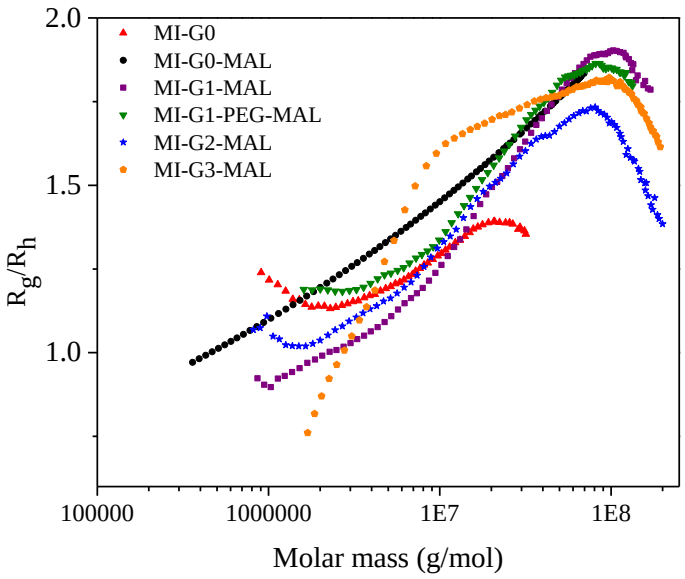

Figure 4.17. Shape factor (R_g/R_h) values of MI-G0 (solid red triangle), MI-G0-MAL (solid black circle), MI-G1-MAL (solid purple square), MI-G1-PEG-MAL (solid olive reverse triangle), MI-G2-MAL (solid blue star) and MI-G3-MAL (solid orange pentagon) over the molar mass measured by AF4-MALLS-DLS.

4.4.7 Analysis of the conformation plots of DenPols

The wealth of information obtained from the fractionation process with AF4-MALLS-DLS allows for the analysis of many parameters. To complement the values obtained for the shape factor, the

scaling law was applied. The slope of the plot log (R_g) vs log (M) is the scaling factor parameter. All the conformation plots were plotted with a linear best fit and a correlation factor of 0.95.

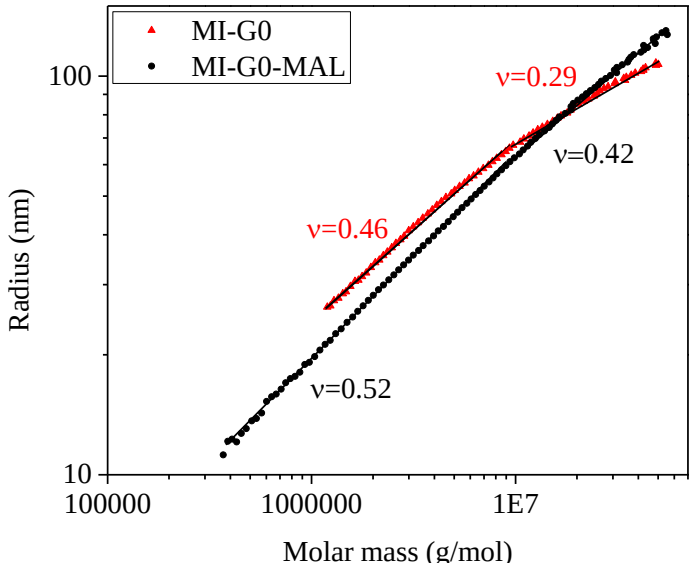

Figure 4.18. R_g over the molar mass determined from AF4-MALLS measurements for MI-G0 (solid red triangle) and MI-G0-MAL (solid black circle) in 10 mM PBS.

The conformation plot for MI-G0 and MI-G0-MAL can be split into two sections for low and high molar mass structures, as seen in Figure 4.18. At lower molar masses, below 1×10^7 g/mol, the behaviour of the slope is linear, for MI-G0 the slope is 0.46 and MI-G0-MAL the slope is 0.52. According to the scaling law these values are indicative of a random coil macromolecule. This is followed by a deviation in the slope with high molar masses for MI-G0, as the slope is 0.29 corresponding to sphere-like shape. There is only a slight decrease for MI-G0-MAL to 0.42, corresponding to a conformation between coil-like and a hard sphere, leaning towards coil-like shape. Therefore, sphere-like clusters are formed from random coil single macromolecules.

A comparison between the conformation plots of MI-G1-MAL and MI-G1-PEG-MAL is displayed in Figure 4.19. The nanostructures of the 1st generation are interesting as the linearity deviates in two instances. The slope indicates that the conformation goes from coil-like to a dense sphere shape with a decreased slope of 0.18 towards higher molar masses. This suggests that sphere-like aggregates are formed from coil-like objects.

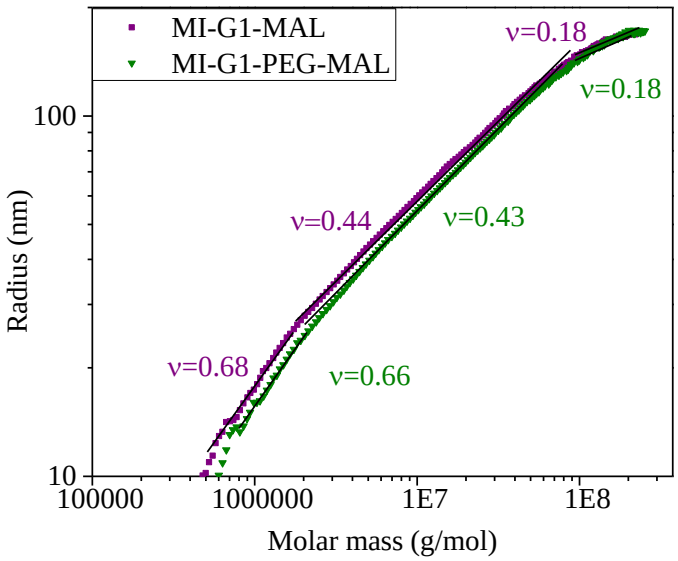

Figure 4.19. R_g over the molar mass determined from AF4-MALS measurements for MI-G1-MAL (solid purple square) and MI-G1-PEG-MAL (solid olive inverted triangle) in 10 mM PBS.

Figure 4.20 shows the conformation plot of MI-G3-MAL with similar linearity deviations to the lower generations, but the deviation occurs at a higher molar mass of 1×10^8 g/mol. The scaling parameter of MI-G2-MAL is 0.46 at low molar masses and the slope deviates to 0.73 with higher molar masses. The scaling parameter corresponds to a coil-like conformation for single macromolecules towards rod-like conformation for aggregates. The deviation in the scaling parameter for MI-G2-MAL corresponds to the values obtained from the shape factor, as elongated aggregates form from random coil single macromolecules.

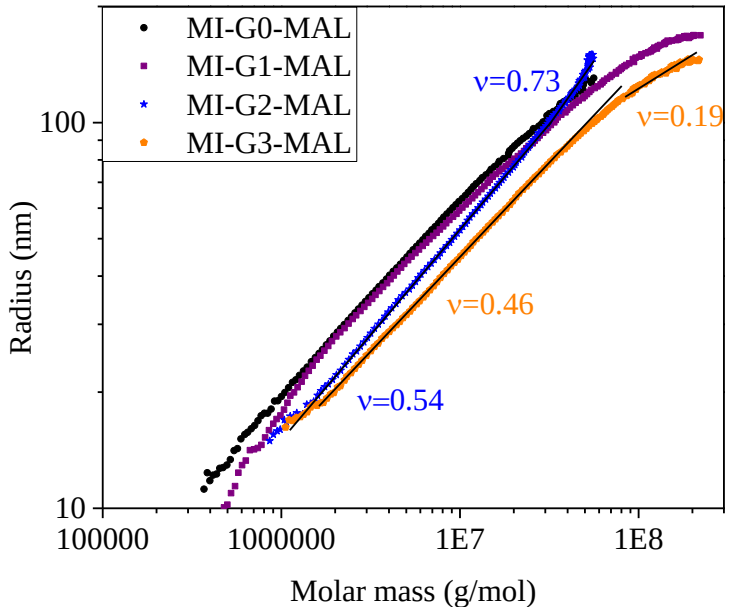

Figure 4.20. R_g over the molar mass determined from AF4-MALLS measurements for MI-G0-MAL (solid black circle), MI-G1-MAL (solid purple square), MI-G2-MAL (solid blue star) and MI-G3-MAL (solid orange pentagon) in 10 mM PBS.

The low molar mass values obtained for the macromolecules from the scaling law agree with the shape factor ratios, confirming that single macromolecules have a random coil-like conformation. Contrary to the low molar mass regions, the high molar mass conformations are more sphere-like and rather compact according to the scaling law. The deviation in the construction of a conformation plot is dependent on the measured molar mass and radii values, each introducing errors. The combination of errors in the two values can lead to deviations in the conformation plot.[34] The error for shape factor values is ± 0.1, this error is important when determining whether an object is a dense sphere or a microgel in the case of MI-G3-MAL. In the case of determining whether an object is sphere-like or rod-like, the error is of critical importance.

4.4.8. Analysis of human serum albumin with AF4-MALLS-DLS

Human serum albumin (HSA) is a model protein with a molar mass of 66.5 kDa and a hydrodynamic radius of 3.51 nm.[42–44] The small size of HSA prevents the analysis of R_g with AF4-MALLS as it results in isotropic scattering for values smaller than 10 nm, thus only the molar mass values were measured. To measure the size of HSA, online DLS and offline batch mode DLS were used.

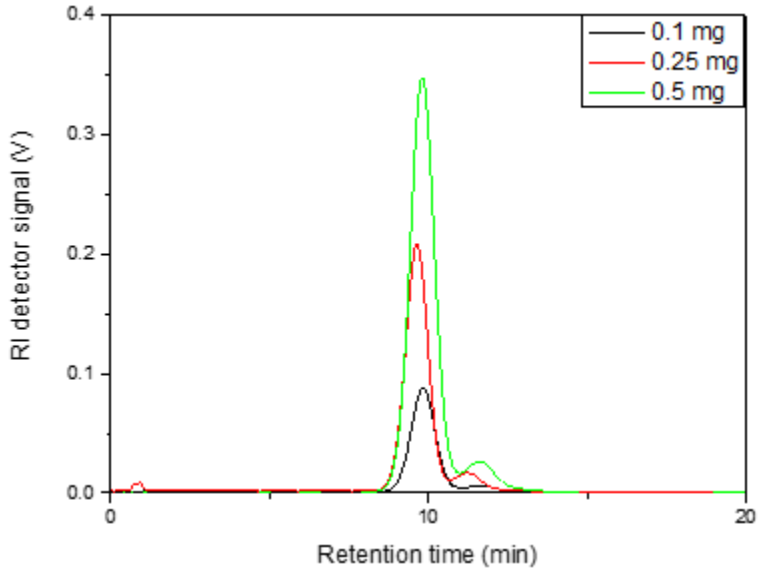

Figure 4.21. Fractograms of HSA, RI detector signal of different concentrations of HSA in 10 mM PBS.

The RI detector signals of different concentrations of HSA are shown in Figure 4.21. It can be observed that with an increase in the concentration there is an increase in the RI detector signal. There are two visible species identified as the monomer and the dimer of HSA.[43] The presence of two species are observed in the MALLS detector signal, see Figure 4.22. For the molar mass measurements, the Zimm mathematical extrapolation was used as HSA is a protein smaller than 50 nm.[45] The peaks elute during the isocratic cross flow of 3 mL/min. There is a constant molar mass reading over the monomer peak, see Figure 4.22.

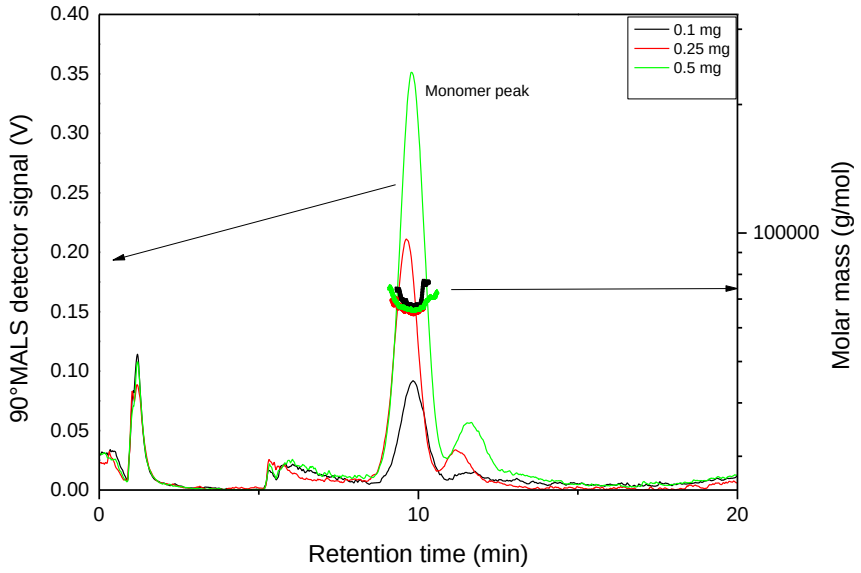

Figure 4.22. Fractograms of HSA, 90° MALLS detector signal of different concentrations of HSA and the measured molar mass readings from AF4-MALLS-DLS measurements.

As seen in Table 4.9 the average molar mass values are in good agreement with the literature value of 66.5 kDa. Concentration-dependent aggregation can be ruled out. The online DLS measurements are between 4.3 and 4.9 nm, which is close to the literature value of 3.51 nm. The dispersity is 1.00, corresponding to a monodisperse/uniform protein.

Table 4.9. Molar mass, dispersity, hydrodynamic radius values at different concentrations of HSA in 10 mM PBS.

Concentration of HSA (mg/mL)	M_w **(kg/mol)**	M_n **(kg/mol)**	$Đ$ (M_w/M_n)	$R_{h,z}$ **(nm)**	$R_{h,batch\ mode\ DLS}$ **(nm)**
0.1	69.8	69.8	1.00	4.3	4.8

0.25	66.3	66.3	1.00	4.9	8.1
0.5	66.5	66.5	1.00	4.5	4.2

The comprehensive analysis of the individual DenPols and HSA was successfully achieved and thus mixtures can be evaluated with AF4-MALLS-DLS.

4.5 Analysis of DenPols and HSA with AF4-MALLS-DLS

To address the need for alternative characterization techniques for studying the interactions between DenPols and HSA, advanced AF4 will be applied. The interactions were investigated by analyzing the changes in molar mass, size, apparent density, and conformation of the DenPol-HSA complexes. Method B was implemented, as used for the individual components, to ensure that fractograms of the DenPols and the mixtures could be compared. Interactions between DenPols with and without sugar moieties and HSA were studied. This was performed by preparing mixtures of DenPols and HSA. The concentration of 1 mg/mL of DenPol was maintained with the increase in the fraction of HSA. The three different masses of HSA added to the 1 mg/mL solution was 0.1, 0.25, and 0.5 mg. The mixtures of DenPols: HSA were in the ratio (1:0), (1:0.1), (1:0.25) and (1:0.5).

MI-G0 with HSA

The complexity of analyzing MI-G0 and HSA is caused by the strong tendency of MI-G0 to form clusters of single macromolecules. The addition of HSA to MI-G0 shows a visible shift of the peak to a later position, illustrated in the MALLS detector signal, see Figure A.1. The RI detector signal shows species eluting after 55 min that make a marginal portion of the sample. It is proposed that the cationic charge of the amino group of MI-G0 and the anionic charge of HSA in neutral aqueous conditions form electrostatic interactions resulting in pronounced aggregation, especially with the absence of the maltose shell to shield the cationic charge.

The determination of molar mass and radius of gyration were not possible for mixtures MI-G0: HSA (1: 0.25) and (1:0.5) as the light scattering signal was low and attempts to obtain a suitable model and fit order for the data was unsuccessful. Thus, only the molar masses for MI-G0 and MI-

G0: HSA (1:0.1) were determined and listed in Table A.1. The addition of HSA led to the increase in M_w, R_g and R_h, indicating electrostatic interactions leading to expanded MI-G0 – HSA complexes with higher molar masses.

MI-G0-MAL with HSA

Figure A.2 shows the MALLS, RI detector signal and molar mass readings. It is evident that there are no changes in the position of the main peak maximum at 27.52 min. There is a decrease in the peak intensity and the peak is slightly narrower for the complexes, showing a less polydisperse DenPol-HSA complex in comparison to MI-G0-MAL. At later elution times, after 55 min, there is a peak with an increased light scattering intensity of the MI-G0-MAL: HSA (1:0.5) mixture. However, there is no peak in the RI detector signal for the species eluting after 55 min. As the retention time increases there is an increase in the molar mass for all mixtures

From the AF4 fractograms it is evident that the peaks of the mixtures are narrower than the peak of the individual MI-G0-MAL. This is demonstrated by the slight smaller dispersity value in Table A.2. The changes in the average molar masses are small. R_g decreases after the addition of HSA indicating a more compact structure, these observations highlight that the interactions between MI-G0-MAL and HSA have an influence on the molecular parameters.

Interactions of HSA with unmodified MI-G0 are stronger than MI-G0-MAL due to the cationic charge on the surface of MI-G0. Maltose on the exterior of the DenPols has a neutral surface but more H-bond active sites compared to MI-G0. The electrostatic interactions between HSA and MI-G0 could form more stable complexes and thus more defined changes are observed in the AF4 fractogram of MI-G0 as compared to MI-G0-MAL.

MI-G1-MAL with HSA

No changes in the position of the MALLS detector signal are observed for MI-G1-MAL: HSA (1:0.1), (1:0.25) and (1:0.5), see Figure A.3. The molar mass readings increase with retention time, indicating a species with varying distributions. The RI detector signal intensity for MI-G1-MAL decreases with the introduction of HSA to the system, less sample is eluting, which can be attributed to numerous factors, such as long focus time or high cross flow, forcing interactions with the semi-permeable membrane.[46] The latter is least likely as there is no peak observed after the cross flow is reduced to 0 mL/min. A reduction in the cross-flow rate could improve the

recovery but this will influence the retention of the non-bound HSA and the resolution. Despite the decrease in the peak intensity, the AF4 protocol was reproducible.

Average molar mass readings decrease with the addition of HSA to MI-G1-MAL as seen in Table A.3. A decrease in the molar mass suggests that HSA disrupts the formation of DenPol-DenPol aggregates. There were marginal deviations in the size of the mixtures compared to individual MI-G1-MAL.

MI-G1-PEG-MAL with HSA

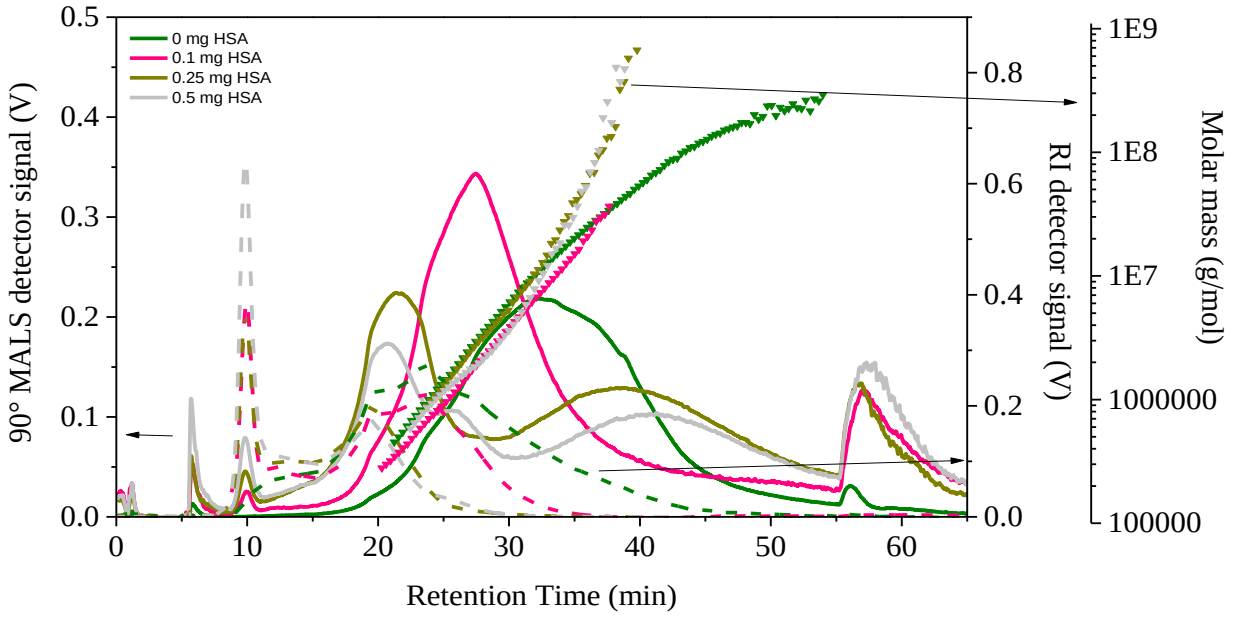

Figure 4.23. Different mixtures of MI-G1-PEG-MAL and HSA in 10 mM PBS measured with AF4-MAL: 90° MALS detector signal with molar masses and RI detector signal. MI-G1-PEG-MAL: HSA (1:0) green solid line, (1:0.1) pink solid line, (1:0.25) brown solid line and (1:0.5) grey solid line.

Introduction of PEG dendrons to the 1st generation DenPols leads to a noticeable increase in the void peak for MI-G1-PEG-MAL: HSA (1: 0.5) because of an insufficient focus time preventing the complete relaxation of the species.[26] However, increasing the focus time can lead to the formation of aggregates. PEG chains are non-ionic, this should lead to non-specific hydrogen bonding interactions with HSA.[47] Figure 4.23 shows the fractograms of MI-G1-PEG-MAL with different amounts of HSA exhibiting unique behaviour in comparison to the lysine-maleimide DenPols. Multimodality is observed for the MALLS detector signal with the incremental addition of HSA. A possible explanation for the multimodality is that during the synthesis of MI-G1-PEG-

MAL, complete modification of the dendrons with the maltose shell was not achieved. Therefore, macromolecules with different degrees of maltose modification and unmodified PEG-moieties are present in the species. These different species form different interactions with HSA leading to the multimodality in the MALLS detector signal. Thus, macromolecules without a maltose shell contain PEG dendrons that are essentially exposed to HSA. The RI detector intensity is low at positions beyond 55 min. Additionally, the peak shifts to earlier retention times with the addition of HSA indicating the elution of species with faster Brownian motion. The presence of HSA could disrupt the suspected aggregation of MI-G1-PEG-MAL forming DenPol-HSA complexes instead of DenPol-DenPol.

Table 4.10. Molar masses, dispersities, radii and dn/dc values determined of MI-G1-PEG-MAL with different ratios of HSA measured with AF4-MALS-DLS.

Mass of HSA (mg)	M_n **(kg/mol)**	M_w **(kg/mol)**	**Đ** (M_w/M_n)	$R_{g,z}$ **(nm)**	$R_{h,z}$ **(nm)**	dn/dc **(mL/g)**
0	2 200	17 100	7.6	117.6± 0.6	62.2± 1.1	0.153
0.1	1 300	3 000	2.3	49.9± 1.9	52.2± 8.7	0.156
0.25	1 400	2 800	2.0	53.5± 8.8	70.9± 15.1	0.156
0.5	1 200	1 700	1.4	43.8± 5.7	99.0± 7.3	0.156

Surprisingly, the molar mass and radius values of the complexes are smaller than MI-G1-PEG-MAL in Table 4.10. With the pronounced aggregation there is a sharp increase in the molar mass exceeding 1×10^9 g/mol for the later eluting peaks. AF4-MALLS can separate a broad range of ultrahigh molar mass samples but when the molar mass values exceed 1×10^9 g/mol the light scattering measurements are no longer reliable.[1] This is a plausible explanation for the observed decrease in the molar mass readings. Thus, no conclusions can be made regarding the molecular parameters. The MALLS detector signal shows a narrower peak for the mixture of MI-G1-PEG-MAL: HSA (1:0.1) and agrees with the dispersity of 2.3.

MI-G2-MAL with HSA

Once again, the void peak shows an increased intensity with the addition of HSA, see Figure A.4. As mentioned, this can be due to insufficient relaxation time or large species ($> 1\,\mu m$). It is evident that there is a change in the peak shape and intensity of the MALLS detector signal of MI-

G2-MAL with the addition HSA. The broadly distributed peak becomes narrower for the mixtures and retention increases. After 40 min, the mixture of MI-G2-MAL: HSA (1:0.1) shows a steep increase to higher molar mass.

$R_{g,z}$ and $R_{h,z}$ of MI-G2-MAL is constant after the addition of HSA. The molar mass readings of MI-G2-MAL in Table A.4 remain constant. The decrease in the MALLS signal intensity for increasing HSA introduced difficulties with the quantification using the Berry extrapolation method. The polynomial degree of 2 was implemented to improve the fit.

MI-G3-MAL with HSA

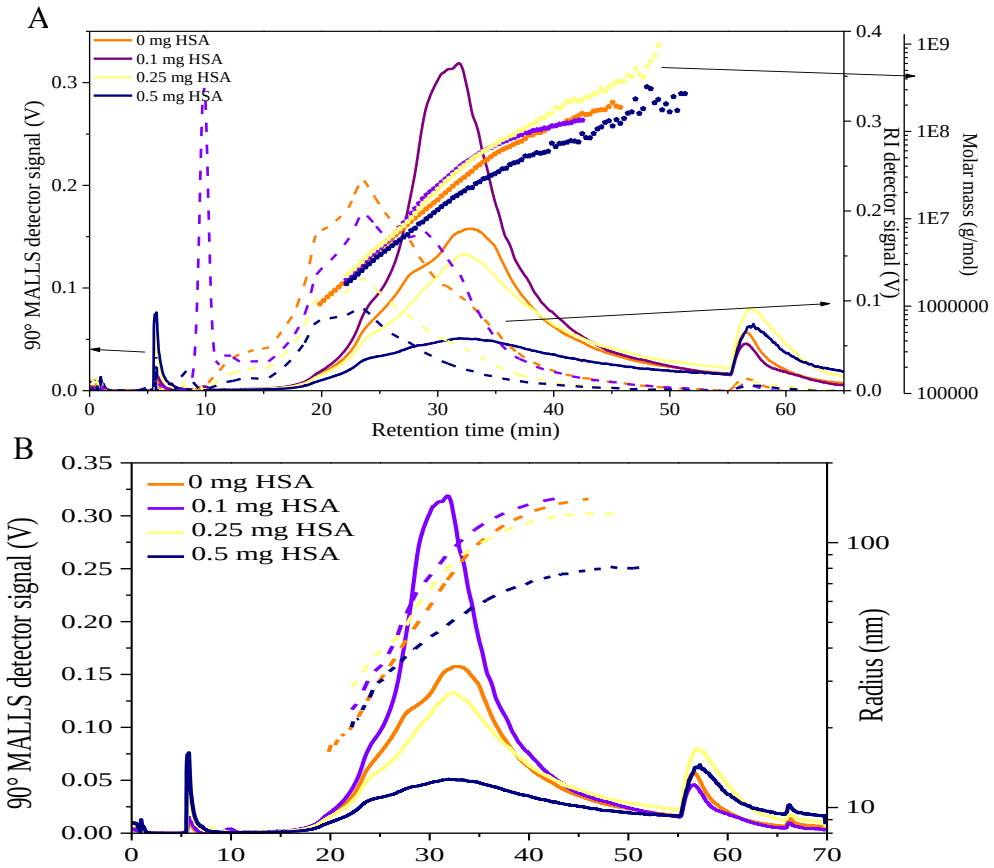

Figure 4.24. Different mixtures of MI-G3-MAL and HSA in 10 mM PBS measured with AF4-MALS, A) 90° MALLS and RI detector signal with molar mass reading, B) 90° MALLS detector signal with radii reading.MI-G3-MAL: HSA (1:0) orange solid line, (1:0.1) purple solid line, (1:0.25) yellow solid line and (1:0.5) navy solid line.

Figure 4.24 A shows a low RI signal intensity for MI-G3-MAL: HSA (1:0.5) that can be attributed to the formation of precipitates after stirring the mixture for 24 hours. With the addition of HSA, a precipitate formed at the bottom of the vial, therefore, larger sized species in the sample were

not injected. The radii of MI-G3-MAL: HSA (1:0.5) plateau below 100 nm compared to the larger radii readings of MI-G3-MAL: HSA (1:0.1) and (1:0.25), see Figure 4.24 B. The reduction of the cross flow to 0 mL/min shows large size species eluting. The RI signal intensity is low for the later eluting species and indicates only a small portion of the species.

Table 4.11 shows the molar masses, dispersities, and radii readings of MI-G3-MAL: HSA (1:0.1), (1:0.25) and (1:0.5). With the addition of 0.1 mg of HSA there is an increase in the M_n to 7 600 kg/mol and M_w to 26 200 kg/mol. The increase in the molar mass can be attributed to a large number of maltose moieties along the polymer backbone with more hydrogen bond sites, and that oligosaccharides can form non-specific hydrogen bonds with HSA.[47] Therefore, more HSA on the surface of the maltose shell results in higher molar masses and larger sizes, displayed in Table 4.11.

Table 4.11. Molar mass, dispersity and radii readings determined for MI-G3-MAL with different ratios of HAS, measured with AF4-MALS-DLS.

Mass of HSA (mg)	M_n **(kg/mol)**	M_w **(kg/mol)**	**Đ** (M_w/M_n)	$R_{g,z}$ **(nm)**	$R_{h,z}$ **(nm)**	**dn/dc (mL/g)**
0	4 100	18 000	4.4	98.0 ± 7.5	53.8± 5.5	0.153
0.1	7 600	26 200	3.5	105.3± 0.7	51.6± 5.9	0.156
0.25	6 600	31 000	4.7	103.7± 1.7	92.8± 23.0	0.156
0.5	6 500	23 000	3.54	129.4± 3.2	78.6± 15.3	0.156

The fractograms for MI-G0-MAL and MI-G1-MAL show minimal changes with the addition of HSA. This is expected as literature has shown that lower generations of maltose-modified glycodendrimers have a lower binding affinity.[47,48] This is due to several parameters that are essential for the binding of HSA, for instance the size, shape, and available sites to form hydrogen bonds. In contrast, MI-G0 showed significant changes in the peak shape and position of the peaks with the formation of DenPol-HSA complexes. MI-G2-MAL showed minimal deviations in molar mass and size. With increased amounts of HSA added to MI-G3-MAL there was precipitation, indicating the formation of large aggregates.

4.5.1 Analysis of the apparent density of DenPol-HSA complexes

To understand the aggregation mechanism and compare the mechanism to the individual DenPols, the apparent density was calculated using the R_g and molar mass data obtained from AF4-MALLS.

The apparent density over the molar mass of MI-G0-MAL and MI-G1-MAL is represented in Figure 4.25 A and B. A decline in the apparent density is displayed for the individual DenPols and the DenPol-HSA complexes, representative of the progression from non-aggregated to aggregated structures. This was observed with the average molar mass and radius readings (Table A.1 and A.2) as there were minimal changes. The decrease in the calculated apparent density with molar mass is usually representative of aggregation or the formation of network-like structures. Network-like structures are generally exhibited by hydrogels with the internal structure having a lower density.[49]

In contrast to the slight changes in the apparent density obtained for MI-G0-MAL and MI-G1-MAL, MI-G1-PEG-MAL shows changes in the compactness of the structure after the addition of HAS (Figure 4.25 C). The apparent density decreases, followed by an increase in the apparent density from molar masses of approximately, 1×10^7 g/mol. The decrease in molar mass indicates, possibly, two populations of aggregates, DenPol-DenPol that have a more compact structure and DenPol-HSA that are less compact. Alternatively, the combination of these aggregates has a lower density. This change in apparent density was previously observed for biohybrid structures, the observation in the apparent density was due to the presence of compact branched and loose structures that were simultaneously present in the sample at high molar masses.[49]

MI-G2-MAL mixtures with 0, 0.1 and 0.25 mg HSA show a decrease in the apparent density, see Figure 4.25 D. With the largest amount of HSA, the apparent density remains between 5 and 15 kg/m^3, indicating that the compactness of the structure is constant as a function of molar mass. The change in the density of MI-G2-MAL: HSA (1:0.5) is small in comparison to mixtures with lower amounts of HSA. These values indicate that the structure is maintained from low to high molar mass species when there is an abundance of HSA.

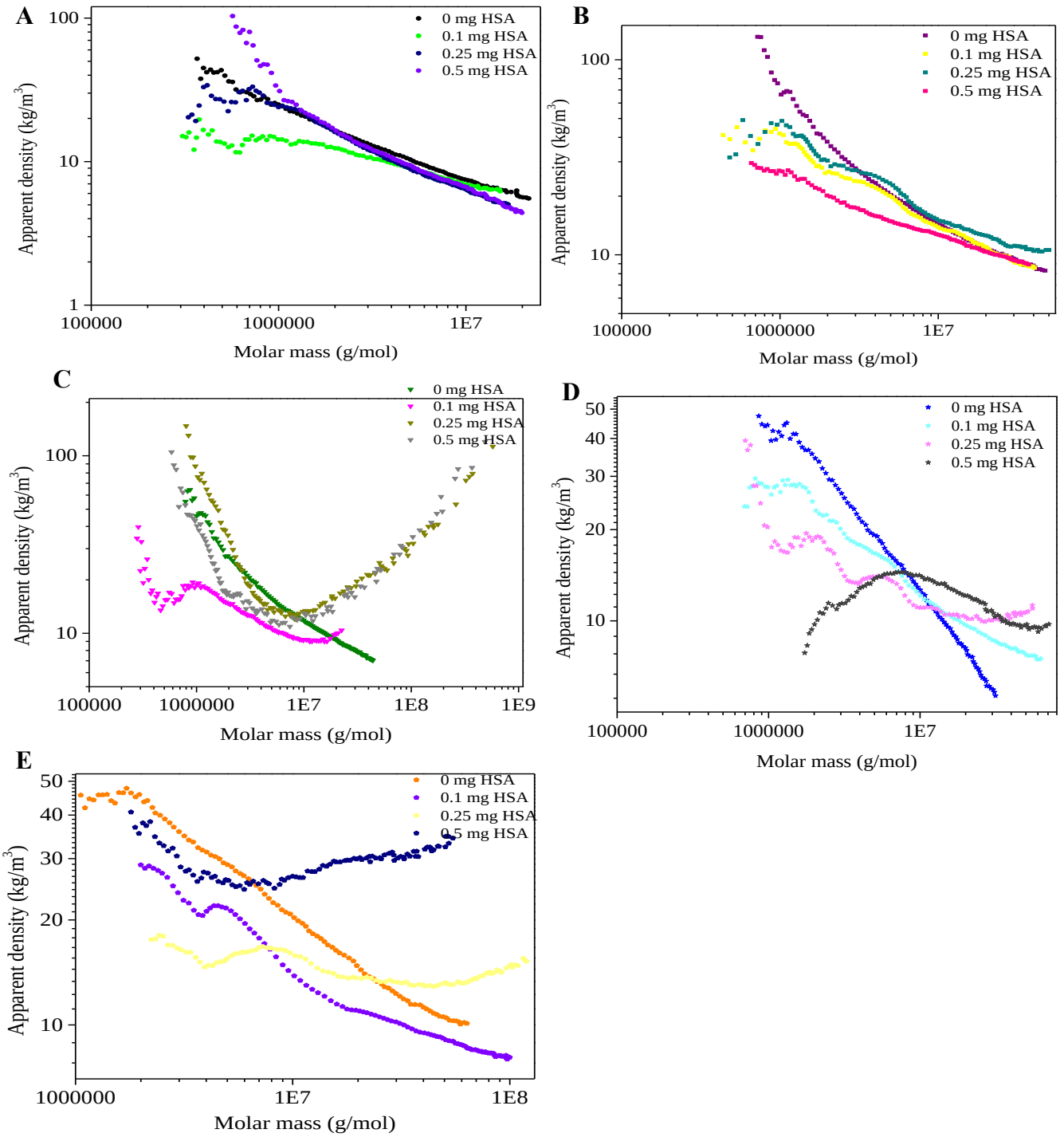

Figure 4.25. Apparent density over molar mass of: A) MI-G0-MAL (solid circle), B) MI-G1-MAL (solid square), C) MI-G1-PEG-MAL (solid inverted triangle), D) MI-G2-MAL (solid star) and E) MI-G3-MAL (solid pentagon).

The apparent density values of MI-G3-MAL with different amounts of HSA display an interesting aggregation mechanism, see Figure 4.25 E. MI-G3-MAL and MI-G3-MAL :HSA (1:0.1) shows a decrease in the apparent density with an increase in the molar mass for the formation of aggregated structures from non-aggregated structures. On the other hand, for MI-G3-MAL: HSA (1:0.25), the apparent density is between 10 -20 kg/m^3 and the apparent density of MI-G3-MAL: HSA (1:0.5) decreases from 40 to 25 kg/m^3 followed by an increase to approximately 35 kg/m^3. This aggregation mechanism is displayed by MI-G1-PEG-MAL: HSA (1:0.25) and (1:0.5).

Progressing towards higher generation numbers there are changes evident in the apparent density with the addition of HSA, this is especially visible with larger amounts of HSA (0.25 and 0.5 mg). The apparent density provides insight into the aggregation mechanism and the influence of HSA on the compactness of the structure. However, the apparent density only shows the presence of an aggregated structure formed but not the architecture of the aggregates. The shape factor will be employed to provide the information about the molecular shape over the molar mass.

4.5.2 Analysis of the shape factor ($\rho = R_g/R_h$) of the DenPol-HSA mixtures

The shape factor, a universal ratio, uses radii that are influenced by molar mass, thus, by applying the ratio the molar mass dependencies are removed.[37] The shape factor is a good quantitative parameter for architectural information of single or clusters of macromolecules. This is crucial for understanding if the conformation of the individual DenPols influences the interactions with HSA and the conformation of DenPol-HSA complexes.

The shape factor and the molar mass distribution (MMD) provide a wealth of information regarding the conformation of the DenPols. Figure 4.26 A shows the shape factor over the MMD of MI-G0-Mal with different amounts of HSA. It is evident that the conformation of MI-G0-MAL is altered with the addition of HSA. These changes were not prevalent in the apparent density calculations and R_h readings. The molar mass and R_g readings deviated slightly from the molar mass of MI-G0-MAL. However, the shape factor illustrates that the formation of aggregated structures and the molecular parameters can show small changes, but the conformation of the complexes can still be influenced. With each subsequent addition of HSA the conformation progresses from a random coil to a hard homogenous sphere even approaching microgel conformation. As a microgel conformation is typically observed between 0.3 to 0.6.[37]

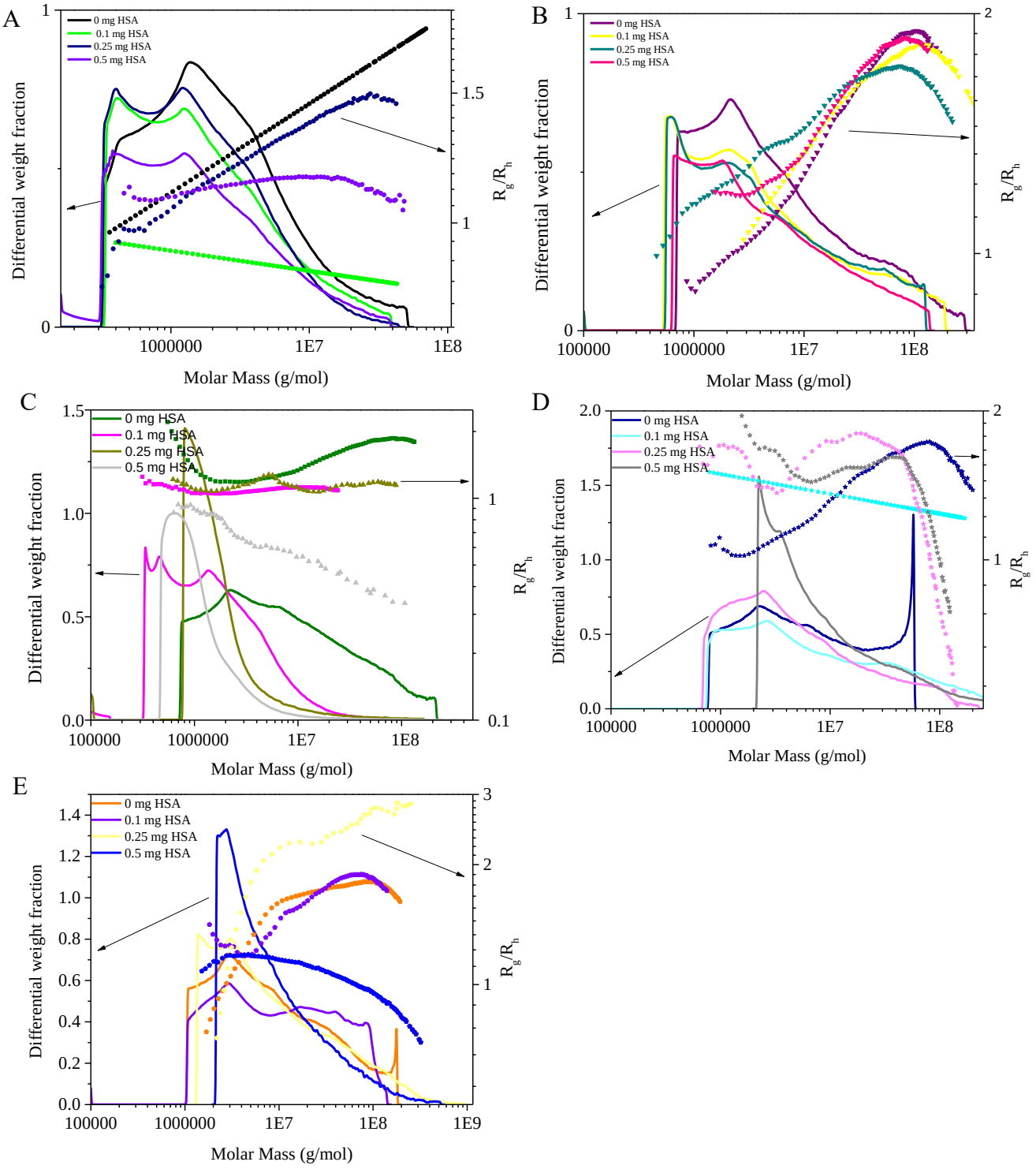

Figure 4.26. Shape factor over molar mass distribution of: A) MI-G0-MAL (solid circle), B) MI-G1-MAL (solid square), C) MI-G1-PEG-MAL (solid upside down triangle), D) MI-G2-MAL (solid star) and E) MI-G3-MAL (solid pentagon).

In addition, the complex formed with MI-G0-MAL: HSA (1: 0.25) exhibited a similar conformational change from a branched random coil to an elongated aggregated structure. The highest amount of HSA shows an R_g/R_h value between approximately 1 and 1.2 over the molar mass distribution, this value is close to 1.225 representative of a hyperbranched polymer. MMD shows the multimodality of the individual MI-G0-MAL as well as the mixtures. As the species moves towards ultrahigh molar masses (above 1×10^7 g/mol) there is a decrease in the differential weight fraction.

MI-G1-MAL with different fractions of HSA are displayed in Figure 4.26 B. The values obtained are within the expected range of 1 and 2 for macromolecules. There are minimal changes in the conformation which was illustrated with the apparent density calculations. The maltose moieties available along the polymer backbone are possibly not easily accessible due to the conformation and the suspected pronounced aggregation of MI-G1-MAL. As a result, there are minimal interactions with HSA.

Figure 4.26 C shows individual MI-G1-PEG-MAL as well as mixtures with different amounts of HSA. There is a noticeable change in the shape factor of MI-G1-PEG-MAL: HSA (1:0.5), the shape factor is within regions below the expected for range of 1 and 2. The shape factor is in regions characteristic of microgels which are essentially cross-linked polymeric nanostructures.[50] These properties, formation of cross-links, are not expected for the intermolecular interactions between MI-G1-PEG-MAL and HSA. An alternative reason could be the movement towards a dense spherically shaped conformation. Comparison of the conformation of MI-G1-PEG-MAL: HSA (1:0.1) and (1:0.25) shows only small deviations as a function of molar mass. The shape factor is 1-1.4, where 1.225 is characteristic for hyperbranched architectures. The MMD becomes narrower and shifts towards lower molar masses with the subsequent addition of HSA. It is evident that the complexes have larger weight fractions at lower molar masses.

Yet, another distinctive change in the shape factor with molar mass shows the interesting role of the multivalent interactions between DenPols and HSA. This is demonstrated with the change in conformation of MI-G2-MAL with the introduction of HSA (see Figure 4.26 D). The conformation of MI-G2-MAL progressed from a spherical shape towards a branched or random coil architecture for the aggregated structures. The conformation of MI-G2-MAL: HSA (1:0.25) shows a decrease from 1.8, which is distinctive for a random coil architecture, towards 0.4 which is in the region for

a microgel species. Similar conformation behaviour is displayed for MI-G2-MAL: HSA (1:0.5). The differential weight fraction shows no symmetry in the curves. The multimodality of the MMD can be attributed to the multiple species existing in individual MI-G2-MAL sample. Regarding the mixtures there is a shift towards higher molar masses and narrower MMD after the addition of 0.5 mg HSA.

A similar conformational deviation displayed for MI-G1-PEG-MAL and MI-G2-MAL is displayed for MI-G3-MAL in Figure 4.26 E. However, with the addition of 0.5 mg HSA, the conformation of the non-aggregated structures, which exist as random coil linear chain to a R_g/R_h of approximately 0.3 displaying a defined transition towards aggregated microgel architecture. Once again, the MMD curves exhibit multimodality, with the shift towards higher molar masses with the addition of 0.5 mg HSA. However, the highest fraction of the species is at lower molar masses, therefore, aggregated structures compose a smaller amount of the entire sample.

The shape factor establishes a relationship between the aggregation mechanism (displayed by the apparent density) and the conformation of the non-aggregated and aggregated species. It is evident that the complexes formed between the DenPols and HSA present noticeable changes in the conformation, especially, with the addition of 0.5 mg of HSA. The differential weight fraction shows that the ultrahigh molar masses contribute a small portion of the overall sample.

4.6 Conclusions

The utilization of batch mode DLS proved advantageous for determining the dependence of the hydrodynamic diameter of the DenPols on concentration and temperature. The broad size distribution of the DenPols emphasized the need of an advanced separation technique to characterize the fractions.

SEC-MALLS analysis was successfully applied to characterize the molar mass of poly (ethylene-*alt*-maleic anhydride) and the Boc-protected DenPols. The degree of polymerization was used to calculate the theoretical molar masses of the DenPols.

An advanced separation technique, AF4-MALLS-DLS was successfully applied for the characterization of ultrahigh molar mass DenPols, HSA and complexes of DenPols-HSA. The molar mass, size and dispersity of the maltose-modified DenPols was obtained. The DenPols contained non-aggregated and aggregated structures. The conformation parameters showed the

random coil architectures of the single macromolecules and clusters with elongated or spherical architectures.

The fractionation process was extended to DenPol-HSA complexes as the protocol was specifically designed to separate the non-bound HSA from the DenPol-HSA complex. The AF4 protocol successfully determined the molar mass, size, and conformation of the complexes. The conformation parameters showed that there are changes in the architectures from randomly branched linear macromolecules to spherical or microgel clusters of macromolecules with high molar masses.

4.7 References

1 M. E. Schimpf, K. D. Caldwell and J. C. Giddings, in *Field-flow fractionation handbook*, ed. M. E. Schimpf, K. D. Caldwell and J.C. Giddings, John Wiley & Sons, Inc., New York, 1st edn, 2000, vol. 1, ch. 1, pp. 3-31.

2 A. Zattoni, D. C. Rambaldi, P. Reschiglian, M. Melucci, S. Krol, A. M. C. Garcia, A. Sanz-Medel, D. Roessner and C. Johann, *J. Chromatogr. A*, 2009, **1216**, 9106–9112.

3 A. Lederer, S. Boye and D. Appelhans, in *ACS Symposium Series*, American Chemical Society, 2018, **1281**, 171–187.

4 A. Mukherjee and V. A. Hackley, *Analyst*, 2018, **143**, 731–740.

5 U. B. Kavurt, M. Marioli, W. T. Kok and D. Stamatialis, *J. Chem. Technol. Biotechnol.*, 2015, **90**, 11–18.

6 M. Glantz, A. Håkansson, H. Lindmark Månsson, M. Paulsson and L. Nilsson, *Langmuir*, 2010, **26**, 12585–12591.

7 R. A. Abbate, N. Raak, S. Boye, A. Janke, H. Rohm, D. Jaros and A. Lederer, *Food Hydrocoll.*, 2019, **92**, 117–124.

8 L. Nilsson, *Food Hydrocoll.*, 2013, **30**, 1–11.

9 S. Boye, D. Appelhans, V. Boyko, S. Zschoche, H. Komber, P. Friedel, P. Formanek, A. Janke, B. I. Voit and A. Lederer, *Biomacromolecules*, 2012, **13**, 4222–4235.

10 J. Stetefeld, S. A. McKenna and T. R. Patel, *Biophys. Rev.*, 2016, **8**, 409–427.

11 R. Xu, *Particuology*, 2015, **18**, 11–21.

12 A. Zhang, L. Shu, Z. Bo and A. D. Schlüter, *Macromol. Chem. Phys.*, 2003, **204**, 328–339.

13 S. M. Sultan, M. R. R. De Planque, P. Ashburn and H. M. H. Chong, *J. Nanomater.*, 2017, **2017**, 1-7

14 J. Madeira Do O, F. Mastrotto, N. Francini, S. Allen, C. F. Van Der Walle, S. Stolnik and G. Mantovani, *J. Mater. Chem. B*, 2018, **6**, 1044–1054.

15 A. Lederer and W. Burchard, in *Hyperbranched Polymers Macromolecules in between Deterministic Linear Chains and Dendrimer Structures*, ed. B. Z. Tang, A. S. Abd-El-Aziz, S. Craig, J. Dong, T. Masuda, C. Weber, the Royal Society of Chemistry, Cambridge, 16th ed., 2015, vol. 1, ch. 5, 88-132.

16 A. Choperena and P. Painter, *Macromolecules*, 2009, **42**, 6159–6165.

17 T. I. Mizan, P. E. Savage and R. M. Ziff, *J. Phys. Chem.*, 1996, **100**, 403–408.

18 A. Gube, L. Jakisch, L. Häußler, K. Schneider, B. Voit and F. Böhme, *Polym. Int.*, 2012, **61**, 157–162.

19 S. Podzimek, T. Vlcek and C. Johann, *J. Appl. Polym. Sci.*, 2001, **81**, 1588–1594.

20 M. Wintermantel, M. Schmidt and M. Antonietti, *Polym. Anal. Charact.*, 1992, 91–103.

21 D. J. Frater, J. W. Mays and C. Jackson, *J. Polym. Sci. Part B Polym. Phys.*, 1997, **35**, 141–151.

22 I. Capron, M. Grisel and G. Muller, *Int. J. Polym. Anal. Charact.*, 1995, **2**, 9–20.

23 M. Gerle, K. Fischer, S. Roos, A. H. E. Müller, M. Schmidt, S. S. Sheiko, S. Prokhorova and M. Möller, *Macromolecules*, 1999, **32**, 2629–2637.

24 M. Leeman, K. G. Wahlund and B. Wittgren, *J. Chromatogr. A*, 2006, **1134**, 236–245.

25 J. Liu, Q. Zhu, S. J. Shire and B. Demeule, in *Field-Flow Fractionation in Biopolymer Anal.*, ed. S. K. R Williams and K. D. Caldwell, Springer Vienna, Vienna, 1st edn, ch. 6, 2012, pp. 89–101.

26 C. R. M. Bria and S. K. R. Williams, *J. Chromatogr. A*, 2016, **1465**, 155–164.

27 H. H. Song, W.-S. Kim, Y. H. Park, E. K. Yu and D. W. Lee, *Bull. Korean Chem. Soc.*, 1999, **20**, 1159–1164.

28 M. Marioli and W. T. Kok, *Anal. Bioanal. Chem.*, 2019, **411**, 2327–2338.

29 A. A. D'souza and R. Shegokar, *Expert Opin. Drug Deliv.*, 2016, **13**, 1257–1275.

30 S. Boye, N. Polikarpov, D. Appelhans and A. Lederer, *J. Chromatogr. A*, 2010, **1217**, 4841–4849.

31 D. Lee and S. K. R. Williams, *J. Chromatogr. A*, 2010, **1217**, 1667–1673.

32 W. F. Reed, *Macromol. Chem. Phys.*, 1995, **196**, 1539–1575.

33 S. R. Bean and G. L. Lookhart, *Cereal Chem.*, 2001, **78**, 608–618.

34 M. Andersson, B. Wittgren and K. G. Wahlund, *Anal. Chem.*, 2003, **75**, 4279–4291.

35 S. K. Ratanathanawongs Williams, M.-A. Benincasa and A. A. Ashames, in *Encyclopedia of Analytical Chemistry*, ed. R. A. Meyers, John Wiley & Sons, Inc., New York, 1st edn, 2016, vol. 1, ch. 2008a, pp. 1-24

36 B. Dhakal, L. Bohé and D. Crich, *J. Org. Chem.*, 2017, **82**, 9263–9269.

37 W. Burchard, *Adv. Polym. Sci.*, 1999, **143**, 114–194.

38 W. Burchard, in *Light Scattering from Polymers*, ed. W. Burchard Springer, Berlin Heidelberg, 1st edn, 1983, vol. 48, ch. , pp. 1–124.

39 J. I. Paez, M. Martinelli, V. Brunetti and M. C. Strumia, *Polymers (Basel).*, 2012, **4**, 355–395.

40 S. Costanzo, L. F. Scherz, T. Schweizer, M. Kröger, G. Floudas, A. Dieter Schlüter and D. Vlassopoulos, *Macromolecules*, 2016, **49**, 7054–7068.

41 F. Dutertre, K. T. Bang, E. Vereroudakis, B. Loppinet, S. Yang, S. Y. Kang, G. Fytas and T. L. Choi, *Macromolecules*, 2019, **52**, 3342–3350.

42 J. K. Armstrong, R. B. Wenby, H. J. Meiselman and T. C. Fisher, *Biophys. J.*, 2004, **87**, 4259–4270.

43 J. Anguizola, R. Matsuda, O. S. Barnaby, K. S. Hoy, C. Wa, E. DeBolt, M. Koke and D. S. Hage, *Clin. Chim. Acta*, 2013, **425**, 64–76.

44 S. C. Rozinek, R. J. Thomas and L. Brancaleon, *Biochem. Biophys. Reports*, 2016, **7**, 295–302.

45 A. Oliva, M. Llabres and J. Farina, *Curr. Drug Discov. Technol.*, 2005, **1**, 229–242.

46 M. E. Schimpf and K. G. Wahlund, *J. Microcolumn Sep.*, 1997, **9**, 535–543.

47 B. Klajnert, D. Appelhans, H. Komber, N. Morgner, S. Schwarz, S. Richter, B. Brutschy, M. Ionov, A. K. Tonkikh, M. Bryszewska and B. Voit, *Chem. - A Eur. J.*, 2008, **14**, 7030–7041.

48 D. Wrobel, D. Appelhans, M. Signorelli, B. Wiesner, D. Fessas, U. Scheler, B. Voit and J. Maly, *Biochim. Biophys. Acta - Biomembr.*, 2015, **1848**, 1490–1501.

49 S. Boye, F. Ennen, L. Scharfenberg, D. Appelhans, L. Nilsson and A. Lederer, *Macromolecules*, 2015, **48**, 4607–4619.

50 Y. Wang, L. Guo, S. Dong, J. Cui and J. Hao, *Adv. Colloid Interface Sci.*, 2019, **266**, 1–20.

Chapter 5

Conclusions

Chapter 5

Conclusions

5.1 Conclusions

In this study, we focused on the application of a versatile and gentle AF4 separation system coupled to MALLS, DLS and RI detectors to characterize DenPols, HSA and DenPols and HSA complexes. The DenPols were synthesized and received from the Department of Bioactive and Responsive Polymers at the Leibniz-Institut für Polymerforschung Dresden (Dresden, Germany). A comparative study between the molar mass, size, molecular size dispersity, apparent density and conformation of the individual DenPols and the DenPol-HSA complexes were performed.

DLS was implemented to study the hydrodynamic size of DenPols and HSA in 10 mM PBS. The polydisperse DenPols showed small changes in the hydrodynamic size with an increase in concentration. The size of MI-G1-MAL, MI-G1-PEG-MAL, MI-G2-MAL, and MI-G3-MAL were similar, as the branching density along the polymer backbone increased but the contour length remained unchanged. The PDI of all the DenPols was above 0.1, therefore the species were all polydisperse. A temperature study displayed minimal changes in the size of the DenPols with elevated temperatures. The PDI showed that the DenPols were polydisperse and separation of DenPols into homogenous fractions was crucial to analyse the size and size distribution.

SEC coupled to MALLS and RI detectors provided the molar mass distribution and dispersity of poly(ethylene-*alt*-maleic anhydride), MI-G0-Boc and MI-G1-Boc. The determination of the molar mass of the polymer backbone was essential for the calculation of the theoretical molar mass values of the DenPols. The MALLS detector signals of MI-G0-Boc and MI-G1-Boc showed a high molar mass shoulder indicating pronounced aggregation in the species. However, the concentration of the high molar masses was low according to the RI detector signal. Therefore, the molar mass values were not strongly influenced by the high molar mass shoulder. SEC-MALLS, with a stationary phase, was not suitable for the characterization of water-soluble ultrahigh molar mass dendronized glycopolymers with extensive branching. Therefore, a technique with an empty channel was desirable for the characterization of DenPols and DenPol-HSA complexes.

The capability of AF4 was displayed by the successful characterization of the molar mass, R_g and R_h of DenPols, HSA and DenPol-HSA complexes. The elution of the DenPols showed broad

MALLS and RI detector signals indicative of a polydisperse sample. In addition, the increase in the molar mass and radii readings showed the presence of expanded, high molar mass structures, suspected as DenPol-DenPol aggregates. The experimental molar mass values of the DenPols exceeded the theoretical molar masses, suggesting aggregation. It was evident from the aggregation number that none of the DenPols were present as only single macromolecules but as clusters of single macromolecules. The aggregation number of MI-G0 was 34, indicating pronounced aggregation possibly because of electrostatic interactions. 1st generation maltose-decorated DenPols had aggregation numbers larger than MI-G2-MAL and MI-G3-MAL, displaying pronounced aggregation and the presence of stable aggregates. It was evident from the aggregation number that there were aggregates present, thus the apparent density was evaluated. The apparent density over the molar mass illustrated non-aggregated lower molar mass structures forming aggregated high molar mass structures. The non-aggregated structures of the DenPols were linear chain random coils forming elongated clusters of single macromolecules, according to the shape factor calculations. The shape factor calculations were complemented, with an additional conformation plot, log R_g vs log M, with the slope corresponding to random coil conformation for the single macromolecules. The ultrahigh molar mass aggregates deviated towards spherical architectures in contrast to the shape factor calculations. However, MI-G2-MAL showed the same aggregation mechanism as random coil conformation for single macromolecules and aggregates were elongated structures. Therefore, the conformation of the high molar masses was not conclusive, based on the two conformational parameters.

The AF4 fractionation process was successfully applied to characterize the molar mass and R_h of HSA. The monomer and dimer peaks of HSA were observed in the MALLS detector signal. HSA eluted during 10 min with a high cross flow and the readings obtained agreed with literature. There was no aggregation dependence on concentration observed.

The successful implementation of the AF4 fractionation process for the individual components was used for the characterization of the DenPol-HSA complexes as non-bound HSA eluted during the first 10 min. The MALLS detector signal of MI-G0-MAL, MI-G1-MAL, MI-G2-MAL, and MI-G3-MAL exhibited minimal changes in the retention time after the addition of HSA. However, the MALLS detector signal of MI-G1-PEG-MAL showed the presence of multimodalities after the addition of HSA. It was proposed that not all the macromolecules were modified with maltose

shells, thus different complexes were formed. The apparent density was studied to determine the change in the aggregation mechanism of the DenPols after the addition of HSA. Distinct changes were observed regarding apparent density over the molar mass of MI-G1-PEG-MAL-HSA, MI-G2-MAL-HSA and MI-G3-MAL-HSA complexes. The apparent density values showed the impact of HSA on the density of the aggregated structures. As the combination of DenPol-HSA and DenPol-DenPol complexes showed an increase in the apparent density towards higher molar masses. The shape factor was evaluated to provide clarity regarding the distinct changes in the aggregation mechanism. The shape factor displayed DenPols with random coil architectures forming dense spherical and swollen macromolecular structures at high molar masses. In addition, the differential weight fractions indicated that ultrahigh molar masses are a marginal fraction of the entire sample. Therefore, the distinct changes in the apparent density and shape factor towards high molar masses were a small contribution towards the entire sample.

These results showed that AF4 is a gentle technique and can be implemented for studying the change in conformation of DenPols when interacting with HSA. A wealth of information was obtained with the implementation of a versatile separation method. The results showed that aggregates with ultrahigh molar masses and DenPol-HSA complexes can be comprehensively characterized. The application of conformational parameters allowed for insight about the architecture of the DenPols and the complexes.

5.2 Future work

Recommendations for possible future work are listed below:

1. Optimize the cross-flow gradient to provide insight of the ultrahigh molar mass fractions. For instance, applying a linear gradient after the exponential gradient to improve analysis of the ultrahigh molar mass fractions.
2. Perform a concentration study of the DenPols with the AF4 method to determine the effect of concentration on the molar mass and size.
3. Use an aqueous system that does not contain a salt to determine the role the salt has on the aggregation of the DenPols and the interactions between DenPols and HSA.
4. Introduce a UV detector as a second concentration detector to quantify the non-bound and bound HSA. This can be performed by obtaining a UV wavelength that only HSA has a signal intensity.

5. Complementary microscopy techniques such as AFM or TEM to provide clarity of the conformation and shape of the DenPols and complexes. Microscopy can improve the understanding of the conformational and shape changes.

Appendix A

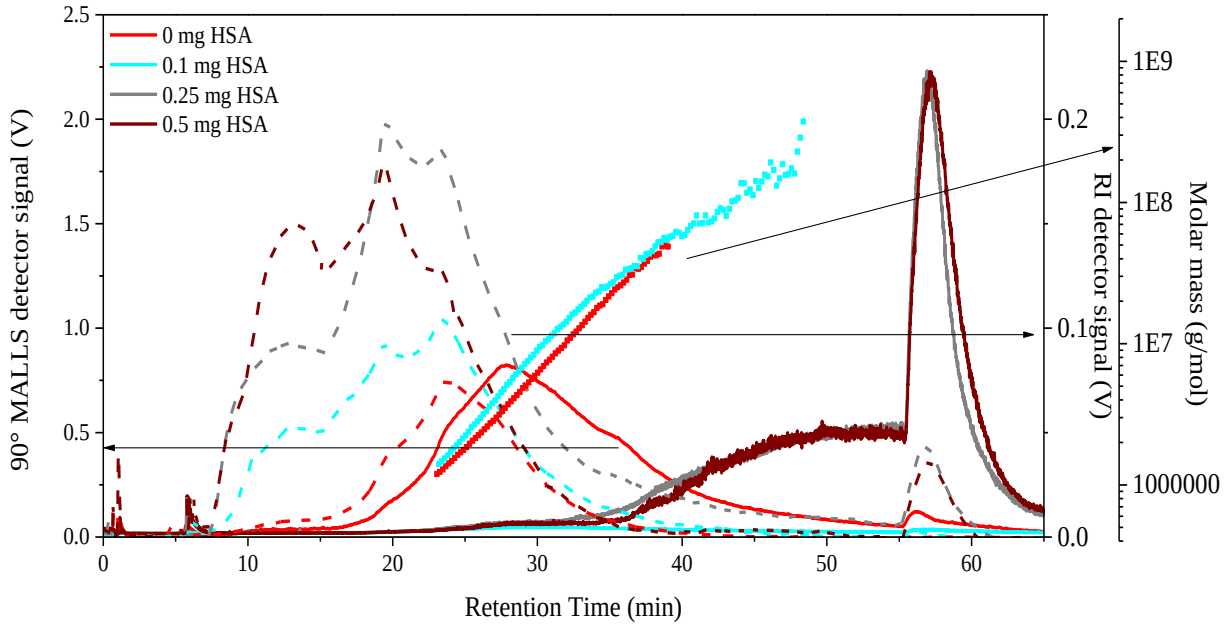

Figure A. 1. Fractograms of different mixtures of MI-G0 and HSA in 0.01 M PBS, measurements: 90° MALLS detector signal, RI detector signal and molar mass: MI-G0 (red), MI-G0:HSA (1: 0.1) (cyan), (1:0.25) (grey) and (1:0.5) (brown).

Table A. 1. Average molar mass, dispersity, size, and dn/dc readings of mixtures of MI-G0 and HSA in 0.01 M PBS.

Mass of HSA (mg)	M_n **(kg/mol)**	M_w **(kg/mol)**	**Đ**	$R_{g,z}$ **(nm)**	$R_{h,z}$ **(nm)**	**dn/dc (mL/g)**
0	2 600	5 500	2.1	80.6 ±15 .0	54.2±15. 6	0.123
0.1	2 000	7 000	3.5	99.0 ± 7. 6	70.0±11. 4	0.156

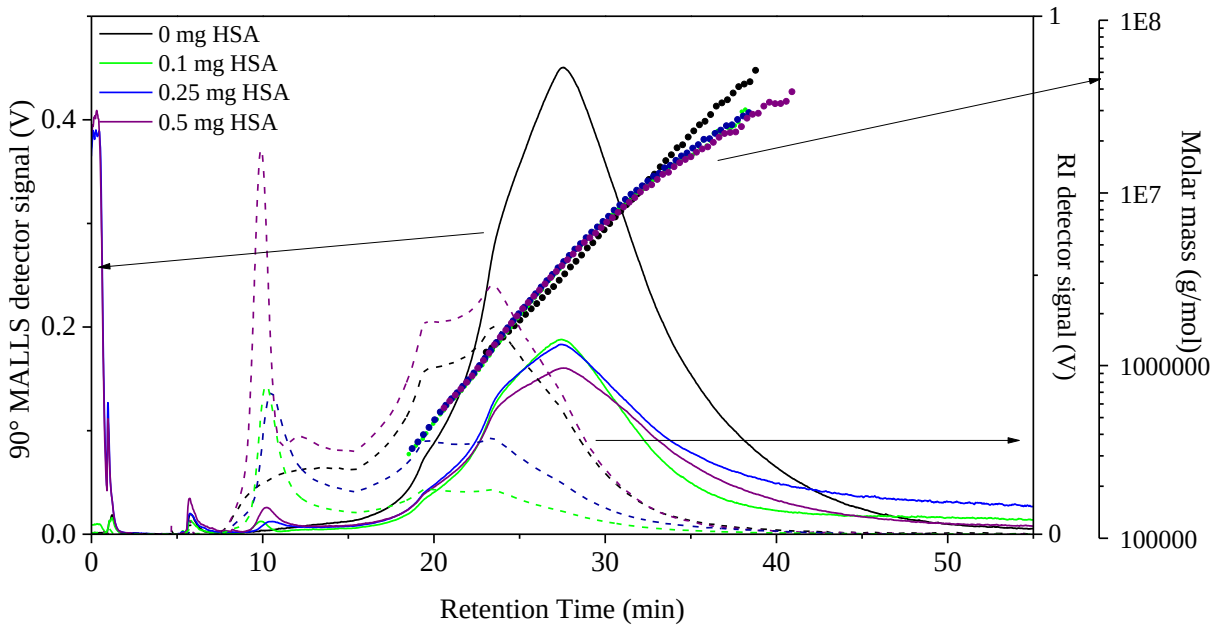

Figure A.2 .Fractograms of different mixtures of MI-G0-MAL and HSA in 10 mM PBS measured with AF4-MALLS, 90° MALLS detector signal, molar mass, RI detector signal: MI-G0-MAL (black), MI-G0-MAL: HSA (1:0.1) green, (1:0.25) blue and (1:0.5) purple.

Table A. 2. Average molar mass, dispersity, size and dn/dc readings of MI-G0-MAL with different ratios of HSA measured with AF4-MALLS-DLS.

Mass of HSA (mg)	M_n **(kg/mol)**	M_w **(kg/mol)**	**Đ** (M_w/M_n)	$R_{g,z}$ **(nm)**	$R_{h,z}$ **(nm)**	**dn/dc (mL/g)**
0	880	3 400	3.9	71.8 ± 1.6	48.5± 1.6	0.153
0.1	980	2 600	2.7	58.4± 0.3	45.3 ± 3.8	0.156
0.25	980	2 900	3.0	66.3 ± 0.6	43.3 ± 8.8	0.156
0.5	1010	3000	3.4	65.0± 0.7	49.5 ± 12.7	0.156

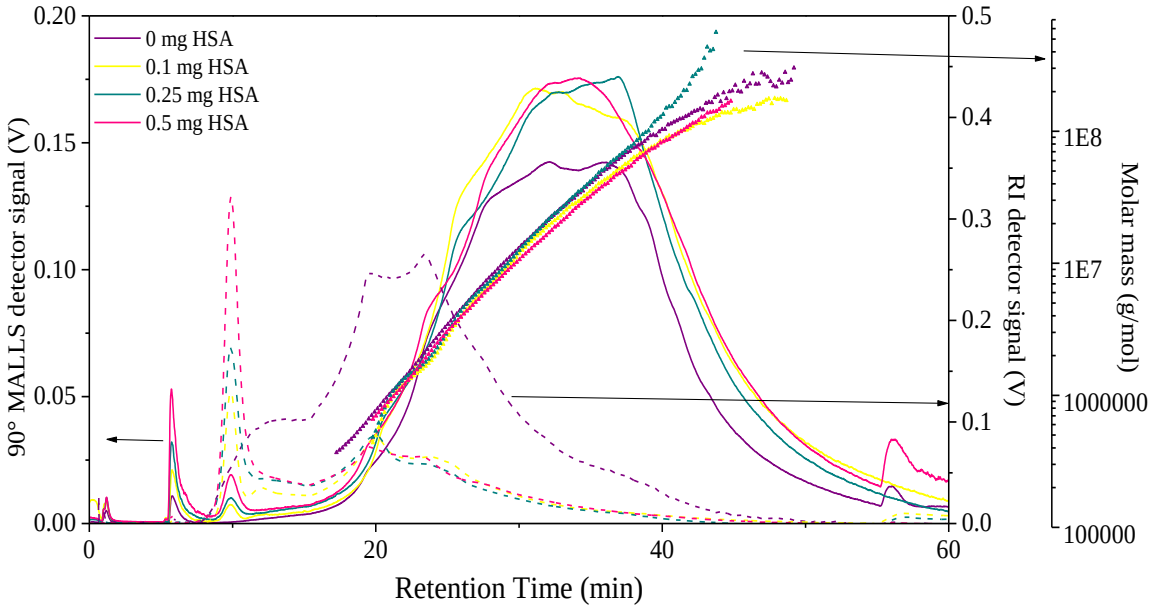

Figure A.3. Fractograms of different mixtures of MI-G1-MAL and HSA in 10 mM PBS measured with AF4-MALLS, a) 90° MALLS detector signal with molar mass distributions, b) 90° MALS detector signal with radius distributions and c) RI detector signal. MI-G1-MAL: HSA (1:0) purple, (1:0.1) yellow, (1:0.25) cyan solid and (1:0.5) pink solid line.

Table A.3.Average molar mass, dispersity, size and dn/dc values determined of MI-G1-MAL with different ratios of HSA measured with AF4-MALLS-DLS.

Mass of HSA (mg)	M_n **(kg/mol)**	M_w **(kg/mol)**	**Đ** (M_w/M_n)	$R_{g,z}$ **(nm)**	$R_{h,z}$ **(nm)**	**dn/dc (mL/g)**
0	2 600	15 200	9.3	122.1± 2.1	62.1± 4.9	0.153
0.1	1 900	15 100	7.7	116.6± 0.6	64.1± 0.3	0.156
0.25	2 000	13 000	6.6	113.7± 8.4	59.8± 6.4	0.156
0.5	2 200	11 700	5.3	115.1± 0.4	62.5± 6.6	0.156

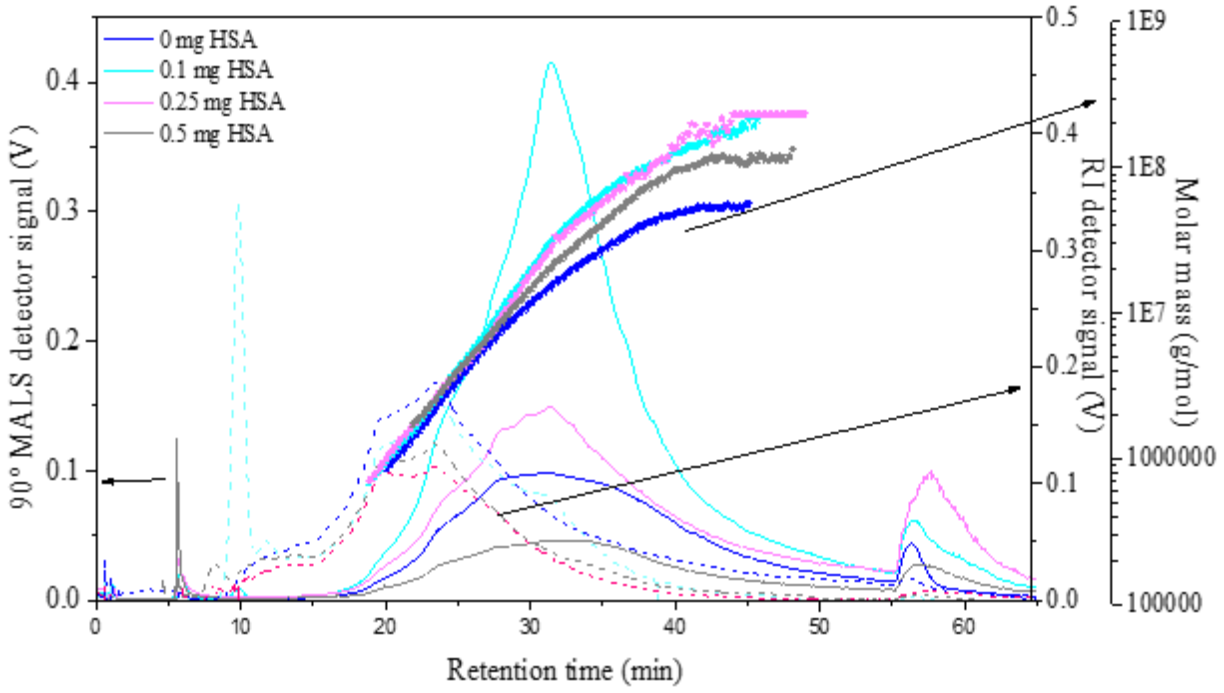

Figure A.4 Fractograms of different mixtures of MI-G2-MAL and HSA in 10 mM PBS measured with AF4-MALLS, 90° MALLS detector signal, molar mass, and RI detector signal. MI-G2-MAL: HSA (1:0) blue, (1:0.1) cyan, (1:0.25) pink and (1:0.5) black.

Table A.4. Average molar mass, dispersity, size and dn/dc values determined for MI-G2-MAL with different ratios of HSA measured with AF4-MALLS-DLS.

Mass of HSA (mg)	M_n **(kg/mol)**	M_w **(kg/mol)**	**Đ** (M_w/M_n)	$R_{g,z}$ **(nm)**	$R_{h,z}$ **(nm)**	**dn/dc (mL/g)**
0	3 000	13 000	4.3	101.1 ± 5.5	69.6± 8.3	0.153
0.1	3 100	19 100	6.2	109 ± 4.5	64.1 ± 12.9	0.156
0.25	2 700	11 200	7.2	92 ± 10.5	89.5 ± 6.2	0.156
0.5	3 800	13 800	4.6	99.3 ± 1.5	70.3 ± 3.4	0.156